UNIVERSITÀ DEGLI STUDI DI PALERMO
Dottorato di Ricerca in Scienze della Terra e del Mare
Dipartimento di Scienze della Terra e del Mare
SSD Geo/03

Architecture and kinematics of forearc basins and intra-caldera resurgences: new insight from the Paola Basin (western offshore Calabria region) and the Campi Flegrei caldera (Campania region)

Ph.D. STUDENT
CORRADINO MARTA

COORDINATOR
PROF. AIUPPA ALESSANDRO

TUTOR
PROF. PEPE FABRIZIO

CO TUTOR
PROF. BERTOTTI GIOVANNI

CYCLE XXXI
YEAR OF QUALIFICATION 2019

Contents

Acknowledges

Completion of this Ph.D. dissertation has been a truly life-changing experience for me and it would not have been possible to do without the support and guidance that I received from many people. I would like to express my sincere gratitude to all of them.

Firstly, I would like to thank my advisor Prof. Fabrizio Pepe for the continuous, unconditional support to my Ph.D. study, for leading me working on diverse exciting projects and for giving me the freedom to work how I desired. I am also grateful for all his contributions of time, ideas, and funding to make my Ph.D. experience productive and stimulating. His joy and enthusiasm for scientific research are contagious and motivational for me. I could not have imagined having a better advisor and mentor for my Ph.D. study.

Besides my advisor, I owe my deepest gratitude to many researchers who offered their helpful support despite their busy schedule. Without their precious feedback my Ph.D. study would not have been achievable. I am grateful to Dr. Marco Sacchi of *Istituto per l'Ambiente Marino e Costiero* of Naples for providing the seismic lines, used for the first chapter of this thesis, and for his helpful comments and input. Special thanks go to Prof. Giovanni Bertotti of Delft University of Technology, who has provided his invaluable contribution in carrying out the research presented in the second chapter of this thesis. I would like to thank Prof. Sean Willett and Prof. Vincenzo Picotti for receiving me at the *ETH Zurich* as a guest student during a stay aboard. I really appreciate the time they have dedicated to me. I recognize the full worth of the hard questions which prompted me to see my research from various perspectives. I am thankful to Dr. Giuseppe Solaro of *Istituto per il Rilevamento Elettromagnetico dell'Ambiente* of Naples for providing DInSAR data used for the first chapter of this dissertation and for his useful suggestions. My deep appreciation goes out to Prof. Carmelo Monaco of *University of Catania*, Prof. Luigi Ferranti of *University of Naples Federico II* and Prof. Rinaldo Nicolich for reviewing parts of this Ph.D. thesis and for providing valuable comments that helped improve it. I also express my thankful to Prof. Andrea Billi of *Sapienza University* of Rome and Prof. Claudio Faccenna of *Roma Tre University* for undertaking the review of my Ph.D. thesis. I acknowledge and appreciate the meticulous work they have done.

I would like to thank my colleagues, Elisabetta, Nicolò and Ciccio, for having make my breaks from research joyful and funny moments and for their encouragement during my Ph.D. period. I am also grateful to my lovely friends, Agata, Ilaria, Luisa, Giulia and Martina, my friends-colleagues Anna Maria and Tiziana, my dear flatmate Emanuela and my cousin Emanuela for having provided me moral and emotional support and for always having been present even from distance. As geologists say, "you rock!"

Last, but not least, a very special gratitude goes out to my mum, dad, Manuel and my aunt Maria Enza who encouraged and helped me at every stage of my life. I would also like to thank them for always believing in me and supporting my choices.

Introduction

This thesis deals with deformation mechanisms at different time and spatial scales ranging from tens to millions of years and from one to tens of kilometers, respectively. The study areas are the Campi Flegrei (Campania region, Italy) and Paola Basin (western offshore Calabria region, Italy).

The Campi Flegrei and its offshore prolongation, the Pozzuoli Bay, represent a natural laboratory for investigating volcano-tectonic deformations at 1yr-1kyr timescale and 1km spatial scale related to the dynamics of the Neapolitan Yellow Tuff (NYT) caldera and its intra-caldera resurgence. Calderas are depressions formed as a consequence of gravitational collapse of overlying rocks into an emptying reservoir following ignimbrite eruptions (Lipman, 2000). Generally, collapse of the caldera floor occurs along a ring fault zone that allows a subsidence up to 3 km and provides a large volume of pyroclastic material. Post-collapse activity includes post-caldera volcanism, resurgence, sedimentation within the caldera depression and hydrothermal processes. In particular, resurgence represents the long-term uplift of the subsided caldera floor to form a dome-like structure. The resurgence develops as dome (Lipman, 2000; R. L. Smith & Bailey, 1968) or disjoint uplifted blocks of the caldera floor rocks (Acocella et al., 2004; Orsi et al., 1991). According to many authors, the uplift of the resurgent dome occurs along inward dipping reverse faults (Brothelande et al., 2016; Kennedy et al., 2004; Mandl, 1988; Orsi et al., 1991; Phillips, 1974; Roche et al., 2000; Walter & Troll, 2001). The development of the fault system can be controlled by the regional tectonics or linked to the reactivation of pre-exiting structures related to caldera collapse (Acocella & Funiciello, 1999; De Natale & Pingue, 1993; Folch & Gottsmann, 2006; Kennedy et al., 2004; Petrinovic et al., 2010; Roche et al., 2000; Saunders, 2004; Vilardo et al., 2010; Walter & Troll, 2001). In the last few decades, the structural elements of the NYT caldera collapse were investigated through a) field data (e.g. Di Vito et al., 1999; Orsi et al., 1996; Vitale & Isaia, 2014), b) high- and very-high reflection seismic data (Alfonsa Milia & Giordano, 2002; M Sacchi et al., 2014), c) tomography images (e.g. Dello Iacono et al., 2009; Judenherc & Zollo, 2004), d) analogue modelling experiments (V Acocella et al., 2004) and e) interferometric synthetic-aperture radar (InSAR) data (e.g. Iuliano et al., 2015; Lundgren et al., 2001; Trasatti et al., 2008; Vilardo et al., 2010). Despite numerous research works, the geometry of the onshore-offshore intra-caldera resurgent dome as well as the relationship between subsurface structures and ground deformations are still poorly understood. In this study, the integrated analysis of high-resolution swath bathymetry, single channel reflection seismics and interferometric synthetic-aperture radar (InSAR) data are used in order to reconstruct the architecture of the NYT intra-caldera resurgence as well as the geometry and kinematics of structures responsible for its development. The results of this research provide new insights into the structural style of restless resurgent calderas.

In order to analyse long term deformations (Myr timescale) occurring at tens of kilometers spatial scale, this research focuses on the Paola Basin, a forearc basin of the Tyrrhenian-Ionian subduction system. Forearc basins are included in the forearc region formed on the overriding plate

of a subduction system between the accretionary prism and volcanic island arc. Forearc basins develop structurally as a consequence of a permanent deformation of the overriding plate in response to subduction and accretion (Dickinson & Seely, 1979). Their evolution is recorded in the depositional sequences resulting by a combination of tectonic processes and sediment supply over millions of years (Laursen et al., 2002; Ryan et al., 2012). The fore-arc region of the Tyrrhenian - Ionian subduction system is located in the area extending from the Aeolian Arc, across the western Calabrian margin and the Calabrian Arc, to the Ionian accretionary wedge. Along the western Calabrian margin, Paola Basin develops as an asymmetric syncline filled by the largest accumulation of Pliocene to present sediments of the forearc region. The depositional sequence records various geological phenomena linked to dynamic interactions between the lower and upper plates of the Tyrrhenian-Ionian subduction system (e.g. subsidence and uplift events). Thus, the Paola Basin and the adjacent northern Calabrian Arc provide new insights into tectono-stratigraphic evolution of the fore-arc region, and its relation with slab roll-back and steepening in a regime of overall convergence. Despite several research works conducted in the upper plate of the Tyrrhenian - Ionian subduction zone (e.g. Argnani & Trincardi, 1988; Guarnieri, 2006; Milia et al., 2009; Pepe et al., 2010), the tectono-stratigraphic evolution of the Paola Basin, the source areas of sediments, and the process responsible for their transport are still poorly known. Furthermore, the mechanisms responsible for the long-term (10^6 years) subsidence in the Paola Basin and uplift in the adjacent Costal Chain are poorly understood and debated as well as the role of contractional, extensional and strike-slip tectonics inside and along the flanks of the basin. In this research, the integrated analysis of EMODnet bathymetry data and a grid of high-penetration, multi-channel seismic-reflection data allows to a) reconstruct the 3D stratigraphic architecture and the Pliocene to Quaternary evolution of the basin; b) constraint the geometry and kinematics of fault systems; c) quantify the vertical movements experienced by different sectors of the basin. Also, the results of this work are combined with the literature knowledge on the horizontal and vertical movements experienced by the northern Calabrian Arc in order to obtain new insights into the long-term deformations of the fore-arc region and the tectonic role of strike-slip fault system formed along the western Calabrian margin.

References

Acocella, V., & Funiciello, R. (1999). The interaction between regional and local tectonics during resurgent doming: the case of the island of Ischia, Italy. *Journal of Volcanology and Geothermal Research*, *88*(1–2), 109–123. https://doi.org/10.1016/S0377-0273(98)00109-7

Acocella, V., Funiciello, R., Marotta, E., Orsi, G., & De Vita, S. (2004). The role of extensional structures on experimental calderas and resurgence. *Journal of Volcanology and Geothermal Research*, *129*(1–3), 199–217.

Argnani, A., & Trincardi, F. (1988). Paola slope basin: evidence of regional contraction on the eastern Tyrrhenian margin. *Memorie Della Società Geologica Italiana*, *44*, 93–105.

Brothelande, E., Peltier, A., Got, J. L., Merle, O., Lardy, M., & Garaebiti, E. (2016). Constraints on the source of resurgent doming inferred from analogue and numerical modeling — Implications on the current feeding system of the Yenkahe dome–Yasur volcano complex (Vanuatu). *Journal of Volcanology and Geothermal Research*, *322*(December 2015), 225–240. https://doi.org/10.1016/j.jvolgeores.2015.11.023

De Natale, G., & Pingue, F. (1993). Ground deformations in collapsed caldera structures. *Journal of Volcanology and Geothermal Research*, *57*(1–2), 19–38.

Dello Iacono, D., Zollo, A., Vassallo, M., Vanorio, T., & Judenherc, S. (2009). Seismic images and rock properties of the very shallow structure of Campi Flegrei caldera (southern Italy). *Bulletin of Volcanology*, *71*(3), 275–284. https://doi.org/10.1007/s00445-008-0222-1

Di Vito, M. A., Isaia, R., Orsi, G., Southon, J. d, De Vita, S., d'Antonio, M., … Piochi, M. (1999). Volcanism and deformation since 12,000 years at the Campi Flegrei caldera (Italy). *Journal of Volcanology and Geothermal Research*, *91*(2–4), 221–246.

Dickinson, W. R., & Seely, D. R. (1979). Structure and stratigraphy of forearc regions. *AAPG Bulletin*, *63*(1), 2–31.

Folch, A., & Gottsmann, J. (2006). Faults and ground uplift at active calderas. *Geological Society, London, Special Publications*, *269*(1), 109–120. https://doi.org/10.1144/GSL.SP.2006.269.01.07

Guarnieri, P. (2006). Plio-Quaternary segmentation of the south Tyrrhenian forearc basin. *International Journal of Earth Sciences*, *95*(1), 107–118. https://doi.org/10.1007/s00531-005-0005-2

Iuliano, S., Matano, F., Caccavale, M., & Sacchi, M. (2015). Annual rates of ground deformation (1993–2010) at Campi Flegrei, Italy, revealed by Persistent Scatterer Pair (PSP) – SAR interferometry. *International Journal of Remote Sensing*, *36*(24), 6160–6191. https://doi.org/10.1080/01431161.2015.1111541

Judenherc, S., & Zollo, A. (2004). The Bay of Naples (southern Italy): Constraints on the volcanic structures inferred from a dense seismic survey. *Journal of Geophysical Research: Solid Earth*, *109*(B10).

Kennedy, B., Stix, J., Vallance, J. W., Lavallée, Y., & Longpré, M. A. (2004). Controls on caldera structure: Results from analogue sandbox modeling. *Bulletin of the Geological Society of America*, *116*(5–6), 515–524. https://doi.org/10.1130/B25228.1

Laursen, J., Scholl, D. W., & von Huene, R. (2002). Neotectonic deformation of the central Chile margin: Deepwater forearc basin formation in response to hot spot ridge and seamount subduction. *Tectonics*, *21*(5), 2-1-2–27. https://doi.org/10.1029/2001TC901023

Lipman, P. W. (2000). Central San Juan caldera cluster: Regional volcanic framework. *SPECIAL PAPERS-GEOLOGICAL SOCIETY OF AMERICA*, 9–70.

Lundgren, P., Usai, S., Sansosti, E., Lanari, R., Tesauro, M., Fornaro, G., & Berardino, P. (2001). Modeling surface deformation observed with synthetic aperture radar interferometry at Campi Flegrei caldera. *Journal of Geophysical Research: Solid Earth*, *106*(B9), 19355–19366.

Mandl, G. (1988). *Mechanics of tectonic faulting*. Elsevier Amsterdam.

Milia, A., & Giordano, F. (2002). Holocene stratigraphy and depositional architecture of eastern Pozzuoli Bay (eastern Tyrrhenian sea margin, Italy): the influence of tectonics and wave-induced currents. *Geo-Marine Letters*, *22*(1), 42–50.

Milia, A., Turco, E., Pierantoni, P. P., & Schettino, A. (2009). Four-dimensional tectono-stratigraphic evolution of the Southeastern peri-Tyrrhenian basins (Margin of Calabria, Italy). *Tectonophysics*, *476*(1–2), 41–56. https://doi.org/10.1016/j.tecto.2009.02.030

Orsi, G., De Vita, S., & Di Vito, M. (1996). The restless, resurgent Campi Flegrei nested caldera (Italy): Constraints on its evolution and configuration. *Journal of Volcanology and Geothermal Research*, *74*(3–4), 179–214. https://doi.org/10.1016/S0377-0273(96)00063-7

Orsi, G., Gallo, G., & Zanchi, A. (1991). Simple-shearing block resurgence in caldera depressions. A model from Pantelleria and Ischia. *Journal of Volcanology and Geothermal Research*, *47*(1–2), 1–11. https://doi.org/10.1016/0377-0273(91)90097-J

Pepe, F., Sulli, A., Bertotti, G., & Cella, F. (2010). Architecture and Neogene to Recent evolution of the western Calabrian continental margin: An upper plate perspective to the Ionian subduction system, central Mediterranean. *Tectonics*, *29*(3), 1–24. https://doi.org/10.1029/2009TC002599

Petrinovic, I. A., Martí, J., Aguirre-Díaz, G. J., Guzmán, S., Geyer, A., & Paz, N. S. (2010). The Cerro Aguas Calientes caldera, NW Argentina: An example of a tectonically controlled, polygenetic collapse caldera, and its regional significance. *Journal of Volcanology and Geothermal Research*, *194*(1–3), 15–26. https://doi.org/10.1016/j.jvolgeores.2010.04.012

Phillips, W. J. (1974). The dynamic emplacement of cone sheets. *Tectonophysics*, *24*(1–2), 69–84.

Roche, O., Druitt, T. H., & Merle, O. (2000). Experimental study of caldera formation. *Journal of Geophysical Research: Solid Earth*, *105*(B1), 395–416. https://doi.org/10.1029/1999JB900298

Ryan, H. F., Draut, A. E., Keranen, K., & Scholl, D. W. (2012). Influence of the Amlia fracture zone on the evolution of the Aleutian Terrace forearc basin, central Aleutian subduction zone. *Geosphere*, *8*(6), 1254–1273. https://doi.org/10.1130/GES00815.1

Sacchi, M., Pepe, F., Corradino, M., Insinga, D. D., Molisso, F., & Lubritto, C. (2014). The Neapolitan Yellow Tuff caldera offshore the Campi Flegrei: Stratal architecture and kinematic reconstruction during the last 15 ky. *Marine Geology*, *354*, 15–33.

Saunders, S. J. (2004). The possible contribution of circumferential fault intrusion to caldera resurgence. *Bulletin of Volcanology*, *67*(1), 57–71. https://doi.org/10.1007/s00445-004-0360-z

Smith, R. L., & Bailey, R. A. (1968). Stratigraphy, structure, and volcanic evolution of the Jemez Mountains, New Mexico. *Special Paper—Geological Society of America*, 447–448.

Trasatti, E., Casu, F., Giunchi, C., Pepe, S., Solaro, G., Tagliaventi, S., … Ricciardi, G. P. (2008).

The 2004–2006 uplift episode at Campi Flegrei caldera (Italy): Constraints from SBAS-DInSAR ENVISAT data and Bayesian source inference. *Geophysical Research Letters*, *35*(7).

Vilardo, G., Isaia, R., Ventura, G., De Martino, P., & Terranova, C. (2010). InSAR Permanent Scatterer analysis reveals fault re-activation during inflation and deflation episodes at Campi Flegrei caldera. *Remote Sensing of Environment*, *114*(10), 2373–2383. https://doi.org/10.1016/j.rse.2010.05.014

Vitale, S., & Isaia, R. (2014). Fractures and faults in volcanic rocks (Campi Flegrei, southern Italy): insight into volcano-tectonic processes. *International Journal of Earth Sciences*, *103*(3), 801–819.

Walter, T. R., & Troll, V. R. (2001). Formation of caldera periphery faults: An experimental study. *Bulletin of Volcanology*, *63*(2–3), 191–203. https://doi.org/10.1007/s004450100135

CHAPTER 1

Architecture and kinematics of the Neapolitan Yellow Tuff intra-caldera resurgence (Pozzuoli Bay, Campi Flegrei): new insights from high-resolution reflection seismics and DInSAR data

NOTE This chapter is a "working in progress" scientific paper in collaboration with F. Pepe, M. Sacchi, L. Ferranti & G. Solaro.

Abstract

Resurgence is the late stage, long-term uplift of a collapse caldera floor to form a dome-like structure. The comprehension of its development and structural pattern is crucial for predicting the caldera behaviour during periods of unrest. This work investigates the resurgent activity of the Neapolitan Yellow Tuff (NYT) caldera (Campi Flegrei - Pozzuoli Bay), using an integrated analysis of high-resolution swath bathymetry, reflection seismic profiles and interferometric synthetic-aperture radar (InSAR) data. The interpretation of the data shows that resurgence affects a ~ 50 km^2 wide almost circular area centred in the Pozzuoli harbor. The resurgent area is surrounded by a ~ 3-4 km wide structural discontinuity corresponding to the Ring Fault Zone (RFZ) that formed during the NYT caldera collapse (~15 ka BP). The uplift of the caldera resurgence occurs along a series of inward-dipping reverse faults of the RFZ characterized by a decreasing-upward inclination of fault planes from ~70° to ~15°. The development of these structures is controlled by the reactivation and deformation of pre-exiting normal faults associated with the NYT caldera collapse. Deformation of reactivated faults often results in folding of overlying and/or juxtaposed strata, in the style of ~ 500 m wide antiformal folds, mostly located along the periphery of the resurgent area. The structural pattern of the resurgence consists of disjoint uplifted blocks of the caldera floor. Two main structural elements are detected inside the resurgent area both off- and onshore, separated by a NNE-SSW trending high-angle normal fault. The most uplifted block comprises the area from Mt Nuovo to La Pietra, whereas the adjacent uplifted sector extends eastwards to include Mt Spina. The morpho-bathymetric expression of the two uplifted blocks is represented by a ~5 km wide antiformal structure, encircled by Bagnoli and Epitaffio valleys. In the hinge zone of the resurgent dome a series of high-angle normal faults form a small apical graben.

Keywords: Caldera, Resurgence, Reverse faults, Campi Flegrei, Pozzuoli Bay.

1.0 Introduction

Collapse calderas represent the surface expression of explosive eruptions in the order of tens to hundreds of km^3 of magma. Following the eruption, a depression forms as a consequence of gravitational collapse of overlying rocks into an emptying reservoir (Lipman, 2000). Generally, calderas subside up to 3 km along boundary faults, and extend from a few of kilometres to tens of kilometres. The caldera shape can be circular or elliptical in plan view, reflecting the influence of the regional tectonics (Holohan et al., 2005). Five end-members of calderas types are defined on the basis of the geometry of their collapse (Cole et al., 2005). In particular, piecemeal collapse calderas consist of several floor blocks and/or multiple collapse centres (Branney & Kokelaar, 1994; Moore & Kokelaar, 1998).

Post-collapse activity frequently involves post-caldera volcanism, resurgence, sedimentation within the caldera depression and hydrothermal processes. Among these activities, the resurgence is

one of the most documented (e.g. Valles, Bonanza caldera, Timber Mountain, Yellowstone, Long valley, La Pacana, Turkey Creek, Cerro Galan, Bennett Lake, Grizzly Peak caldera, Campi Flegrei, Toba). Resurgence is defined as the long-term uplift of a caldera floor portion to form a dome-like structure, up to thousands of meters high. Several authors agree that resurgence results from a magmatic overpressure associated with a renewed upward migration of magma (du Bray & Pallister, 1999; Gazis et al., 1995; Kennedy et al., 2012; Lipman, 2000; Marsh, 1984; Smith & Bailey, 1968). The uplift dynamics varies from doming (R. L. Smith & Bailey, 1968) to disjointing in differentially uplifted blocks of the caldera floor rocks (Acocella et al., 2004; Orsi et al., 1991).

Current models on the deformation pattern related to the resurgence are proposed based on field studies, geophysical data, remote sensing, numerical and analogue experiments. As the caldera floor is pushed upward, the intra-caldera deposits fold, fracture, and fault, forming on the whole a dome-like structure. Frequently, a depression bounded by normal faults forms on top of the dome structure (Brothelande et al., 2016; Lipman, 1984; Self, Goff, Gardner, Wright, & Kite, 1986). The uplifted area is confined within pre-existing collapse calderas (Acocella & Funiciello, 1999; De Natale & Petrazzuoli, 1997; Giuseppe De Natale & Pingue, 1993; Orsi et al., 1991). According to many authors, resurgent domes are bordered by inward dipping reverse faults (Brothelande et al., 2016; Kennedy et al., 2004; Mandl, 1988; Morán-Zenteno et al., 2004; Orsi et al., 1991; Phillips, 1974; Roche et al., 2000; Walter & Troll, 2001), but its formation throughout outward dipping systems is also proposed (Tibaldi & Vezzoli, 1998). The development of the fault system can be controlled by the regional tectonics or linked to the reactivation of pre-exiting structures related to caldera collapse (Acocella & Funiciello, 1999; Folch & Gottsmann, 2006; Hon, 1987; Kennedy et al., 2004; Morán-Zenteno et al., 2004; De Natale & Pingue, 1993; Petrinovic et al., 2010; Roche et al., 2000; Saunders, 2004; Vilardo et al., 2010; Walter & Troll, 2001). The reactivation of moderately to steeply (typically 50–60°) dipping normal faults as reverse faults occurs preferentially in the area of most intense fluid overpressures (Sibson, 1995).

This work focuses on the Campi Flegrei volcanic area and its offshore sector, the Pozzuoli bay, characterized by ground deformations associated with the dynamics of the NYT caldera collapse-resurgence system. In the last few decades, the structural elements of the NYT caldera collapse were inferred on the basis of a) field data (e.g. Orsi et al., 1996; Vitale & Isaia, 2014; Di Vito et al., 1999), b) high- and very-high reflection seismic data (Milia & Giordano, 2002; Sacchi et al., 2014), c) tomography images (Dello Iacono et al., 2009; Judenherc & Zollo, 2004), d) analogue modelling experiments (Acocella et al., 2000; 2004). Also, recent ground deformations at Campi Flegrei were documented using interferometric synthetic-aperture radar (InSAR) technique (e.g. Lundgren et al., 2001; Iuliano et al., 2015; Trasatti et al., 2015; Vilardo et al., 2010). InSAR data highlight that the recent subsidence (1992–1999) and uplift (since 2005) phases are associated with the development of the resurgent dome in the NYT intra-caldera region. Despite numerous research works, the geometry of the onshore-offshore intra-caldera resurgence as well as the relationship

between subsurface structures and ground deformation are still poorly understood. In this study, the integrated analysis of bathymetric, seismic reflection and satellite data allowed to reconstruct the architecture of the NYT intra-caldera resurgence as well as the geometry and kinematics of structures responsible for its development. The results of this research provide new insights into the structural style of restless resurgent calderas.

2.0 Geological framework

2.1 The Campi Flegrei-Pozzuoli bay volcanic district

The Campi Flegrei represent an active volcanic district placed along the Tyrrhenian margin of the Campania region (southern Italy) (Fig. 1). The volcanic area is structurally dominated by a caldera collapse and a resurgent dome uplifted in the inner caldera region (Florio et al., 1999; Giudicepietro, 1993; Dello Iacono et al., 2009; Judenherc & Zollo, 2004; De Natale et al., 2006; Orsi et al., 1996; Rosi & Sbrana, 1987; Sacchi et al., 2014; 2009; Scarpati et al., 1993; Wohletz et al., 1995). The caldera structure consists of a ~16 km wide sub-circular depression formed in the central sector of the Campi Flegrei and its offshore prolongation, the Pozzuoli bay, during the eruption of the Neapolitan Yellow Tuff (NYT), a 30–50 km3 Dense Rock Equivalent (DRE) ignimbrite dated at ~15 ka BP (Deino et al., 2004). Following the NYT eruption, about 70 monogenic phreato-magmatic vents developed inside the NYT caldera collapse (Di Renzo et al., 2011; Di Vito et al., 1999; Fedele et al., 2011; Isaia et al., 2009). The most recent eruption occurred at Monte Nuovo in 1538 A.D. (De Natale et al., 2006; Rosi & Sbrana, 1987).

According to several authors, NW–SE, NE–SW, and N–S striking faults occurred along the Campi Flegrei area during and after the development of the NYT caldera (Acocella, 2008; Bruno, 2004; Milia et al., 2003; Orsi et al., 1999; Rosi & Sbrana, 1987). The NE-SW and subordinate NW-SE extensional faults are the main structures controlling volcanic activity (Fig. 1). In particular, the NW-SE trending fracture system is the most widespread during the resurgence development (Acocella, 2010; Orsi et al., 1996).

The NYT inner caldera deformation was explained through a simple-shearing block resurgence mechanism by Orsi et al., 1991b; 1996. This model consists in the formation of several blocks bounded by sub-vertical fault planes and characterized by differential vertical displacement. According to Orsi et al., 1996, the most uplifted area is located between the Pozzuoli harbour and La Solfatara and bounded by inferred high-angle reverse faults. Some authors found that inner caldera ground deformation predominantly occurs along re-activated caldera ring-faults, intra-caldera faults, and eruptive fissures (De Natale & Petrazzuoli, 1997; De Natale & Pingue, 1993; Vilardo et al., 2010).

Offshore, the caldera collapse led to the formation of concentric normal faults along the Ring Fault Zone (RFZ) defined by Sacchi et al., 2014 (Fig.1). Diffused occurrence of pore fluids was recognized within the stratigraphic succession cut by the RFZ, especially in the western sector of the

bay, culminating in the formation of fluids vents (Carmisciano et al., 2013). The RFZ encircles the NYT resurgent dome, that displays a diameter of ~ 5 km and is located in the northern sector of the Pozzuoli bay (Sacchi et al., 2014).

2.2 Ground deformation at Campi Flegrei

Over the last 15 kyrs, ground deformation on long- (resurgence) and short- (bradyseisms) time scales affected the inner caldera region (Cinque et al., 1985; Isaia et al., 2009; G. Orsi et al., 1996; Di Vito et al., 1999). The most uplifted part of the caldera floor includes La Starza marine terrace, presently at 30 to 55 m above sea level (a.s.l). This sector uplifted up to about 90 m with an average rate in the order of 9–12 mm/year between 10.5 ka PB and 4.0 ka PB (Sacchi et al., 2014). During the same time, subsidence occurred in the southern part of the Pozzuoli bay (Scandone et al., 2006).

Historical ground deformation was well documented by marine incrustations on Roman and Middle Ages edifices as well as submerged archaeological remains. Particularly, the ruins of an ancient Roman market, the "Serapeum", recorded a post-Roman subsidence phase in the area of Pozzuoli harbor (Dvorak & Mastrolorenzo, 1991; Parascandola, 1947) with an average rate of ~1.5–2.0 cm/year (Troiano et al., 2011). Also, the discovery of Roman archaeological remains at water depth of ~10 m suggests a post-Roman subsidence along the western coast of the Pozzuoli Bay (Orsi et al., 1996; Passaro et al., 2013). Several, rapid and intense uplift episodes interrupted the trend of subsidence, in association with eruptive activity such as the 1538 AD Monte Nuovo eruption (Bellucci et al., 2006; Dvorak & Mastrolorenzo, 1991; Troiano et al., 2011).

Since 1905, ground-based topographic levelling networks, integrated with a global positioning system (GPS) monitoring network and interferometric data, record the unrest episodes of the NYT caldera. The major uplifts of 170 and 180 cm were estimated at Pozzuoli harbor in 1970–71 and 1982–84, respectively (Battaglia et al., 2006; Dvorak & Berrino, 1991; Del Gaudio et al., 2010; De Natale et al., 2006). After two decades of prevailing subsidence, the Campi Flegrei area experienced uplift periods (e.g. 2005-2006; 2012-2013), alternating with subsidence phases or stationary deformation trends (Bottiglieri et al., 2010; D'Auria et al., 2015; De Martino et al., 2014; Del Gaudio et al., 2010). The pattern of recent uplifts was radially symmetric with decreasing deformation velocity values moving from the Pozzuoli harbor towards the borders of the NYT caldera (Iuliano et al., 2015; Samsonov et al., 2014; Trasatti et al., 2015; Vilardo et al., 2010). The last phase of ground uplift occurred between April 2012 and January 2013, reaching ~11 cm with a maximum rate of 3 cm/month (Elisa Trasatti et al., 2015). Ground deformation was interpreted as the effect of magmatic intrusions at shallow depth (D'Auria et al., 2015).

3.0 Materials and methods

This study is based on the integrated analysis of a) multibeam bathymetry, b) a grid of high and very high-resolution seismic reflection data, and c) differential synthetic aperture radar interferometric (DinSAR) data.

3.1 Multibeam bathymetry

The high-resolution grid Digital Terrain Model (DTM) with cell size of ~10 m is a part of the swath bathymetry data acquired by the IAMC-CNR in the Pozzuoli Bay (see Sacchi et al., 2014 for details of acquisition and processing). The hill-shaded GeoTIFF images of the bathymetry dataset was created within GeoSuite AllWorks and Global Mapper software. The color ramp for the GeoTIFF images was scaled between the sea level and the maximum measured water depth. Ambient lighting is from NNE (30°) at 50° above the horizon, and vertical exaggeration is 4.8×.

3.2 Seismic reflection data acquisition and processing

Seismic data consist of over 600 km of single channel (Geo-Source Sparker, Sub-bottom Chirp) reflection seismic profiles recorded in the Pozzuoli Bay between 2007 and 2013. Seismic profiles are primarily acquired along NNW–SSE to NNE–SSW directions and subordinately along WNW–ESE direction (Fig. 1b). The software used for the acquisition of navigation data is the PDS-2000 RESON which provides the DGPS positioning data to all the instrumentation operating on board. High- and very high-resolution data were recorded using a single channel streamer with an active section of 2.8 m, containing seven high resolution hydrophones, for 1.3 s two-way time (t.w.t.) at a 10 kHz (0.1 ms) sampling rate. The Sub-Bottom Chirp profiler operated with a 16 transducer Benthos Chirp II system in a wide frequency band (2–7 kHz), with a long pulse (20–30 ms). Sparker data were acquired using a 1 kJ power supply with a multi-tip sparker array, a ringing-free system operating with a shot rate of 1.5 s, and a base frequency of ~800 Hz.

Processing of seismic data was performed using the Geo-Suite AllWorks software. The processing sequence applied to the dataset included the following operators: a) spherical divergence correction, b) bandpass (300–2000 Hz) filter, c) swell filter, d) traces mixing, e) predictive deconvolution, f) time varying gain and g) muting of water column. Signal penetration was found to exceed 500 ms (twt). Vertical resolution reached up to 0.5 m near the seafloor.

Seismic interpretation allowed to reconstruct the stratigraphic architecture of depositional systems and elements. Following the analysis of acoustic facies, the thickness of sediment and volcanic features were derived from time to depth conversion using velocities of 2000 m/s for the pre NYT deposits, 1600-1800 m/s for the post-NYT deposits and 1500 m/s for the water column. Seismic velocity values were derived from the correlation between seismic units and lithostratigraphic data available in literature (Di Vito et al., 1999; Rosi & Sbrana, 1987). In order to

better display the internal and external geometry stratigraphic units, the depth-converted sections are illustrated with vertical exaggeration up to 6×.

3.3 The Campi Flegrei DInSAR data

DInSAR data were exploited in order to characterize the geometry of the active structures associated with the intra-caldera resurgence. To do this, the study time intervals were chosen on the basis of the recent positive bradiseismic crisis documented in the literature (Iuliano et al., 2015 and references therein). In particular, we collected a series of ENVISAT and COSMO-SkyMed satellite SAR images to generate hundreds of interferograms by exploiting the well-developed Small BAseline Subsets (SBAS) method (Berardino et al, 2002; Trasatti et al., 2008). This method allowed us to retrieve mean displacement velocity maps and corresponding time series with a standard deviation of approximately 1 mm/y for each investigated coherent pixel, in agreement with previous studies (Casu et al.,2006). Interferograms were computed using SAR images acquired by a) the ENVISAT satellites on ascending and descending orbits in the period July 2005-November 2006; b) the COSMO-SkyMed satellite on ascending orbit in the period January 2009-November 2016. Finally, deformation velocity maps were imported into Surfer software to improve data visualization and interpretation.

4.0 Data and results

4.1. Seafloor morphology of the Pozzuoli Bay

The Pozzuoli bay covers a ~ 30 km^2 wide area and reaches a maximum depth of ~115 m below sea level (b.s.l.) close to Nisida Island (Fig. 2). Morpho-bathymetric analysis reveals that the inner continental shelf varies in width from 1.8 km western offshore of Pozzuoli harbor and 1.6 km between the Bagnoli district and Nisida Island to less than a few hundred metres offshore Baia. Along the western sector of the bay, a pronounced break in the continental shelf profile is detected at water depths varying from~ 30 m b.s.l. to the NW to ~ 40 m b.s.l. to the SE.

A series of stepped terraced surfaces cut the north-eastern sector of the inner continental shelf over a distance of ~500 m. In particular, three terraced surfaces at depth of 10 m, 17 m and 27 m b.s.l., extending for ~100 m, are identified between offshore of Pozzuoli harbour and La Pietra (profile 1 in Fig. 2), whereas, only two terraced surfaces are detected in the inner continental shelf to the East of La Pietra (profile 2 in Fig. 2). These surfaces lie at depth of 15 and 27 m b.s.l. and extend for ~180 m.

A convex-upward area was recognized in the northern sector of the bay (Fig. 2). It is characterized by an elliptical shape, elongated in WNW-ESE direction. The morphological structure is ~ 50 m high and its flanks have an inclination of less than 3°. Two depressed zones extending in NNW–SSE (Epitaffio valley) and NE–SW (Bagnoli valley) directions bound the convex-upward area. At the top, a WNW-ESE ~ 1 km wide depressed zone was detected (profile 3 in Fig. 2).

4.2. Definition of seismic units

Seven seismic stratigraphic units were defined on the basis of their stratal architecture as well as seismic characters such as amplitude, lateral continuity and frequency of internal reflectors. From bottom to top they are named NYT, CF, SRD, GF1, HD1, GF2 and HD2 (Fig. 3). Unit NYT shows discontinuous, medium frequency and high to moderate-amplitude reflections (Fig. 3a and b, CDPs 1800-2500). It is bounded at the top by a major unconformity and represents the acoustic basement for the sparker source in the study area. Unit CF is characterized by layered, continuous, medium frequency and moderate to low-amplitude reflectors (Fig. 3c). Locally, the occurrence of fluids reduces reflection amplitudes, fading the base of unit CF as well as its internal pattern (Fig. 3b). Unit SRD displays parallel, continuous, medium to high frequency and low to moderate amplitude reflectors. Locally, reflections are characterized by a convergent pattern towards the northern sector of the Pozzuoli bay (Fig. 3c). The top of unit SRD is represented by a well-defined, high-amplitude reflector. The upper part of the seismic stratigraphic succession (UD in Fig. 3b and c) includes units GF1, HD1, GF2 and HD2. Units GF1 and GF2 have medium frequency, moderate to high-amplitude, and may locally appear transparent due to chaotic reflections (Fig. 3d). In the eastern sector of the bay, unit GF2 can be divided into two subunits, namely GF2.a and GF2.b (Fig. 4a and b). Subunit GF2.a has a chaotic internal geometry and it is bounded at the top by a high-amplitude, hummocky reflector. Whereas, subunit GF2.b displays parallel and continuous reflectors. Units HD1 and HD2 are defined by continuous, parallel and medium to low-amplitude reflections (Fig. 3d). Unit HD2 is bounded at top by the seafloor, and at bottom by a high-amplitude reflector. A well-defined, high-amplitude and continuous reflector, labelled VT, is detected from the southern to the northern sector of the bay. Along the inner continental shelf break, unit HD2 is characterized by a series of prograding reflectors and exhibits a wedge shape (Fig. 3e).

4.3. Seismic stratigraphic interpretation

The stratigraphic architecture and structures of the NYT caldera-resurgent system were interpreted along depth-converted seismic sections crossing the Pozzuoli Bay in WNW–ESE and N–S directions. In all seismic profiles the acoustic basement is represented by unit NYT. This unit can be correlated with the Neapolitan Yellow Tuff deposits widespread around the whole of Campi Flegrei and outcropping along the Posillipo hill (Scarpati et al., 1993b). The NYT deposits deepen from ~ 140 m b.s.l to ~ 230 m b.s.l moving from the southern sector of Pozzuoli offshore to the central part of the bay (Fig. 3b and 5) and rise up to ~ 70 m b.s.l in correspondence of the antiformal structure located in the northern part of the Pozzuoli offshore (Fig. 7). The deepening of the NYT deposits occurs across a series of high-angle normal faults, dipping ~60°–70° towards the inner part of the caldera (Figs. 3b and 5). The normal fault system defines a curvilinear trend in plan view and it was recognized in all seismic profiles throughout the bay. The outermost normal fault was inferred

on the basis of the tilted reflections towards the inner side of the caldera, and it was interpreted as the structural limit of the NYT caldera. On the whole, the set of normal faults define the Ring Fault Zone (RFZ) formed as a consequence of the NYT caldera collapse (Lipman, 2000 and references therein).

Several inner-dipping reverse faults were identified inside the RFZ, close to its inner boundary. These structures are characterized by fault planes with an upward decreasing inclination and often associated with synthetic faults that accommodate volcano tectonic deformation. On profile Msk_112 the reverse fault dips westwards with a decreasing inclination from 65° to 20° upward (Fig. 7b around CDP 500, and c). Whereas, the fault plain changes its inclination from ~50° to 15° upward in the west-central sector of the bay (Fig. 5b around CDP 56500). Moving to the East, the occurrence of fluids partially obscure the seismic signal, but the geometry of reflections allows to infer the presence of the reverse fault (Fig. 5d around CDP 600). Anticline structures form in correspondence of the reverse faults.

Most of the caldera collapse depression is filled by unit CF. Its maximum thickness is ~ 100 m in the central sector of the caldera and decreases towards the outer boundary of the RFZ, down to a few tens of meters (Figs. 3b, 5b and d). On the basis of its stratigraphic position, unit CF can be interpreted as the first volcaniclastic deposits overlying the NYT. Strata of unit CF are cut by the normal faults forming the RFZ. The seismic signal of unit CF is locally obliterated due to the diffused occurrence of fluids ascending to the upper layers through the fault system.

Deposits of Unit SRD overlay unit CF with a thickness decreasing from ~ 30 m, measured in the southern sector of the Pozzuoli Bay, to less than 10 m ten of meters close to the antiformal structure in the central-northern part of the bay (Figs. 3b, 5 and 7b). Unit SRD displays a convergent pattern of internal reflections from the anticlines associated to the reverse faults towards the north. Unit GF1 and GF2 exhibit a lens-shaped geometry and pinch out along the flank of the antiformal structure located in the northern sector of the bay (Fig. 3b and d). Both units were interpreted as the seismic expression of gravity flow deposits, on the basis of their external and internal geometries. The lower gravity flow GF1 is ~ 5 m thick in the western sector of the bay and reaches its maximum thickness of ~10 m in the central part, while it is absent to the east. The upper gravity flow GF2 displays a minimum thickness of ~10 m in the central sector of the bay and increases up to ~ 16m and 12m in the western and eastern sector, respectively. GF2 deposits are divided into two distinct subunits, GF2.a and GF2.b (Fig. 4b). The chaotic internal geometry of GF2.a suggests high energy and/or turbulence during the sediment transport. Because of the turbulence, the finer sediment fraction is raised and suspended in the water column. Successively, the well-stratified deposits of GF2.b form for slow deposition of finer sediments (Fig. 4c). Units GF2.a and GF2.b are interpreted as representing respectively the body and the tail of the GF2 gravity flow deposits.

The layered units HD1 and HD2 are interpreted as epiclastic deposits widespread in the Pozzuoli Bay. Unit HD1 separates the gravity flows deposits of unit GF1 from those of unit GF2,

whereas unit HD2 overlays unit GF2 (Figs. 3b and d; 4d). Unit HD1 is characterized by a thickness less than ~ 8m, whereas the maximum thickness of HD2 is of ~ 10m reached in the central sector of the bay. A well-defined, high-amplitude and continuous reflector, named VT, is detected inside the deposits of unit HD2 from the southern to the northern sectors of the bay (Fig. 3d and e). Along the shelf break, deposits of unit HD2 form a ~270 m long prograding wedge. It is limited by toplap/offlap and downlap surfaces at top and bottom, respectively (Fig. 3e). The water depth of the prograding wedge decreases from 43 m b.s.l. in the eastern sector of the bay to 28 m b.s.l. in the westernmost side. Landwards, an erosional surface truncates the oblique reflectors of unit HD2 as well as the underlying units.

The northern area of the Pozzuoli bay is characterized by the occurrence of a broad ~5 km wide antiformal structure (Fig. 7b). In the hinge zone of the antiformal structure, a series of high-angle normal faults cut the stratigraphic sequence, reaching the seafloor (Fig. 7d). The average dip of the faults is ~60°–70° whereas vertical displacement of individual faults is up to ~10 m. Overall, they form a ~2 km wide "graben-like" structure.

4.4. Deformation velocity patterns at Campi Flegrei

The deformation velocity field of the Campi Flegrei displays positive values for both ERS orbits from July 2005 to November 2006 (Fig. 6 a and b). An exception is represented by the Vomero area, where negative values were recorded by the ERS ascending orbit. An elliptical area extending from the Mt Nuovo to Mt Spina shows higher deformation velocities respect to the surroundings. Velocity values are in the range from 1 cm/year up to 3.2 cm/year, recorded by both orbits at the Pozzuoli harbor. The velocity field of the elliptical area can be divided in two adjacent sectors, labelled S1 and S2, based on the deformation velocity pattern related to both orbits (Fig. 6a). Particularly, the sector S1 is characterized by a gradual change in velocity from 1 cm/y to 2.5 cm/year, moving from Monte Nuovo to La Pietra zone for a distance of ~ 5 km. Whereas, the sector S2 displays an abrupt decreasing in velocity from 2.5 cm/year to 1 cm/year from La Pietra zona to Mt Spina, over a distance of ~2 km.

During the four analyzed periods between 2009 and 2016, the western and central sectors of the Campi Flegrei display positive values of deformation velocity for the COSMO SkyMed ascending orbit (Fig. 6c, d, e and f). The highest values of deformation velocity reach 2.5 cm/year, 9 cm/year and 6 cm/year at the Pozzuoli harbor, respectively, in the periods January 2009 – December 2011, January 2012 – December 2012, and June 2014 – November 2016. Conversely, negative velocities are observed in the eastern sector of the Campi Flegrei, including Baia, Fuorigrotta, Soccavo and Vomero zones. The deformation velocity pattern of the sectors S1 and S2 is recognized in the maps related to the periods 2009 –2011, 2012, 2014 –2016 (Fig. 6c, d and f). Velocity values of sector S1 decrease north-westwards from 2 cm/year to 0.5 cm/year in the period 2009 – 2011, from 4 cm/year to 2 cm/year during the year 2012, and from 3 cm/year to 1 cm/year in the period

2014 – 2016. In the sector S2, deformation velocity values decrease abruptly from 1.5 cm/year to 0.5 cm/year in the period 2009 – 2011, from 4 cm/year to 0.5 cm/year during the year 2012, and from 3 cm/year to 0.5 cm/year in the period 2014 – 2016.

A positive velocity field characterizes the Campi Flegrei between January 2013 and June 2014, with the exception of the Fuorigrotta and Soccavo areas (Fig. 6e). Velocity values are lower with respect to the other study periods, reaching a maximum value of just 1.5 cm/year at the Pozzuoli harbor. Sectors S1 and S2 do not display different behaviour during this time interval.

5.0 Discussion

5.1. Architecture of the NYT caldera-resurgent system

The NYT caldera is characterized by an almost circular shape in plan view with radius of ~8 km (Fig. 8). The caldera consists of a concentric structure including a ~4 km wide circular ring (RFZ) and an inner caldera resurgent dome. The RZF is defined by a series of inner-dipping normal faults that accommodates a generalized subsidence of the Pozzuoli bay. The outer boundary of the fault zone extends for about ~9 km from Capo Miseno offshore to Nisida Island. The inner boundary develops offshore, between Baia and Mt Spina. The normal fault system displays a remarkable pattern of migration from the inner boundary of the RFZ towards the outer area. This pattern is in accordance with analogue models that simulate the caldera collapse in which the development of normal faults formation proceeds from the interior towards the periphery of the caldera structure (Roche et al., 2000; Walter and Troll, 2001).

An inner-dipping reverse fault system is located in the western, central and northeastern sectors of the RZF, close to its inner boundary (Figs. 3b, 5, 7 and 8). These structures are characterized by fault planes with an upwards decreasing inclination from ~60°-70° to ~15°-20°. The lower part of fault planes show a geometry of normal fault as suggested by a major thickness of CF deposits in correspondence of the hanging wall (Figs. 3b CDPs 1600-1700; 5b around CDP 56500; 7c). Fault offsets involve strata from the lower part to unit CF in the western sector (Fig. 3b) and reaches unit HD1 in the northeastern sector (Fig. 7c). Deformation also include folding of the overlying units, to form~ 500 m wide antiformal structures (Figs. 3b, 5, 7c). The divergent pattern of reflectors within unit SRD was recognized from the anticline structures until the top of the antiformal structure located in northern sector of the Pozzuoli bay (Fig. 3b CDPs 1700-2500). This pattern suggests that the deposition of unit SRD occurred during the uplift of the antiformal structure. According to analogue models of resurgent doming superimposed on caldera collapses (Acocella et al., 2000; Kennedy et al., 2004; Roche et al., 2000; Walter & Troll, 2001) the high-angle inner-dipping reverse faults can be interpreted as the pre-existing fault system that formed during the caldera collapse and was inverted during the deformation of the resurgent dome. Most of the reactivated normal faults are located in the western and central part of RFZ, where pore fluids ascend through the faults reaching the seafloor. The preferential reactivation of moderately to steeply

(typically 50–60°) dipping normal faults in the area of intense fluid pressure is in agreement with the results of previous studies (e.g. Sibson, 1995).

The resurgent structure of the NYT caldera affects a ~ 50 km^2 wide almost circle area centred in the Pozzuoli harbor (Fig.8). It extends from the folded zone associated with the reverse faults until the antiformal structure detected in the northern sector of the Pozzuoli bay (Fig. 7b; 8). The antiformal structure also has a morpho-bathymetric expression in the most uplifted inner sector of the resurgent area. Epitaffio and Bagnoli valleys correspond to the depressed areas that form at the transition between the inner resurgent dome and the anticlines associated with the reverse faults, in agreement with the structures observed in the analogue models (Acocella et al., 2000 and refers therein). In the hinge zone of the antiformal structure, a series of normal faults delineate a small structural depression (i.e. apical graben) (Fig. 7d). Most individual faults of the apical graben deform the seafloor, suggesting they are active structures. The development of these faults can be explained as the consequence of the extension regime in the area of maximum convex curvature of the resurgent area.

An effect of the evolution of the resurgence is clearly expressed by the southward migration of the basin depocenter through time. The shift of depocenters is recorded by the distribution pattern of gravity flows deposits of units GF1 and GF2 (Fig. 4d and e) in the western and central sectors of the Pozzuoli bay. Based on lateral variation in thickness variation and the pattern of bedding dip within these units, it is possible to classify this area as a migrating growth syncline (*sensu* Salles et al., 2011). Conversely, no remarkable shift of basin depocenters is observed in the easternmost part of the Pozzuoli bay, outside the resurgent area (Fig. 4a).

5.2 The inner resurgent dome of the Campi Flegrei-Pozzuoli bay area

In the Pozzuoli bay the inner resurgent sector of the NYT cadera can be divided in two adjacent part, labeled A and B, on the basis of series of geo-morphological markers (mostly erosional and depositional terraces) located at different water depths. Three ~100 m long terraced surfaces were detected over a distance of ~ 500 m in the sector A, whereas sector B is characterized by two ~180 m long terraced surfaces over a distance of ~ 500 m. Along the inner shelf profile, infralittoral prograding wedges were identified and mapped (Fig. 8). The high-amplitude reflector VT, was recognized throughout all prograding wedges (Fig. 3e). This seismic horizon can be correlated with the tephra layer deposited during the eruption of Vesuvius of 79 AD (Sacchi et al., 2014). Water depths above the infralittoral prograding wedges decreases from East (~ 40 m b.s.l.) to West (~ 28 m b.s.l.) in sector A, whereas a water depth of ~ 42 m b.s.l. was recognized in sector B (Fig. 8). These sectors are divided by a NNE-SSW trending high-angle normal fault (Fig. 5d around CDP 70), located approximately off La Pietra (Fig. 8). By considering the occurrence of three less extended terraced surfaces of the sector A compared to two more extended terraced surfaces of sector B as

well as the westwards decreasing water depth of the prograding wedges of the sector A, the western and central sectors of the Pozzuoli bay uplift faster than the eastern one.

Onland, the interpretation of the deformation velocity maps of the Campi Flegrei showed that deformation pattern consists of two adjacent sectors, named S1 and S2, uplifting compared to the surrounding area. Sector S1 is characterized by higher values of deformation velocity respect to sector S2 during the period 2005-2016. Sector S1 is placed in the western and central part of the Campi Flegrei, from Mt Nuovo until the coastal cliff bordering La Pietra zone, whereas S2 extends eastwards until the slopes of Mt Spina. Sectors S1 and S2 correspond to the onshore extension of sectors A and B, as defined in the inner continental shelf. Accordingly, the slopes of Mt Spina and La Pietra are interpreted as the topographic expression of the two structures detected in the seismic profiles along the continental shelf. The boundaries of the two sectors correspond to areas of high and medium strain documented by Acocella, 2010 (Fig. 1). Also, the eastern limit of sector S2 lies along an alignment of recent eruptive vents that postdate the NYT eruption (D'Antonio et al., 1999; Smith et al., 2011).

The simple-shearing block resurgence model can explain the formation of the NYT intra-caldera resurgence. At the beginning of the deformation, pre-exiting high-angle faults define the edges of the resurgent blocks. Uplift occurs along reverse faults that reactivate normal faults formed during the NYT caldera collapse. These structures are located along the periphery of the resurgent area. The inner resurgent sector develops in the form of two major uplifted blocks, separated by a NNE-SSW trending high-angle normal fault in correspondence of La Pietra zone (Figs. 8 and 9). Such pattern is observed in ring-fault bounded resurgent structures such as the Ischia, Pantelleria islands (Orsi et al., 1991; Acocella and Funiciello, 1999) and Bodrum resurgent caldera system (Ulusoy et al., 2004).

6.0 Conclusions

The analysis of bathymetric and seismic reflection data acquired in the Pozzuoli Bay, coupled with the interpretation of ground deformation maps of the Campi Flegrei, provided new insights into the structural pattern of the NYT resurgent caldera. The main results can be summarized as follows:

1) The NYT collapse caldera has an almost circle shape with radius of ~8 km. The structural pattern consists of the ~3-4 km wide ring fault zone that surrounds an uplifted intra caldera region. The caldera depression hosts up to 100 m thick stratigraphic succession, including marine epiclastic sediments, volcaniclastic layers and gravity flow deposits.
2) In the Pozzuoli bay, the ring fault zone corresponds to a series of ~60° inward dipping normal faults that accommodate the collapse of the NYT caldera floor from ~140 m up to ~230 m moving from the southern sector of the bay towards its central part. The development of the normal faults proceeded from the inner region of the caldera outward, causing its enlargement

through time. In the southern sector of the bay, the ring fault zone is characterized by the occurrence of fluids that ascend through the faults reaching the seafloor.

3) The resurgence occurs over a ~ 50 km^2 wide almost circle area centred on the Pozzuoli harbour. A ~5 km wide antiformal structure, surrounded by Bagnoli and Epitaffio valleys, was detected inside the offshore resurgent area. A series of high-angle normal faults forms a graben-like structure at the crest of the resurgent dome as a consequence of the extension regime in the area of maximum curvature of the antiformal structure.
4) An inward-dipping reverse fault system is responsible for the uplift of the resurgence. The fault planes are characterized by upwards decreasing inclinations from ~70° to ~15°. Both the fault planes geometry and the thickness of the involved deposits suggest that the reverse faults reactivate pre-exiting normal faults developed during the NYT caldera collapse.
5) The resurgence consists of disjoint uplifted blocks of the caldera floor rocks. Two main blocks are detected inside the resurgent area, separated by a NNE-SSW trending high-angle normal fault. The most uplifted block includes the area from Mt Nuovo to La Pietra, and the adjacent uplifted sector extends eastwards until Mt Spina.

Captions

Figure 1. Morpho-structural map of the Neapolitan Yellow Tuff caldera (after Wohletz et al., 1995; Orsi et al. 1996; Di Vito et al., 1999; Milia and Torrente, 2003; Bruno, 2004; Sacchi et al., 2014). Location of eruptive vents younger than the NYT eruption are after D'Antonio et al. 1999. Strain distribution in the Campi Flegrei with high and medium wide range of spacing (S) is also shown (after Acocella, 2010). The direction of elongation of the rectangle indicates the orientation of the associated structures. a) Location of the investigated area. b) Location of the seismic profile dataset used in this study.

Figure 2. Morpho-bathymetric map of the Pozzuoli Bay. Abbreviations: EV, Epitaffio valley; BV, Bagnoli valley; T, thalweg of the EV–BV morpho-structural depression; V.E., vertical exaggeration.

Figure 3. a) Msk_113 Sparker profile. Inset shows its location. b) Depth-converted Msk_113 profile and its seismic facies interpretation. Boxes show seismo-stratigraphic units recognized on seismic Sparker (c) and Sub-Bottom Chirp profiles (d and e). Abbreviations: s.b.m., sea bottom multiple; V.E., vertical exaggeration; ICSB: inner continental shelf break.

Figure 4. a) Depth-converted CAFE_034 Sub-Bottom Chirp profile and its seismic facies interpretation. b) Particular of the gravity flow deposits (GF unit) showing the two subunits recognized on the CAFE_034 profile and c) its line drawing. Dark green shading indicates the body (subunit GF2.a) of the gravity flow. Light green shading indicates sediments deposited by settling of a suspended material (subunit GF2.b). d) Depth-converted CAFE_028 Sub-Bottom Chirp profile and its seismic facies interpretation. e) Line drawing of a part of the CAFE_028 profile showing the migration of the depocenter in the Epitaffio valley. Insets show the location of the Chirp profiles. Abbreviations: Di, vector velocity; D1 and D2, basin depocenters; V.E., vertical exaggeration.

Figure 5. a) Depth-converted Msk_114 Sparker profile and b) its seismic facies interpretation. c) Depth-converted Msk_115 Sparker profile and d) its seismic facies interpretation. Insets show the location of the profiles. V.E., vertical exaggeration.

Figure 6. Deformation velocity maps computed from the a) ascending and b) descending ENVISAT data acquired between July 2005 and November 2006, and ascending COSMO-SkyMed data (c, d, e and f) acquired between January 2009 and November 2016. The velocity maps are superimposed on the DTM of the Campi Flegrei. Abbreviations: B, Baia; N, Mt Nuovo; Ls, La Starza terrace; P, Pozzuoli harbor; Lp, La Pietra; M, Mt Spina; F, Fuorigrotta; S, Soccavo; V, Vomero.

Figure 7. a) Depth-converted Msk_112 Sparker profile and b) its interpretation. Inset shows the location of the profile. c) Detail of the reverse fault formed by the reactivation of the caldera collapse normal fault. d) Particular of the graben-like structure on the top of the antiformal structure,

recognized on Chirp seismic profile. Abbreviations: VD, vertical displacement; V.E., vertical exaggeration.

Figure 8. Morpho-structural map of the NYT caldera and intra-caldera resurgence. S1 and S2 are the two main uplifted sectors recognized on the deformation velocity maps of the Campi Flegrei. The location of the infralittoral prograding wedges derive from the interpretation of Sub-Bottom Chirp profiles. Abbreviations: EV, Epitaffio valley; BV, Bagnoli valley.

Figure 9. Schematic section across the NYT intra-caldera resurgence from the north-eastern area of the Campi Flegrei to Nisida Island, in the south-western sector of the Pozzuoli Bay. Inset shows the location of the section.

References

Acocella, V. (2008). Activating and reactivating pairs of nested collapses during calderaforming eruptions: Campi Flegrei (Italy). *Geophysical Research Letters*, *35*(17), 1–5. https://doi.org/10.1029/2008GL035078

Acocella, V. (2010). Evaluating fracture patterns within a resurgent caldera: Campi Flegrei, Italy. *Bulletin of Volcanology*, *72*(5), 623–638. https://doi.org/10.1007/s00445-010-0347-x

Acocella, V., Cifelli, F., & Funiciello, R. (2000). <Acocella et al. Analogue models of collapse calderas and resurgent domes.pdf>, *104*, 81–96. https://doi.org/10.1016/S0377-0273(00)00201-8

Acocella, V., & Funiciello, R. (1999). The interaction between regional and local tectonics during resurgent doming: the case of the island of Ischia, Italy. *Journal of Volcanology and Geothermal Research*, *88*(1–2), 109–123. https://doi.org/10.1016/S0377-0273(98)00109-7

Acocella, V., Funiciello, R., Marotta, E., Orsi, G., & De Vita, S. (2004). The role of extensional structures on experimental calderas and resurgence. *Journal of Volcanology and Geothermal Research*, *129*(1–3), 199–217.

Allen, P. A., & Allen, J. R. (1990). Basin analysis: principles & applications: Blackwell Science. Oxford, UK.

Argnani, A., & Savelli, C. (1999). Cenozoic volcanism and tectonics in the southern Tyrrhenian sea: Space-time distribution and geodynamic significance. *Journal of Geodynamics*, *27*(4–5), 409–432. https://doi.org/10.1016/S0264-3707(98)00025-8

Argnani, A., & Trincardi, F. (1988). Paola slope basin: evidence of regional contraction on the eastern Tyrrhenian margin. *Memorie Della Società Geologica Italiana*, *44*, 93–105.

Avedik, F., Hirn, A., Renard, V., Nicolich, R., Olivet, J. L., & Sachpazi, M. (1996). "Single-bubble" marine source offers new perspectives for lithospheric exploration. *Tectonophysics*, *267*(1–4), 57–71.

Avedik, F., Nicolich, R., Hirn, A., Maltezou, F., McBride, J., & Cernobori, L. (1995). Appraisal of a new, high-energy and low-frequency seismic pulse generating method on a deep seismic reflection profile in the Central Mediterranean Sea. *First Break*, *13*(7), 277–290.

Barberi, F., Gasparini, P., Innocenti, F., & Villari, L. (1973). Volcanism of the southern Tyrrhenian Sea and its geodynamic implications. *Journal of Geophysical Research*, *78*(23), 5221–5232.

Battaglia, M., Troise, C., Obrizzo, F., Pingue, F., & De Natale, G. (2006). Evidence for fluid migration as the source of deformation at Campi Flegrei caldera (Italy). *Geophysical Research Letters*, *33*(1).

Beccaluva, L., Gabbianelli, G., Lucchini, F., Rossi, P. L., & Savelli, C. (1985). Petrology and K/Ar ages of volcanics dredged from the Eolian seamounts: implications for geodynamic evolution of the southern Tyrrhenian basin. *Earth and Planetary Science Letters*, *74*(2–3), 187–208.

Bellucci, F., Woo, J., Kilburn, C. R. J., & Rolandi, G. (2006). Ground deformation at Campi Flegrei, Italy: implications for hazard assessment. *Geological Society, London, Special Publications*, *269*(1), 141–157.

Berardino, P., Fornaro, G., Lanari, R., & Sansosti, E. (2002). A new algorithm for surface deformation monitoring based on small baseline differential SAR interferograms. *IEEE Transactions on Geoscience and Remote Sensing*, *40*(11), 2375–2383.

Bertotti, G., Picotti, V., Chilovi, C., Fantoni, R., Merlini, S., & Mosconi, A. (2001). Neogene to quaternary sedimentary basins in the South Adriatic (Central Mediterranean): Foredeeps and lithospheric buckling. *Tectonics*, *20*(5), 771–787. https://doi.org/10.1029/2001TC900012

Bigi, G., Castellarin, A., Catalano, R., Coli, M., Cosentino, D., Dal Piaz, G. V, … Praturlon, A. (1989). Synthetic structural-kinematic map of Italy, scale 1: 2.000. 000. *CNR, Progetto Finalizzato Geodinamica, Roma*.

Bonardi, G., Cavazza, W., Perrone, V., & Rossi, S. (2001). Calabria-Peloritani terrane and northern Ionian sea. In *Anatomy of an orogen: The Apennines and adjacent Mediterranean basins* (pp. 287–306). Springer.

Bortoluzzi, G., Polonia, A., Torelli, L., Artoni, A., Carlini, M., Carone, S., … Stanghellini, G. (2017). Styles and rates of deformation in the frontal accretionary wedge of the Calabrian Arc (Ionian Sea): Controls exerted by the structure of the lower African plate. *Italian Journal of Geosciences*, *136*(3), 347–364. https://doi.org/10.3301/IJG.2016.11

Bottiglieri, M., Falanga, M., Tammaro, U., De Martino, P., Obrizzo, F., Godano, C., & Pingue, F. (2010). Characterization of GPS time series at the Neapolitan volcanic area by statistical analysis. *Journal of Geophysical Research: Solid Earth*, *115*(B10).

Branney, M. J., & Kokelaar, P. (1994). Volcanotectonic faulting, soft-state deformation, and rheomorphism of tuffs during development of a piecemeal caldera, English Lake District. *Geological Society of America Bulletin*, *106*(4), 507–530.

Brothelande, E., Peltier, A., Got, J. L., Merle, O., Lardy, M., & Garaebiti, E. (2016). Constraints on the source of resurgent doming inferred from analogue and numerical modeling — Implications on the current feeding system of the Yenkahe dome–Yasur volcano complex (Vanuatu). *Journal of Volcanology and Geothermal Research*, *322*(December 2015), 225–240. https://doi.org/10.1016/j.jvolgeores.2015.11.023

Brozzetti, F., Cirillo, D., Liberi, F., Piluso, E., Faraca, E., De Nardis, R., & Lavecchia, G. (2017). Structural style of Quaternary extension in the Crati Valley (Calabrian Arc): Evidence in support of an east-dipping detachment fault. *Italian Journal of Geosciences*, *136*(3), 434–453. https://doi.org/10.3301/IJG.2017.11

Bruno, P. P. (2004). Structure and evolution of the Bay of Pozzuoli (Italy) using marine seismic reflection data: implications for collapse of the Campi Flegrei caldera. *Bulletin of Volcanology*, *66*(4), 342–355.

Burg, J.-P., & Podladchikov, Y. (2000). From buckling to asymmetric folding of the continental lithosphere: Numerical modelling and application to the Himalayan syntaxes. *Geological Society, London, Special Publications*, *170*(1), 219–236.

Capozzi, R., & Picotti, V. (2003). Pliocene sequence stratigraphy, climatic trends and sapropel formation in the Northern Apennines (Italy). *Palaeogeography, Palaeoclimatology, Palaeoecology*, *190*, 349–371. https://doi.org/10.1016/S0031-0182(02)00614-4

Carminati, E., Cavazza, W., Roure, F., Spakman, W., Stampfli, G. M., & Ziegler, P. A. (2004). TRANSMED Transect III: Massif Central-Provence-Gulf of Lion-Provençal Basin-Sardinia-Tyrrhenian Basin-Southern Apennines-Apulia-Adriatic Sea-Albanides-Balkans-Moesian Platform. *Cavazza, W., Roure, F., Spakman, Stampfli, GM and Ziegler, PA, Eds., The TRANSMED Atlas: The Mediterranean Region from Crust to Mantle: Heidelberg, Springer-Verlag*.

Carminati, E., & Doglioni, C. (2005). EUROPE| Mediterranean Tectonics.

Carminati, E., Wortel, M. J. R., Spakman, W., & Sabadini, R. (1998). The role of slab detachment processes in the opening of the western–central Mediterranean basins: some geological and geophysical evidence. *Earth and Planetary Science Letters*, *160*(3–4), 651–665.

Carmisciano, C., Grassi, M., Cocchi, L., Masetti, G., Filippone, M., Ricci, E., … Berrino, G. (2013). RICAMAR2013-RIlievi per la Caratterizzazione dell'Ambiente MARino nel Golfo di Pozzuoli.

Carobene, L. (2003). Genesi, età, sollevamento ed erosione dei terrazzi marini di Crosia-Calopezzati (Costa ionica della Calabria-Italia). *Il Quaternario*, *16*(1), 43–90.

Casu, F., Manzo, M., & Lanari, R. (2006). A quantitative assessment of the SBAS algorithm performance for surface deformation retrieval from DInSAR data. *Remote Sensing of Environment*, *102*(3–4), 195–210.

Cattaneo, A., Correggiari, A., Langone, L., & Trincardi, F. (2003). The late-Holocene Gargano subaqueous delta, Adriatic shelf: sediment pathways and supply fluctuations. *Marine Geology*, *193*(1–2), 61–91.

Cattaneo, A., Trincardi, F., Asioli, A., & Correggiari, A. (2007). The Western Adriatic shelf clinoform: energy-limited bottomset. *Continental Shelf Research*, *27*(3–4), 506–525. https://doi.org/10.1016/j.csr.2006.11.013

Cavazza, W., & DeCelles, P. G. (1998). Upper Messinian siliciclastic rocks in southeastern Calabria (southern Italy): palaeotectonic and eustatic implications for the evolution of the central Mediterranean region. *Tectonophysics*, *298*(1–3), 223–241.

Chiarabba, C., De Gori, P., & Speranza, F. (2008). The southern Tyrrhenian subduction zone: deep geometry, magmatism and Plio-Pleistocene evolution. *Earth and Planetary Science Letters*, *268*(3–4), 408–423.

Cianflone, G., & Calabria, U. (2015). Preliminary study of the surface ground displacements in the Crati Valley (Calabria) by means of InSAR data, (November).

Cinque_1985.

Cinque, A., Rolandi, G. t, & Zamparelli, V. (1985). L'estensione dei depositi marini olocenici nei Campi Flegrei in relazione alla vulcano-tettonica. *Bollettino Della Società Geologica Italiana*, *104*(2), 327–348.

Cloetingh, S., & Burov, E. (2011). Lithospheric folding and sedimentary basin evolution: a review and analysis of formation mechanisms. *Basin Research*, *23*(3), 257–290.

Cocchi, L., Passaro, S., Tontini, F. C., & Ventura, G. (2017a). Volcanism in slab tear faults is larger than in island-arcs and back-arcs. *Nature Communications*, *8*(1). https://doi.org/10.1038/s41467-017-01626-w

Cocchi, L., Passaro, S., Tontini, F. C., & Ventura, G. (2017b). Volcanism in slab tear faults is larger than in island-arcs and back-arcs. *Nature Communications*, *8*(1), 1451. https://doi.org/10.1038/s41467-017-01626-w

Cole, J. W., Milner, D. M., & Spinks, K. D. (2005). Calderas and caldera structures: A review. *Earth-Science Reviews*, *69*(1–2), 1–26. https://doi.org/10.1016/j.earscirev.2004.06.004

Colella, A. (1988). Fault-controlled marine Gilbert-type fan deltas. *Geology*, *16*(11), 1031–1034. Retrieved from http://dx.doi.org/10.1130/0091-7613(1988)016%3C1031:FCMGTF%3E2.3.CO

D'Agostino, N., D'Anastasio, E., Gervasi, A., Guerra, I., Nedimović, M. R., Seeber, L., & Steckler, M. (2011). Forearc extension and slow rollback of the Calabrian Arc from GPS measurements. *Geophysical Research Letters*, *38*(17), 1–6. https://doi.org/10.1029/2011GL048270

D'Antonio, M., Civetta, L., Orsi, G., Pappalardo, L., Piochi, M., Carandente, A., … Isaia, R. (1999). The present state of the magmatic system of the Campi Flegrei caldera based on a reconstruction of its behavior in the past 12 ka. *Journal of Volcanology and Geothermal Research*, *91*(2), 247–268.

D'Auria, L., Pepe, S., Castaldo, R., Giudicepietro, F., Macedonio, G., Ricciolino, P., … Zinno, I. (2015). Magma injection beneath the urban area of Naples: A new mechanism for the 2012-2013 volcanic unrest at Campi Flegrei caldera. *Scientific Reports*, *5*(August), 1–11. https://doi.org/10.1038/srep13100

Damuth, J. E. (1980). Use of high-frequency (3.5–12 kHz) echograms in the study of near-bottom sedimentation processes in the deep-sea: a review. *Marine Geology*, *38*(1–3), 51–75.

De Martino, P., Guardato, S., Tammaro, U., Vassallo, M., & Iannaccone, G. (2014). A first GPS measurement of vertical seafloor displacement in the Campi Flegrei caldera (Italy). *Journal of Volcanology and Geothermal Research*, *276*, 145–151. https://doi.org/10.1016/j.jvolgeores.2014.03.003

De Natale, G., & Pingue, F. (1993). Ground deformations in collapsed caldera structures. *Journal of Volcanology and Geothermal Research*, *57*(1–2), 19–38.

De Natale, G., Troise, C., Pingue, F., Mastrolorenzo, G., Pappalardo, L., Battaglia, M., & Boschi, E. (2006). The Campi Flegrei caldera: unrest mechanisms and hazards. *Geological Society, London, Special Publications*, *269*(1), 25–45. https://doi.org/10.1144/GSL.SP.2006.269.01.03

De Ritis, R., Dominici, R., Ventura, G., Nicolosi, I., Chiappini, M., Speranza, F., … Sonnino, M. (2010). A buried volcano in the Calabrian Arc (Italy) revealed by high-resolution aeromagnetic data. *Journal of Geophysical Research: Solid Earth*, *115*(11), 1–18. https://doi.org/10.1029/2009JB007171

Deino, A. L., Orsi, G., de Vita, S., & Piochi, M. (2004). The age of the Neapolitan Yellow Tuff caldera-forming eruption (Campi Flegrei caldera–Italy) assessed by 40 Ar/39 Ar dating method. *Journal of Volcanology and Geothermal Research*, *133*(1), 157–170.

Del Ben, A., Barnaba, C., & Taboga, A. (2008). Strike-slip systems as the main tectonic features in the Plio-Quaternary kinematics of the Calabrian Arc. *Marine Geophysical Researches*, *29*(1), 1–12. https://doi.org/10.1007/s11001-007-9041-6

Del Gaudio, C., Aquino, I., Ricciardi, G. P., Ricco, C., & Scandone, R. (2010). Unrest episodes at Campi Flegrei: A reconstruction of vertical ground movements during 1905-2009. *Journal of Volcanology and Geothermal Research*, *195*(1), 48–56. https://doi.org/10.1016/j.jvolgeores.2010.05.014

Dello Iacono, D., Zollo, A., Vassallo, M., Vanorio, T., & Judenherc, S. (2009). Seismic images and rock properties of the very shallow structure of Campi Flegrei caldera (southern Italy). *Bulletin of Volcanology*, *71*(3), 275–284. https://doi.org/10.1007/s00445-008-0222-1

Di Renzo, V., Arienzo, I., Civetta, L., D'Antonio, M., Tonarini, S., Di Vito, M. A., & Orsi, G. (2011). The magmatic feeding system of the Campi Flegrei caldera: architecture and temporal evolution. *Chemical Geology*, *281*(3), 227–241.

Di Vito, M. A., Isaia, R., Orsi, G., Southon, J. d, De Vita, S., d'Antonio, M., … Piochi, M. (1999). Volcanism and deformation since 12,000 years at the Campi Flegrei caldera (Italy). *Journal of Volcanology and Geothermal Research*, *91*(2–4), 221–246.

Dickinson, W. R., & Seely, D. R. (1979). Structure and stratigraphy of forearc regions. *AAPG Bulletin*, *63*(1), 2–31.

Doglioni, C., Gueguen, E., Harabaglia, P., & Mongelli, F. (1999). On the origin of west-directed subduction zones and applications to the western Mediterranean. *Geological Society, London, Special Publications*, *156*(1), 541–561.

du Bray, E. A., & Pallister, J. S. (1999). Recrystallization and anatexis along the plutonic-volcanic contact of the Turkey Creek caldera, Arizona. *Geological Society of America Bulletin*, *111*(1), 143–153.

Dvorak, J. J., & Berrino, G. (1991). Recent ground movement and seismic activity in Campi Flegrei, southern Italy: Episodic growth of a resurgent dome. *Journal of Geophysical Research: Solid Earth*, *96*(B2), 2309–2323.

Dvorak, J. J., & Mastrolorenzo, G. (1991). *The mechanisms of recent vertical crustal movements in Campi Flegrei caldera, southern Italy* (Vol. 263). Geological Society of America.

Faccenna, C., Becker, T. W., Lucente, F. P., Jolivet, L., & Rossetti, F. (2001). History of subduction and back arc extension in the Central Mediterranean. *Geophysical Journal International*, *145*(3), 809–820.

Faccenna, C., Funiciello, F., Civetta, L., D Antonio, M., Moroni, M., & Piromallo, C. (2007). Slab disruption, mantle circulation, and the opening of the Tyrrhenian basins. *SPECIAL PAPERS-GEOLOGICAL SOCIETY OF AMERICA*, *418*, 153.

Fedele, L., Insinga, D. D., Calvert, A. T., Morra, V., Perrotta, A., & Scarpati, C. (2011). 40 Ar/39 Ar dating of tuff vents in the Campi Flegrei caldera (southern Italy): toward a new chronostratigraphic reconstruction of the Holocene volcanic activity. *Bulletin of Volcanology*, *73*(9), 1323–1336.

Ferranti, L., Antonioli, F., Mauz, B., Amorosi, A., Dai Pra, G., Mastronuzzi, G., … Verrubbi, V. (2006). Markers of the last interglacial sea-level high stand along the coast of Italy: Tectonic implications. *Quaternary International*, *145–146*, 30–54. https://doi.org/10.1016/j.quaint.2005.07.009

Ferranti, L., Burrato, P., Pepe, F., Santoro, E., Mazzella, M. E., Morelli, D., … Vannucci, G. (2014). An active oblique-contractional belt at the transition between the Southern Apennines and Calabrian Arc: The Amendolara Ridge, Ionian Sea, Italy. *Tectonics*, *33*(11), 2169–2194. https://doi.org/10.1002/2014TC003624

Ferranti, L., Monaco, C., Antonioli, F., Maschio, L., Kershaw, S., & Verrubbi, V. (2007). The contribution of regional uplift and coseismic slip to the vertical crustal motion in the Messina Straits, southern Italy: Evidence from raised Late Holocene shorelines. *Journal of Geophysical Research: Solid Earth*, *112*(6). https://doi.org/10.1029/2006JB004473

Ferranti, L., Santoro, E., Mazzella, M. E., Monaco, C., & Morelli, D. (2009). Active transpression in the northern Calabria Apennines, southern Italy. *Tectonophysics*, *476*(1–2), 226–251. https://doi.org/10.1016/j.tecto.2008.11.010

Ferrari, L., & Manetti, P. (1993). Geodynamic framework of the Tyrrhenian volcanism: a review. *Acta Vulcanol*, *3*, 1–10.

Finetti, I. R. (2005). *CROP project: deep seismic exploration of the central Mediterranean and Italy* (Vol. 1). Elsevier.

Florio, G., Fedi, M., Cella, F., & Rapolla, A. (1999). The Campanian Plain and Phlegrean Fields: structural setting from potential field data. *Journal of Volcanology and Geothermal Research*, *91*(2–4), 361–379.

Folch, A., & Gottsmann, J. (2006). Faults and ground uplift at active calderas. *Geological Society, London, Special Publications*, *269*(1), 109–120. https://doi.org/10.1144/GSL.SP.2006.269.01.07

Frezzotti, M. L., Peccerillo, A., & Panza, G. (2009). Carbonate metasomatism and CO2 lithosphere–asthenosphere degassing beneath the Western Mediterranean: an integrated model arising from petrological and geophysical data. *Chemical Geology*, *262*(1–2), 108–120.

Galli, P., & Bosi, V. (2003). Catastrophic 1638 earthquakes in Calabria (southern Italy): New insights from paleoseismological investigation. *Journal of Geophysical Research: Solid Earth*, *108*(B1).

Gamberi, F., & Rovere, M. (2010). Mud diapirs, mud volcanoes and fluid flow in the rear of the Calabrian Arc Orogenic Wedge (southeastern Tyrrhenian sea). *Basin Research*, *22*(4), 452–464.

Gazis, C. A., Lanphere, M., Taylor Jr, H. P., & Gurbanov, A. (1995). 40Ar/39Ar and 18O/16O studies of the Chegem ash-flow caldera and the Eldjurta Granite: Cooling of two late Pliocene igneous bodies in the Greater Caucasus Mountains, Russia. *Earth and Planetary Science Letters*, *134*(3–4), 377–391.

Gillot, P. Y. (1987). Histoire volcanique des Iles Eoliennes: arc insulaire ou complexe orogénique anulaire. *Doc. Trav. IGAL*, *11*, 35–42.

Giudicepietro, F. (1993). La dinamica recente dell'area vulcanica flegrea. Ph. D. thesis, 179 pp., Univ. of Naples, Naples, Italy.

Gliozzi, E. (1987). I terrazzi delpleistocene superiore della peninsola do Crotone (Calabria). *Geologica Romana*, *26*, 17–49.

Guarnieri, P. (2006). Plio-Quaternary segmentation of the south Tyrrhenian forearc basin. *International Journal of Earth Sciences*, *95*(1), 107–118. https://doi.org/10.1007/s00531-005-0005-2

Gueguen, E., Doglioni, C., & Fernandez, M. (1998). On the post-25 Ma geodynamic evolution of the western Mediterranean. *Tectonophysics*, *298*(1–3), 259–269.

Gulick, S. P. S., Meltzer, A. S., & Clarke Jr, S. H. (2002). Effect of the northward-migrating Mendocino triple junction on the Eel River forearc basin, California: Stratigraphic development. *Geological Society of America Bulletin*, *114*(2), 178–191.

Gutscher, M., Kukowski, N., Malavieille, J., & Lallemand, S. (1998). Episodic imbricate thrusting and underthrusting: Analog experiments and mechanical analysis applied to the Alaskan accretionary wedge. *Journal of Geophysical Research: Solid Earth*, *103*(B5), 10161–10176.

Gvirtzman, Z., & Nur, A. (2001). Residual topography, lithospheric structure and sunken slabs in the central Mediterranean. *Earth and Planetary Science Letters*, *187*(1–2), 117–130.

Holohan, E. P., Troll, V. R., Walter, T. R., Münn, S., McDonnell, S., & Shipton, Z. K. (2005). Elliptical calderas in active tectonic settings: An experimental approach. *Journal of*

Volcanology and Geothermal Research, *144*(1–4 SPEC. ISS.), 119–136. https://doi.org/10.1016/j.jvolgeores.2004.11.020

Hon, K. (1987). Geologic and petrologic evolution of the Lake city caldera, San Juan Mountains, Colorado. University of Colorado.

Isaia, R., Marianelli, P., & Sbrana, A. (2009). Caldera unrest prior to intense volcanism in Campi Flegrei (Italy) at 4.0 ka BP: Implications for caldera dynamics and future eruptive scenarios. *Geophysical Research Letters*, *36*(21).

Iuliano, S., Matano, F., Caccavale, M., & Sacchi, M. (2015). Annual rates of ground deformation (1993–2010) at Campi Flegrei, Italy, revealed by Persistent Scatterer Pair (PSP) – SAR interferometry. *International Journal of Remote Sensing*, *36*(24), 6160–6191. https://doi.org/10.1080/01431161.2015.1111541

Jacques, E., Monaco, C., Tapponnier, P., Tortorici, L., & Winter, T. (2001). Faulting and earthquake triggering during the 1783 Calabria seismic sequence. *Geophysical Journal International*, *147*(3), 499–516.

Judenherc, S., & Zollo, A. (2004). The Bay of Naples (southern Italy): Constraints on the volcanic structures inferred from a dense seismic survey. *Journal of Geophysical Research: Solid Earth*, *109*(B10).

Kastens, K., Mascle, J., Auroux, C., Bonatti, E., Broglia, C., Channell, J., … Hasegawa, S. (1988). ODP Leg 107 in the Tyrrhenian Sea: Insights into passive margin and back-arc basin evolution. *Geological Society of America Bulletin*, *100*(7), 1140–1156.

Kennedy, B., Stix, J., Vallance, J. W., Lavallée, Y., & Longpré, M. A. (2004). Controls on caldera structure: Results from analogue sandbox modeling. *Bulletin of the Geological Society of America*, *116*(5–6), 515–524. https://doi.org/10.1130/B25228.1

Kennedy, B., Wilcock, J., & Stix, J. (2012). Caldera resurgence during magma replenishment and rejuvenation at Valles and Lake City calderas. *Bulletin of Volcanology*, *74*(8), 1833–1847. https://doi.org/10.1007/s00445-012-0641-x

Kukowski, N., Lallemand, S. E., Malavieille, J., Gutscher, M.-A., & Reston, T. J. (2002). Mechanical decoupling and basal duplex formation observed in sandbox experiments with application to the Western Mediterranean Ridge accretionary complex. *Marine Geology*, *186*(1–2), 29–42.

Lambeck, K. (1983). The role of compressive forces in intracratonic basin formation and mid-plate orogenies. *Geophysical Research Letters*, *10*(9), 845–848.

Laursen, J., Scholl, D. W., & von Huene, R. (2002). Neotectonic deformation of the central Chile margin: Deepwater forearc basin formation in response to hot spot ridge and seamount subduction. *Tectonics*, *21*(5), 2-1-2–27. https://doi.org/10.1029/2001TC901023

Li, Z., & Schieber, J. (2018). Detailed facies analysis of the Upper Cretaceous Tununk Shale Member, Henry Mountains Region, Utah: Implications for mudstone depositional models in epicontinental seas. *Sedimentary Geology*, *364*(May), 141–159. https://doi.org/10.1016/j.sedgeo.2017.12.015

Lipman, P. W. (1984). The roots of ash flow calderas in western North America: windows into the tops of granitic batholiths. *Journal of Geophysical Research: Solid Earth*, *89*(B10), 8801–8841.

Lipman, P. W. (2000). Central San Juan caldera cluster: Regional volcanic framework. *SPECIAL*

PAPERS-GEOLOGICAL SOCIETY OF AMERICA, 9–70.

Liu, J. P., Xu, K. H., Li, A. C., Milliman, J. D., Velozzi, D. M., Xiao, S. B., & Yang, Z. S. (2007). Flux and fate of Yangtze River sediment delivered to the East China Sea. *Geomorphology*, *85*(3–4), 208–224. https://doi.org/10.1016/j.geomorph.2006.03.023

Locardi, E. (1993). Dynamics of deep structures in the Tyrrhenian-Apennines area and its relation to neotectonics. *Il Quaternario*, *6*, 59–66.

Loreto, M. F., Fracassi, U., Franzo, A., Del Negro, P., Zgur, F., & Facchin, L. (2013). Approaching the seismogenic source of the Calabria 8 September 1905 earthquake: New geophysical, geological and biochemical data from the S. Eufemia Gulf (S Italy). *Marine Geology*, *343*(September 1905), 62–75. https://doi.org/10.1016/j.margeo.2013.06.016

Loreto, M. F., Pepe, F., De Ritis, R., Ventura, G., Ferrante, V., Speranza, F., … Sacchi, M. (2015). Geophysical investigation of Pleistocene volcanism and tectonics offshore Capo Vaticano (Calabria, southeastern Tyrrhenian Sea). *Journal of Geodynamics*, *90*, 71–86. https://doi.org/10.1016/j.jog.2015.07.005

Lundgren, P., Usai, S., Sansosti, E., Lanari, R., Tesauro, M., Fornaro, G., & Berardino, P. (2001). Modeling surface deformation observed with synthetic aperture radar interferometry at Campi Flegrei caldera. *Journal of Geophysical Research: Solid Earth*, *106*(B9), 19355–19366.

Maesano, F. E., Tiberti, M. M., & Basili, R. (2017). The Calabrian Arc: Three-dimensional modelling of the subduction interface. *Scientific Reports*, *7*(1), 1–15. https://doi.org/10.1038/s41598-017-09074-8

Malinverno, A., Cafiero, M., Ryan, W. B. F., & Cita, M. B. (1981). Distribution of messinian sediments and erosional surfaces beneath the tyrrhenian sea-geodynamic implications. *Oceanologica Acta*, *4*(4), 489–495.

Mandl, G. (1988). *Mechanics of tectonic faulting*. Elsevier Amsterdam.

MARSH, B. D. (1984). Mechanics and energetics of magma formation and ascension. *Studies in Geophysics. Explosive Volcanism: Inception, Evolution, and Hazards*, 67–83.

Mattei, M., Cifelli, F., & D'Agostino, N. (2007). The evolution of the Calabrian Arc: Evidence from paleomagnetic and GPS observations. *Earth and Planetary Science Letters*, *263*(3–4), 259–274. https://doi.org/10.1016/j.epsl.2007.08.034

Mattei, M., Cipollari, P., Cosentino, D., Argentieri, A., Rossetti, F., Speranza, F., & Di Bella, L. (2002). The Miocene tectono-sedimentary evolution of the southern Tyrrhenian Sea: Stratigraphy, structural and palaeomagnetic data from the on-shore Amantea basin (Calabrian Arc, Italy). *Basin Research*, *14*(2), 147–168. https://doi.org/10.1046/j.1365-2117.2002.00173.x

Mattei, M., Speranza, F., Argentieri, A., Rossetti, F., Sagnotti, L., & Funiciello, R. (1999). Extensional tectonics in the Amantea basin (Calabria, Italy): A comparison between structural and magnetic anisotropy data. *Tectonophysics*, *307*(1–2), 33–49. https://doi.org/10.1016/S0040-1951(99)00117-1

Mazzoli, S., D'Errico, M., Aldega, L., Corrado, S., Invernizzi, C., Shiner, P., & Zattin, M. (2008). Tectonic burial and "young" (<10 Ma) exhumation in the southern Apennines fold-and-thrust belt (Italy). *Geology*, *36*(3), 243–246. https://doi.org/10.1130/G24344A.1

Milia, A., & Giordano, F. (2002). Holocene stratigraphy and depositional architecture of eastern Pozzuoli Bay (eastern Tyrrhenian sea margin, Italy): the influence of tectonics and wave-

induced currents. *Geo-Marine Letters*, *22*(1), 42–50.

Milia, A., Torrente, M. M., Russo, M., & Zuppetta, A. (2003). Tectonics and crustal structure of the Campania continental margin: relationships with volcanism. *Mineralogy and Petrology*, *79*(1–2), 33–47.

Milia, A., Turco, E., Pierantoni, P. P., & Schettino, A. (2009). Four-dimensional tectono-stratigraphic evolution of the Southeastern peri-Tyrrhenian basins (Margin of Calabria, Italy). *Tectonophysics*, *476*(1–2), 41–56. https://doi.org/10.1016/j.tecto.2009.02.030

Minelli, L., & Faccenna, C. (2010). Evolution of the Calabrian accretionary wedge (central Mediterranean). *Tectonics*, *29*(4).

Molin, P., Dramis, F., & Palmieri, E. (2002). The Pliocene-Quaternary uplift of the Ionian northern Calabria coastal belt between Corigliano Calabro and Capo Trionto. *Studi Geologici Camerti, Vol. Spec.*, 135–145.

Monaco, C., Tortorici, L., & Paltrinieri, W. (1998). Structural evolution of the Lucanian Apennines, southern Italy. *Journal of Structural Geology*, *20*(5), 617–638.

Monaco et al., 1998 Southern Apennines.pdf. (n.d.).

Moore, I., & Kokelaar, P. (1998). Tectonically controlled piecemeal caldera collapse: A case study of Glencoe volcano, Scotland. *Geological Society of America Bulletin*, *110*(11), 1448–1466.

Morán-Zenteno, D. J., Alba-Aldave, L. A., Solé, J., & Iriondo, A. (2004). A major resurgent caldera in southern Mexico: The source of the late Eocene Tilzapotla ignimbrite. *Journal of Volcanology and Geothermal Research*, *136*(1–2), 97–119. https://doi.org/10.1016/j.jvolgeores.2004.04.002

Morelli, C., Giese, P., Cassinis, R., Colombi, B., Guerra, I., Luongo, G., … Schutte, K. G. (1975). Crustal structure of Southern Italy. A seismic refraction profile between Puglia-Calabria-Sicily. *Boll. Geofis. Teor. Appl*, *18*, 183–210.

Natale, D., & Petrazzuoli, M. (1997). of the crest chamber I ...., *24*(13), 1555–1558.

Neri, G., Orecchio, B., Totaro, C., Falcone, G., & Presti, D. (2009). Subduction beneath southern Italy close the ending: Results from seismic tomography. *Seismological Research Letters*, *80*(1), 63–70.

Nicolosi, I., Speranza, F., & Chiappini, M. (2006). Ultrafast oceanic spreading of the Marsili Basin, southern Tyrrhenian Sea: Evidence from magnetic anomaly analysis. *Geology*, *34*(9), 717–720.

Noda, A. (2016). Forearc basins: Types, geometries, and relationships to subduction zone dynamics. *Bulletin of the Geological Society of America*, *128*(5–6), 879–895. https://doi.org/10.1130/B31345.1

Olivetti, V., Cyr, A. J., Molin, P., Faccenna, C., & Granger, D. E. (2012). Uplift history of the Sila Massif, southern Italy, deciphered from cosmogenic ^{10}Be erosion rates and river longitudinal profile analysis. *Tectonics*, *31*(3), 1–19. https://doi.org/10.1029/2011TC003037

Orecchio, B., Presti, D., Totaro, C., D'Amico, S., & Neri, G. (2015). Investigating slab edge kinematics through seismological data: The northern boundary of the Ionian subduction system (south Italy). *Journal of Geodynamics*, *88*, 23–35. https://doi.org/10.1016/j.jog.2015.04.003

Orsi, G., Civetta, L., Del Gaudio, C., De Vita, S., Di Vito, M. A., Isaia, R., … Ricco, C. (1999). Short-term ground deformations and seismicity in the resurgent Campi Flegrei caldera (Italy): An example of active block-resurgence in a densely populated area. *Journal of Volcanology and Geothermal Research*, *91*(2–4), 415–451. https://doi.org/10.1016/S0377-0273(99)00050-5

Orsi, G., De Vita, S., & Di Vito, M. (1996). The restless, resurgent Campi Flegrei nested caldera (Italy): Constraints on its evolution and configuration. *Journal of Volcanology and Geothermal Research*, *74*(3–4), 179–214. https://doi.org/10.1016/S0377-0273(96)00063-7

Orsi, G., Gallo, G., & Zanchi, A. (1991). Simple-shearing block resurgence in caldera depressions. A model from Pantelleria and Ischia. *Journal of Volcanology and Geothermal Research*, *47*(1–2), 1–11. https://doi.org/10.1016/0377-0273(91)90097-J

Panza, G. F., Peccerillo, A., Aoudia, A., & Farina, B. (2007). Geophysical and petrological modelling of the structure and composition of the crust and upper mantle in complex geodynamic settings: the Tyrrhenian Sea and surroundings. *Earth-Science Reviews*, *80*(1–2), 1–46.

Parascandola, A. (1947). *I fenomeni bradisismici del Serapeo di Pozzuoli*. Stabilmento tipografico G. Genovese.

Passaro, S., Barra, M., Saggiomo, R., Di Giacomo, S., Leotta, A., Uhlen, H., & Mazzola, S. (2013). Multi-resolution morpho-bathymetric survey results at the Pozzuoli–Baia underwater archaeological site (Naples, Italy). *Journal of Archaeological Science*, *40*(2), 1268–1278.

Pepe, F., Bertotti, G., & Cloetingh, S. (2004). Tectono-stratigraphic modelling of the North Sicily continental margin (southern Tyrrhenian Sea). *Tectonophysics*, *384*(1–4), 257–273.

Pepe, F., Sulli, A., Bertotti, G., & Cella, F. (2010). Architecture and Neogene to Recent evolution of the western Calabrian continental margin: An upper plate perspective to the Ionian subduction system, central Mediterranean. *Tectonics*, *29*(3), 1–24. https://doi.org/10.1029/2009TC002599

Petrinovic, I. A., Martí, J., Aguirre-Díaz, G. J., Guzmán, S., Geyer, A., & Paz, N. S. (2010). The Cerro Aguas Calientes caldera, NW Argentina: An example of a tectonically controlled, polygenetic collapse caldera, and its regional significance. *Journal of Volcanology and Geothermal Research*, *194*(1–3), 15–26. https://doi.org/10.1016/j.jvolgeores.2010.04.012

Phillips, W. J. (1974). The dynamic emplacement of cone sheets. *Tectonophysics*, *24*(1–2), 69–84.

Piromallo, C., & Morelli, A. (2003). P wave tomography of the mantle under the Alpine-Mediterranean area. *Journal of Geophysical Research: Solid Earth*, *108*(B2).

Polonia, A., Torelli, L., Mussoni, P., Gasperini, L., Artoni, A., & Klaeschen, D. (2011). The Calabrian Arc subduction complex in the Ionian Sea: Regional architecture, active deformation, and seismic hazard. *Tectonics*, *30*(5).

Pontevivo, A., & Panza, G. F. (2006). The lithosphere-asthenosphere system in the Calabrian Arc and surrounding seas–Southern Italy. *Pure and Applied Geophysics*, *163*(8), 1617–1659.

Puga-Bernabéu, Á., Martín, J. M., Braga, J. C., & Sánchez-Almazo, I. M. (2010). Downslope-migrating sandwaves and platform-margin clinoforms in a current-dominated, distally steepened temperate-carbonate ramp Guadix Basin, Southern Spain. *Sedimentology*, *57*(2), 293–311. https://doi.org/10.1111/j.1365-3091.2009.01079.x

Qiu, J., Liu, J., Saito, Y., Yang, Z., Yue, B., Wang, H., & Kong, X. (2014). Sedimentary evolution

of the Holocene subaqueous clinoform off the southern Shandong Peninsula in the Western South Yellow Sea. *Journal of Ocean University of China*, *13*(5), 747–760. https://doi.org/10.1007/s11802-014-2227-z

Rehault, J. P., Moussat, E., & Fabbri, A. (1987). Structural evolution of the Tyrrhenian back-arc basin. *Marine Geology*, *74*(1–2), 123–150.

Robustelli, G., Lucà, F., Corbi, F., Pelle, T., Dramis, F., Fubelli, G., … Cugliari, D. (2009). Alluvial terraces on the Ionian coast of northern Calabria, southern Italy: Implications for tectonic and sea level controls. *Geomorphology*, *106*(3–4), 165–179. https://doi.org/10.1016/j.geomorph.2008.12.010

Roche, O., Druitt, T. H., & Merle, O. (2000). Experimental study of caldera formation. *Journal of Geophysical Research: Solid Earth*, *105*(B1), 395–416. https://doi.org/10.1029/1999JB900298

Rosi, M., & Sbrana, A. (1987). *Phlegrean fields* (Vol. 9). Consiglio nazionale delle ricerche.

Ryan, H. F., Draut, A. E., Keranen, K., & Scholl, D. W. (2012). Influence of the Amlia fracture zone on the evolution of the Aleutian Terrace forearc basin, central Aleutian subduction zone. *Geosphere*, *8*(6), 1254–1273. https://doi.org/10.1130/GES00815.1

Sacchi, M., Alessio, G., Aquino, I., Esposito, E., Molisso, F., Nappi, R., … Violante, C. (2009). Risultati preliminari della campagna oceanografica CAFE_07–Leg 3 nei Golfi di Napoli e Pozzuoli, Mar Tirreno orientale. *Quaderni Di Geofisica*.

Sacchi, M., Pepe, F., Corradino, M., Insinga, D. D., Molisso, F., & Lubritto, C. (2014). The Neapolitan Yellow Tuff caldera offshore the Campi Flegrei: Stratal architecture and kinematic reconstruction during the last 15 ky. *Marine Geology*, *354*, 15–33.

Salles, L., Ford, M., Joseph, P., De Veslud, C. L. C., & Le Solleuz, A. (2011). Migration of a synclinal depocentre from turbidite growth strata: the Annot syncline, SE France. *Bulletin de La Societe Geologique de France*, *182*(3), 199–220. https://doi.org/10.2113/gssgfbull.182.3.199

Samsonov, S. V., Tiampo, K. F., Camacho, A. G., Fernández, J., & González, P. J. (2014). Spatiotemporal analysis and interpretation of 1993-2013 ground deformation at Campi Flegrei, Italy, observed by advanced DInSAR. *Geophysical Research Letters*, *41*(17), 6101–6108. https://doi.org/10.1002/2014GL060595

Santo, A. P., & Clark, A. H. (1994). Volcanological evolution of Aeolian Arc, Italy: Inferences from 40Ar/39Ar ages of Filicudi rocks. IAVCEI Congress, Abstract Volume, Ankara, 1994. Savelli, C. 2000. Two-stage progression of volcanism 8–0 Ma in the central Mediterranean southern Italy. *Journal of Geodynamics*, *31*, 87–104.

Saunders, S. J. (2004). The possible contribution of circumferential fault intrusion to caldera resurgence. *Bulletin of Volcanology*, *67*(1), 57–71. https://doi.org/10.1007/s00445-004-0360-z

Savelli, C. (1988). Late Oligocene to Recent episodes of magmatism in and around the Tyrrhenian Sea: implications for the processes of opening in a young inter-arc basin of intra-orogenic (Mediterranean) type. *Tectonophysics*, *146*(1–4), 163–181.

Scandone, R., Giacomelli, L., & Speranza, F. F. (2006). The volcanological history of the volcanoes of Naples: a review. *Developments in Volcanology*, *9*, 1–26.

Scarpati, C., Cole, P., & Perrotta, A. (1993a). The Neapolitan Yellow Tuff—a large volume

multiphase eruption from Campi Flegrei, southern Italy. *Bulletin of Volcanology*, *55*(5), 343–356.

Scarpati, C., Cole, P., & Perrotta, A. (1993b). The Neapolitan Yellow Tuff - A large volume multiphase eruption from Campi Flegrei, Southern Italy. *Bulletin of Volcanology*, *55*(5), 343–356. https://doi.org/10.1007/BF00301145

Self, S., Goff, F., Gardner, J. N., Wright, J. V, & Kite, W. M. (1986). Explosive rhyolitic volcanism in the Jemez Mountains: Vent locations, caldera development and relation to regional structure. *Journal of Geophysical Research: Solid Earth*, *91*(B2), 1779–1798.

Shulgin, A., Kopp, H., Klaeschen, D., Papenberg, C., Tilmann, F., Flueh, E. R., … Djajadihardja, Y. (2013). Subduction system variability across the segment boundary of the 2004/2005 Sumatra megathrust earthquakes. *Earth and Planetary Science Letters*, *365*, 108–119.

Sibson, R. H. (1995). Selective fault reactivation during basin inversion: potential for fluid redistribution through fault-valve action. *Geological Society, London, Special Publications*, *88*(1), 3–19.

Slingerland, R., & Keen, T. R. (1999). Sediment transport in the Western Interior Seaway of North America: Predictions from a climate-ocean-sediment model.

Smith, R. L., & Bailey, R. A. (1968). Stratigraphy, structure, and volcanic evolution of the Jemez Mountains, New Mexico. *Special Paper—Geological Society of America*, 447–448.

Smith, V. C., Isaia, R., & Pearce, N. J. G. (2011). Tephrostratigraphy and glass compositions of post-15 kyr Campi Flegrei eruptions: implications for eruption history and chronostratigraphic markers. *Quaternary Science Reviews*, *30*(25–26), 3638–3660.

Spence, G. D., Hyndman, R. D., Davis, E. E., & Yorath, C. J. (1991). Seismic structure of the northern Cascadia accretionary prism: evidence from new multichannel seismic reflection data. *Continental Lithosphere: Deep Seismic Reflections*, *22*, 257–263.

Spina, V., Tondi, E., Galli, P., & Mazzoli, S. (2009). Fault propagation in a seismic gap area (northern Calabria, Italy): Implications for seismic hazard. *Tectonophysics*, *476*(1–2), 357–369.

Spina, V., Tondi, E., & Mazzoli, S. (2011). Complex basin development in a wrench-dominated back-arc area: Tectonic evolution of the Crati Basin, Calabria, Italy. *Journal of Geodynamics*, *51*(2–3), 90–109. https://doi.org/10.1016/j.jog.2010.05.003

Stephenson, R. A., & Cloetingh, S. (1991). Some examples and mechanical aspects of continental lithosphere folding.

Tansi, C., Muto, F., Critelli, S., & Iovine, G. (2007). Neogene-Quaternary strike-slip tectonics in the central Calabrian Arc (southern Italy). *Journal of Geodynamics*, *43*(3), 393–414. https://doi.org/10.1016/j.jog.2006.10.006

Thomson, S. N. (1994). Fission track analysis of the crystalline basement rocks of the Calabrian Arc, southern Italy: evidence of Oligo-Miocene late-orogenic extension and erosion. *Tectonophysics*, *238*(1–4), 331–352.

Thomson, S. N., Stöckhert, B., Rauche, H., & Brix, M. R. (1998). Apatite fission-track thermochronology of the uppermost tectonic unit of Crete, Greece: implications for the post-Eocene tectonic evolution of the Hellenic subduction system. In *Advances in Fission-Track Geochronology* (pp. 187–205). Springer.

Tibaldi, A., & Vezzoli, L. (1998). The space problem of caldera resurgence: an example from Ischia Island, Italy. *Geologische Rundschau*, *87*(1), 53–66.

Tortorici, L., Monaco, C., Tansi, C., & Cocina, O. (1995). Recent and active tectonics in the Calabrian arc (Southern Italy). *Tectonophysics*, *243*(1–2), 37–55.

Totaro, C., Orecchio, B., Presti, D., Scolaro, S., & Neri, G. (2016). Seismogenic stress field estimation in the Calabrian Arc region (south Italy) from a Bayesian approach. *Geophysical Research Letters*, *43*(17), 8960–8969. https://doi.org/10.1002/2016GL070107

Trasatti, E., Casu, F., Giunchi, C., Pepe, S., Solaro, G., Tagliaventi, S., Ricciardi, G. P. (2008). The 2004–2006 uplift episode at Campi Flegrei caldera (Italy): Constraints from SBAS-DInSAR ENVISAT data and Bayesian source inference. *Geophysical Research Letters*, *35*(7).

Trasatti, E., Polcari, M., Bonafede, M., & Stramondo, S. (2015). Geodetic constraints to the source mechanism of the 2011-2013 unrest at Campi Flegrei (Italy) caldera. *Geophysical Research Letters*, *42*(10), 3847–3854. https://doi.org/10.1002/2015GL063621

Troiano, A., Di Giuseppe, M. G., Petrillo, Z., Troise, C., & De Natale, G. (2011). Ground deformation at calderas driven by fluid injection: modelling unrest episodes at Campi Flegrei (Italy). *Geophysical Journal International*, *187*(2), 833–847.

Ulusoy, I., Cubukcu, E., Aydar, E., Labazuy, P., Gourgaud, A., & Vincent, P. M. (2004). Volcanic and deformation history of the Bodrum resurgent caldera system (southwestern Turkey). *Journal of Volcanology and Geothermal Research*, *136*(1–2), 71–96. https://doi.org/10.1016/j.jvolgeores.2004.03.016

Van Dijk, J. P., Bello, M., Brancaleoni, G. P., Cantarella, G., Costa, V., Frixa, A., … Zerilli, A. (2000). A regional structural model for the northern sector of the Calabrian Arc (southern Italy). *Tectonophysics*, *324*(4), 267–320. https://doi.org/10.1016/S0040-1951(00)00139-6

Vilardo, G., Isaia, R., Ventura, G., De Martino, P., & Terranova, C. (2010). InSAR Permanent Scatterer analysis reveals fault re-activation during inflation and deflation episodes at Campi Flegrei caldera. *Remote Sensing of Environment*, *114*(10), 2373–2383. https://doi.org/10.1016/j.rse.2010.05.014

Vitale, S., & Isaia, R. (2014). Fractures and faults in volcanic rocks (Campi Flegrei, southern Italy): insight into volcano-tectonic processes. *International Journal of Earth Sciences*, *103*(3), 801–819.

Walter, T. R., & Troll, V. R. (2001). Formation of caldera periphery faults: An experimental study. *Bulletin of Volcanology*, *63*(2–3), 191–203. https://doi.org/10.1007/s004450100135

Westaway, R. (1993). Quaternary uplift of southern Italy. *Journal of Geophysical Research: Solid Earth*, *98*(B12), 21741–21772.

Wohletz, K., Orsi, G., & De Vita, S. (1995). Eruptive mechanisms of the Neapolitan Yellow Tuff interpreted from stratigraphie, chemical, and granulometric data. *Journal of Volcanology and Geothermal Research*, *67*(4), 263–290.

Wortel, M. J. R., & Spakman, W. (2000). Subduction and slab detachment in the Mediterranean-Carpathian region. *Science*, *290*(5498), 1910–1917.

Zecchin, M., Caffau, M., Civile, D., Critelli, S., Di Stefano, A., Maniscalco, R., … Roda, C. (2012). The Plio-Pleistocene evolution of the Crotone Basin (southern Italy): Interplay between sedimentation, tectonics and eustasy in the frame of Calabrian Arc migration. *Earth-Science Reviews*, *115*(4), 273–303. https://doi.org/10.1016/j.earscirev.2012.10.005

Figures

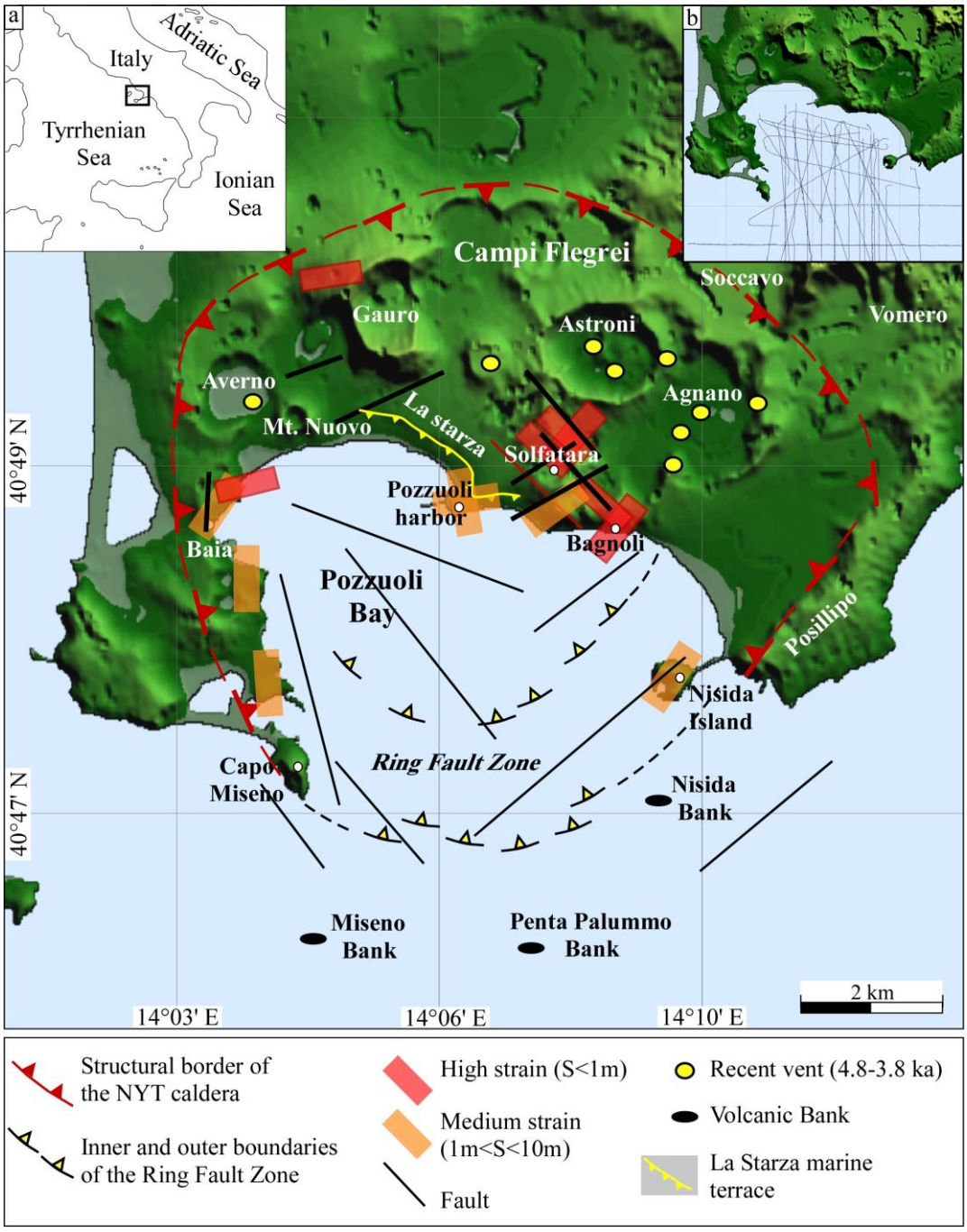

Figure 1. Corradino et al.

Figure 1. Morpho-structural map of the Neapolitan Yellow Tuff caldera (after Wohletz et al., 1995; Orsi et al. 1996; Di Vito et al., 1999; Milia and Torrente, 2003; Bruno, 2004; Sacchi et al., 2014). Location of eruptive vents younger than the NYT eruption are after D'Antonio et al. 1999. Strain distribution in the Campi Flegrei with high and medium wide range of spacing (S) is also shown (after Acocella, 2010). The direction of elongation of the rectangle indicates the orientation of the associated structures. a) Location of the investigated area. b) Location of the seismic profile dataset used in this study.

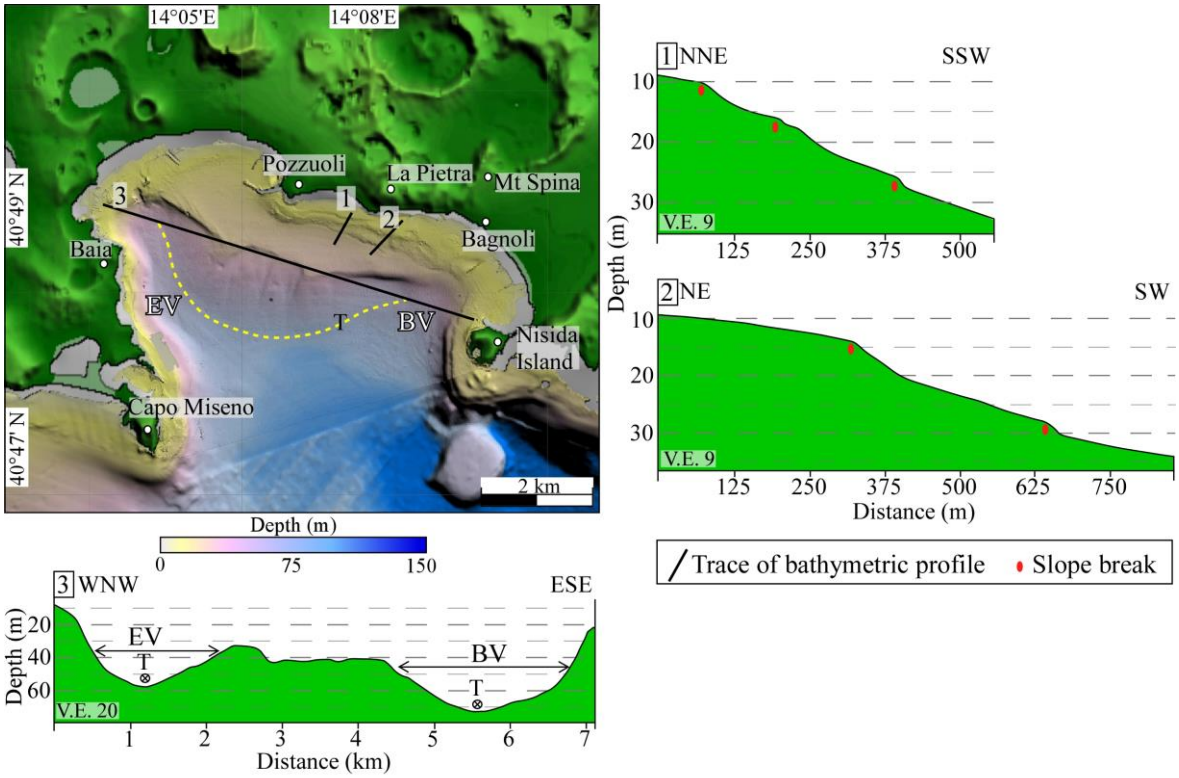

Figure 2. Corradino et al.

Figure 2. Morpho-bathymetric map of the Pozzuoli Bay. Abbreviations: EV, Epitaffio valley; BV, Bagnoli valley; T, thalweg of the EV–BV morpho-structural depression; V.E., vertical exaggeration.

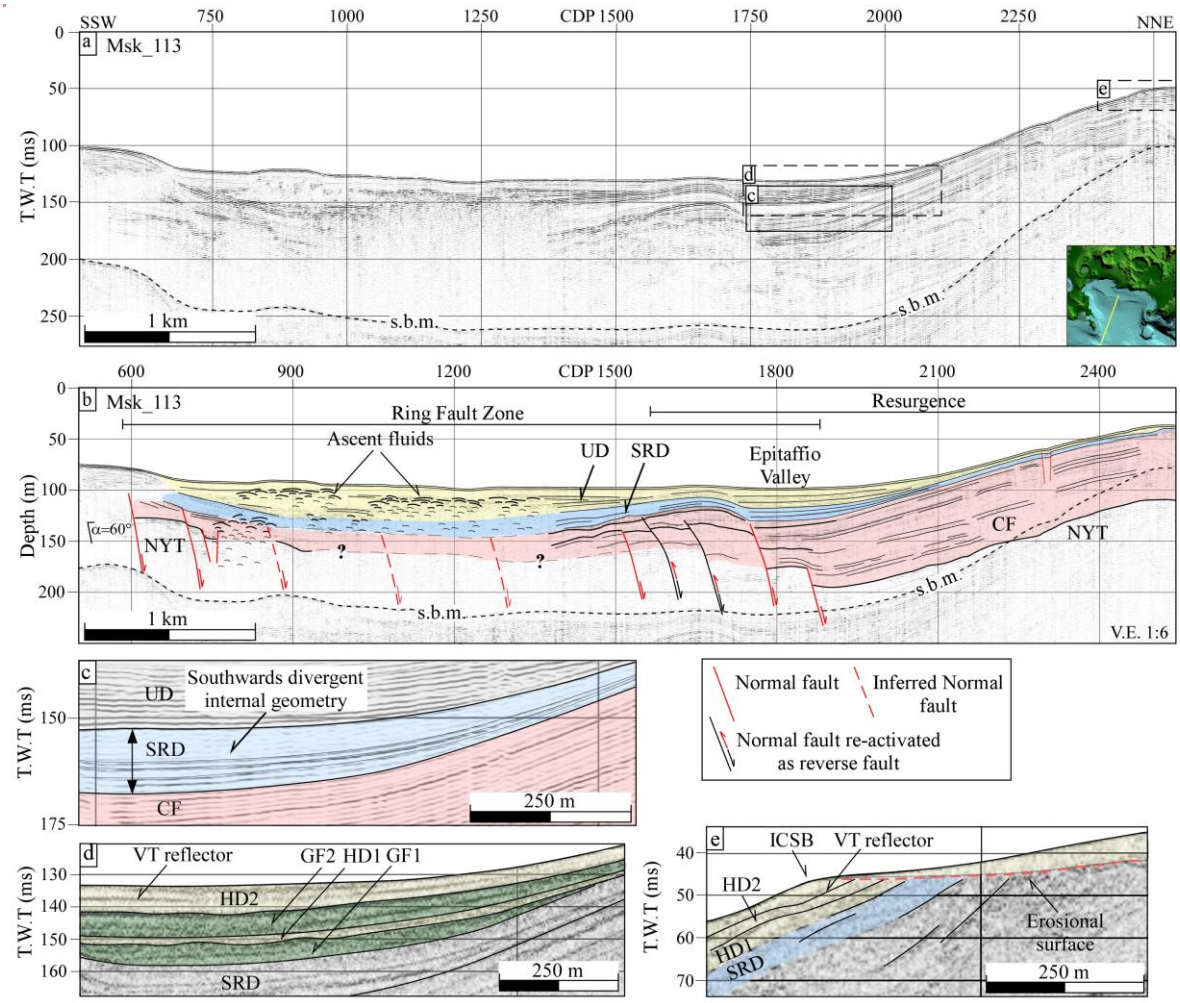

Figure 3. Corradino et al.

Figure 3. a) Msk_113 Sparker profile. Inset shows its location. b) Depth-converted Msk_113 profile and its seismic facies interpretation. Boxes show seismo-stratigraphic units recognized on seismic Sparker (c) and Sub-Bottom Chirp profiles (d and e). Abbreviations: s.b.m., sea bottom multiple; V.E., vertical exaggeration; ICSB: inner continental shelf break.

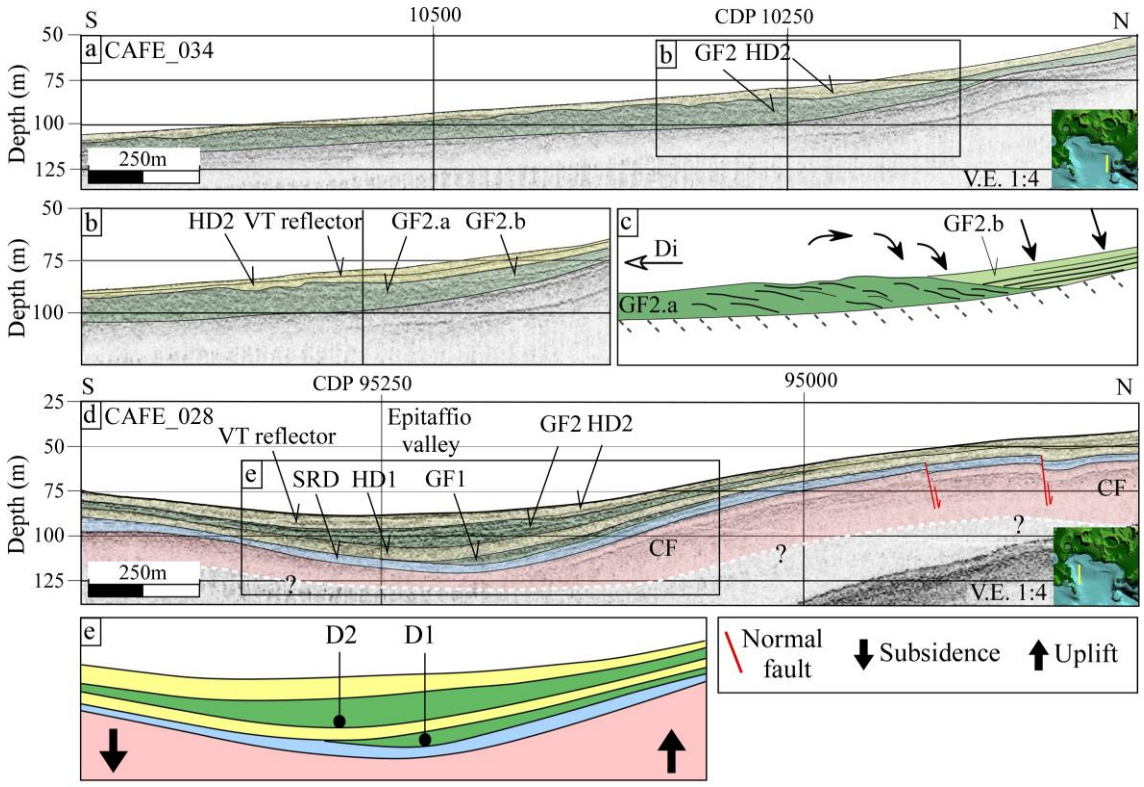

Figure 4. Corradino et al.

Figure 4. a) Depth-converted CAFE_034 Sub-Bottom Chirp profile and its seismic facies interpretation. b) Particular of the gravity flow deposits (GF unit) showing the two subunits recognized on the CAFE_034 profile and c) its line drawing. Dark green shading indicates the body (subunit GF2.a) of the gravity flow. Light green shading indicates sediments deposited by settling of a suspended material (subunit GF2.b). d) Depth-converted CAFE_028 Sub-Bottom Chirp profile and its seismic facies interpretation. e) Line drawing of a part of the CAFE_028 profile showing the migration of the depocenter in the Epitaffio valley. Insets show the location of the Chirp profiles. Abbreviations: Di, vector velocity; D1 and D2, basin depocenters; V.E., vertical exaggeration.

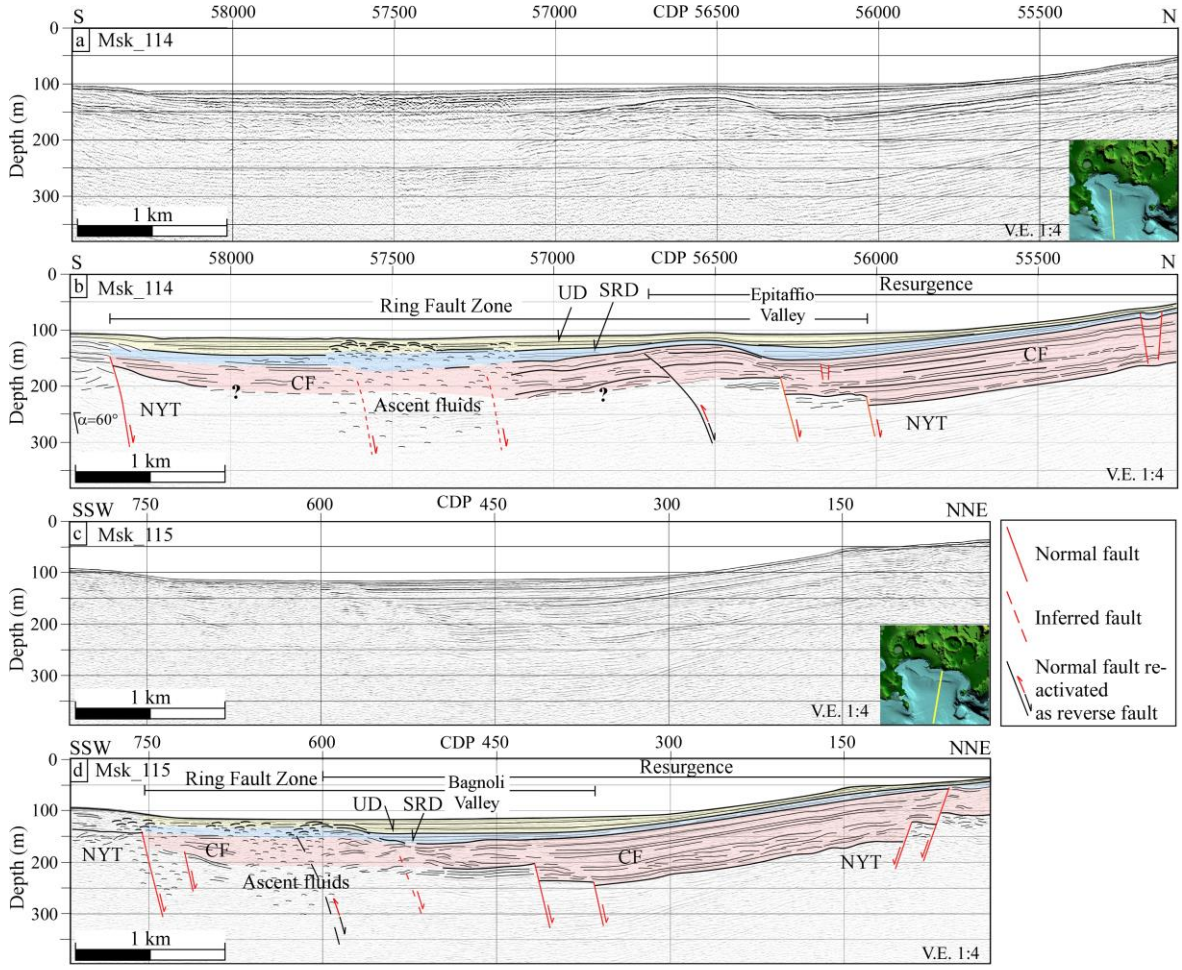

Figure 5. Corradino et al.

Figure 5. a) Depth-converted Msk_114 Sparker profile and b) its seismic facies interpretation. c) Depth-converted Msk_115 Sparker profile and d) its seismic facies interpretation. Insets show the location of the profiles. V.E., vertical exaggeration.

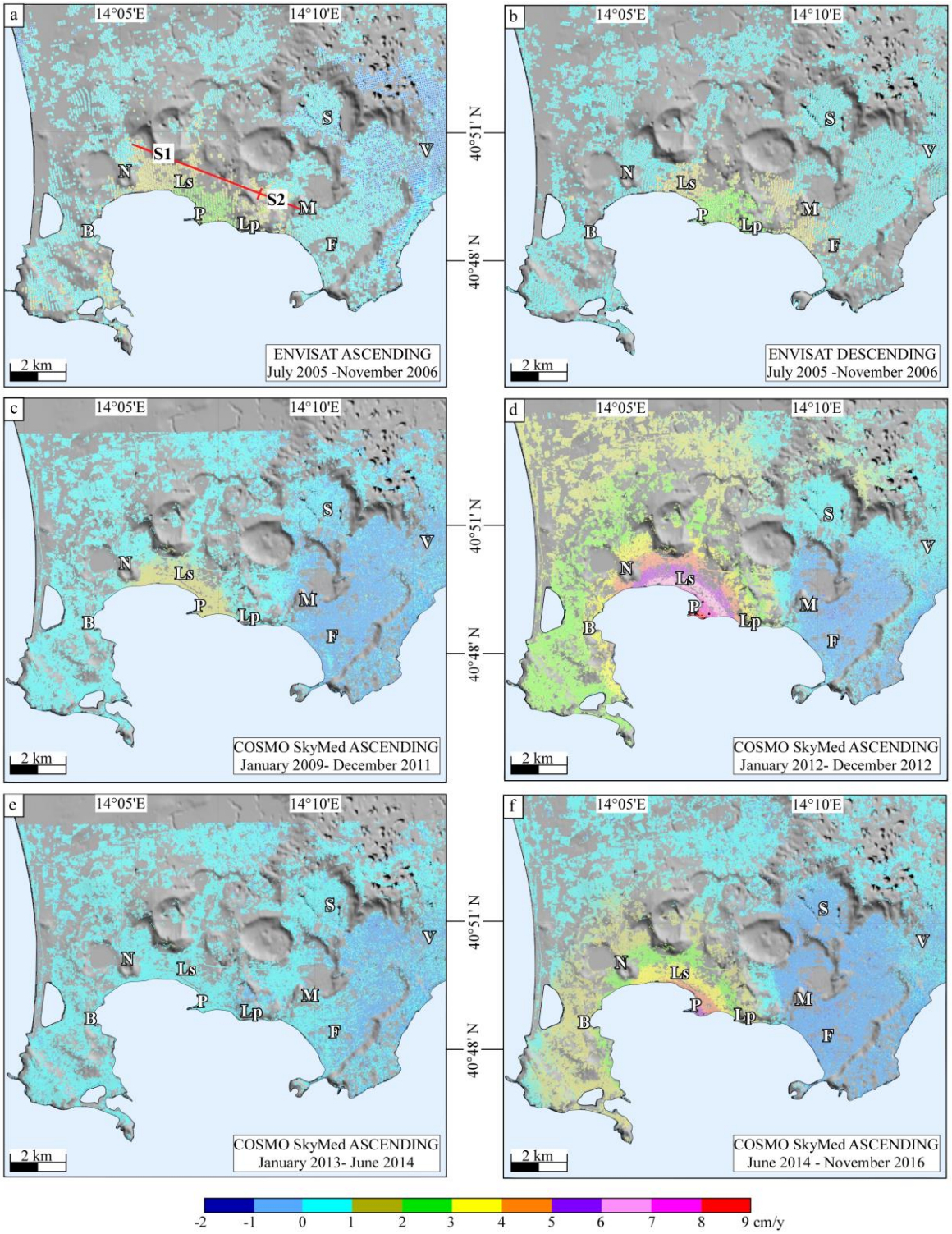

Figure 6. Corradino et al.

Figure 6. Deformation velocity maps computed from the a) ascending and b) descending ENVISAT data acquired between July 2005 and November 2006, and ascending COSMO-SkyMed data (c, d, e and f) acquired between January 2009 and November 2016. The velocity maps are superimposed on the DTM of the Campi Flegrei. Abbreviations: B, Baia; N, Mt Nuovo; Ls, La Starza terrace; P, Pozzuoli harbor; Lp, La Pietra; M, Mt Spina; F, Fuorigrotta; S, Soccavo; V, Vomero.

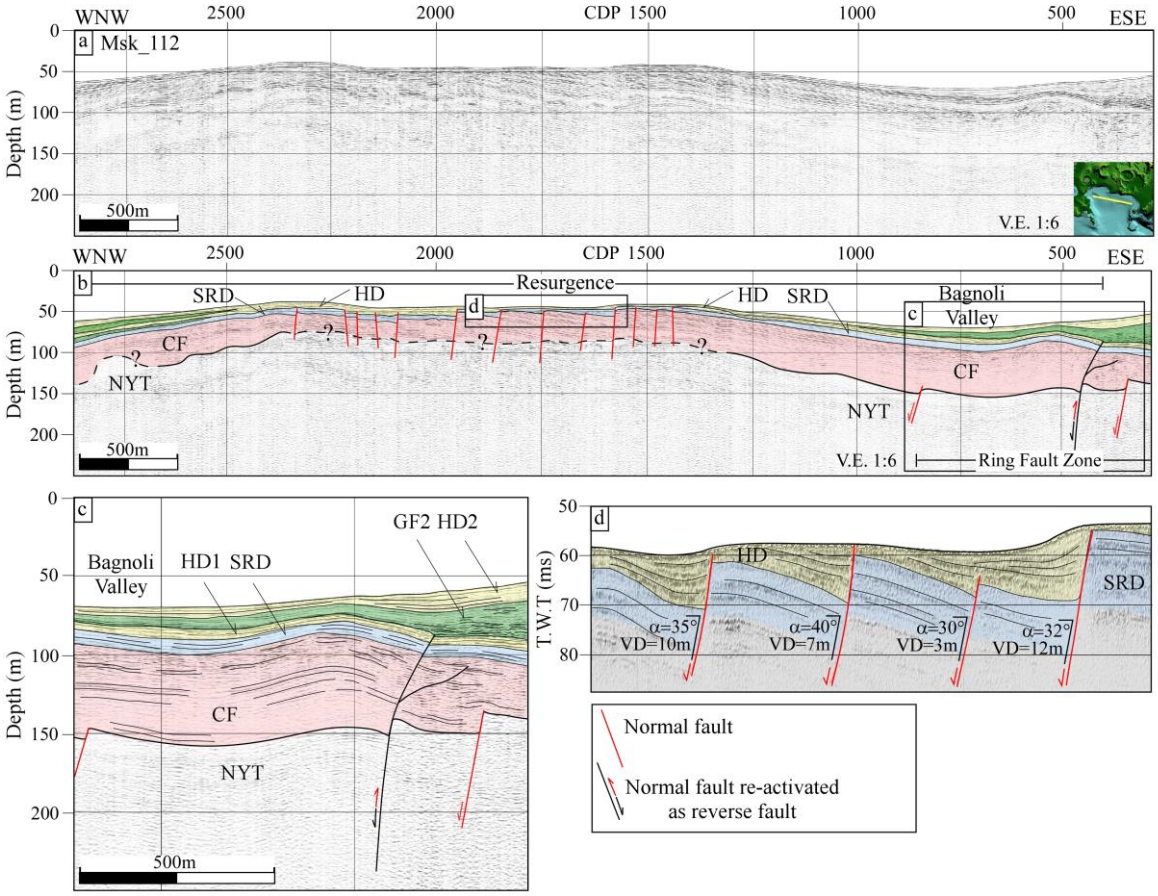

Figure 7. Corradino et al.

Figure 7. a) Depth-converted Msk_112 Sparker profile and b) its interpretation. Inset shows the location of the profile. c) Detail of the reverse fault formed by the reactivation of the caldera collapse normal fault. d) Particular of the graben-like structure on the top of the antiformal structure, recognized on Chirp seismic profile. Abbreviations: VD, vertical displacement; V.E., vertical exaggeration.

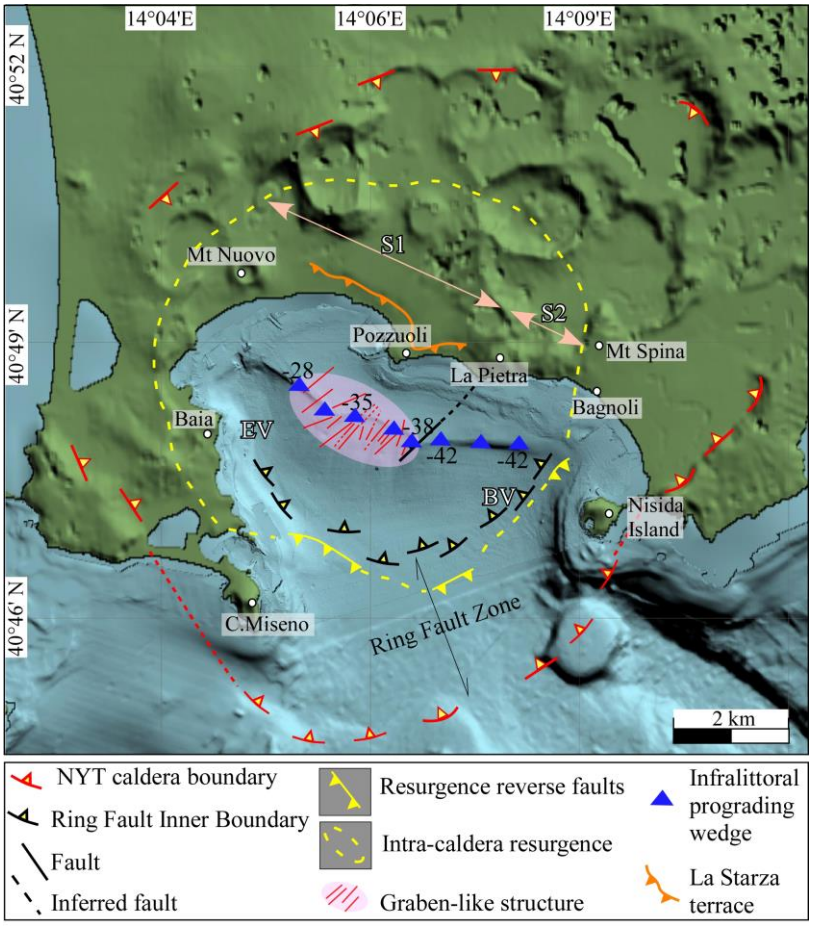

Figure 8. Corradino et al.

Figure 8. Morpho-structural map of the NYT caldera and intra-caldera resurgence. S1 and S2 are the two main uplifted sectors recognized on the deformation velocity maps of the Campi Flegrei. The location of the infralittoral prograding wedges derive from the interpretation of Sub-Bottom Chirp profiles. Abbreviations: EV, Epitaffio valley; BV, Bagnoli valley.

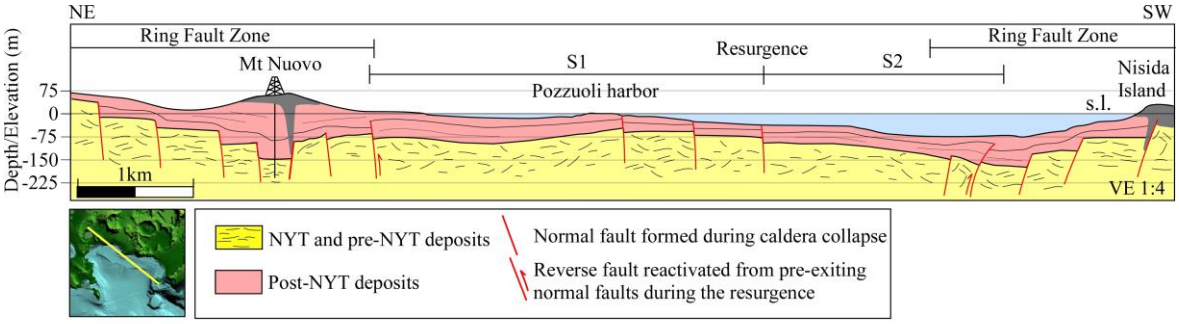

Figure 9. Corradino et al.

Figure 9. Schematic section across the NYT intra-caldera resurgence from the north-eastern area of the Campi Flegrei to Nisida Island, in the south-western sector of the Pozzuoli Bay. Inset shows the location of the section.

CHAPTER 2

3D Architecture and Plio-Quaternary evolution of the Paola Basin: Insights into the Fore-arc of the Tyrrhenian-Ionian Subduction System

NOTE This chapter is a scientific paper submitted to "*Basin Research*" journal. The authors are the followings: M. Corradino, F. Pepe, G. Bertotti, V. Picotti, C. Monaco & R. Nicolich.

Abstract

Fore-arc basins are segments of fore-arc regions that form structurally in response to a variety of subduction zone processes. The sedimentary infill records the complex tectono-stratigraphic evolution of basin associated with subduction system, and thus, allows deciphering the formation mechanisms of basins developed in compressional intraplate settings. We analyse these processes in the Paola Basin, a fore-arc basin of the Tyrrhenian-Ionian subduction system, by using reflection seismic profiles and bathymetric data. The Paola Basin is a NNW-SSE trending asymmetric syncline, bounded by the offshore sector of the Coastal Chain to the East and by the regional-scale Paola Anticline to the West. It hosts up to 5.5 km thick Plio-Quaternary deposits, most of them showing eastward-dipping clinoforms. These latter are associated to shelfal progradation, supplied from the north *via* longshore currents, dispersing sediments from unknown Apenninic/Sila entry points. A local circulation of longshore currents flowed southwards and dispersed sediments from unknown Apenninic/Sila entry points. An aggradational internal geometry characterizes the uppermost part of the sedimentary infill with a thickness decreasing westwards, suggesting a sediment supply from the Coastal Chain. In the Early Pliocene, the proto Paola Basin extended from the Paola Anticline up to the western flank of the Sila Massif. Since ~ 3.5 Ma, the uplift of the Coastal Chain shortened the proto Paola Basin, leading to the separation of the basin from the Crati basin. Short wavelength (~ 80 km) lithospheric buckling, caused by a ENE-WSW oriented, arc-normal paleo-stress field, is the most likely mechanism that explains the pattern of tectonic subsidence of the Paola Basin, the uplift of the Paola Anticline and part of the uplift experienced by Sila Massif during the Plio-Quaternary. Kilometre-scale, strike-slip restraining and releasing bends are widely spread over the hinge zone of the Paola Anticline, defining the Paola Ridge. Their formation is compatible with an NW-SE oriented maximum stress axis meanwhile strike-slip fault accommodates the arc-parallel component of the plate motion. The change in direction from ENE-WSW to NW-SE of the maximum stress axis in the fore-arc region is a consequence of the transition from orthogonal to oblique subduction, associated to the bending of the Northern Calabria Arc. Regional uplift and folding of the Northern Calabrian Arc induced tensile stress resulting in the formation of N-S trending normal faults in the extrados of the Sila Massif anticline. In this context, the Paola Basin can be defined as a "Neutral Accretionary-type" forearc basin.

Keywords: Calabrian Arc, Ionian Sea, Fore-arc basin, Lithospheric buckling, Longshore current

1.0 Introduction

Fore-arc basins are segments of fore-arc region that develop on the overriding plate of a subduction system between accretionary prism and volcanic island arcs. They form structurally in response to a variety of subduction zone processes (Dickinson & Seely, 1979). The sedimentary infill, resulting by interaction of tectonic process and sediment supply, records the evolution of the fore-arc basin associated with subduction processes (Laursen et al., 2002; Ryan et al., 2012).

Recently, Noda (2016) proposes a classification scheme for fore-arc basins considering both the material transfer between the two plates (accretionary or non-accretionary) and the long-term strain field in the basin (compressional or extensional) and surrounding areas.

The relative movements of the African and European plates and the subduction and retreat of the Adriatic-Ionian plate mainly controlled the Neogene to Recent tectono-stratigraphic evolution of the western and central Mediterranean (Carminati & Doglioni, 2005; Carminati et al., 1998; Faccenna et al., 2001). These movements produced regional shortening leading to the development of an accretionary wedge. From Oligocene to Pleistocene times, contractional/transpressional and extensional episodes took place within the existing portion of the accretionary wedge. Extensional tectonics resulted in the opening of back-arc basins younger towards the East (e.g. Liguro-Provençal, Vavilov and Marsili basins; Faccenna et al., 2007; Gueguen et al., 1998; Rehault et al., 1987; Carminati et al., 2004). The retreat of the Ionian plate also caused the formation of volcanic seamounts along arc-shaped structures, which become younger from West to southeast (Argnani & Savelli, 1999; Locardi, 1993; Savelli, 1988).

The fore-arc region of the Tyrrhenian-Ionian subduction system is located in the area extending from the Aeolian Arc, across the western Calabrian continental margin and the adjacent continental domain, the Calabrian arc, to the Ionian accretionary wedge (Fig.1a). The latter differ considerably in length, style of tectonic deformation and regional slope angle moving along the fore-arc region in the north- and south-east directions (Minelli & Faccenna, 2010; Polonia et al., 2011). The lithospheric setting of the "Tyrrhenian-Ionian Subduction zone" is generally illustrated through schematic cross sections in a NW–SE direction extending from the southern Tyrrhenian to the Ionian foreland (e.g. Faccenna et al., 2001; Maesano et al., 2017; Neri et al., 2009). On the contrary, the structural setting of the overriding plate in the area extending from the Paola Ridge to the Apulia Escarpment remains poorly documented.

The Paola Basin is an asymmetric syncline that contains the largest accumulation of Pliocene to present sediments of the fore-arc region (Bigi et al., 1989). The depositional sequences record various geological phenomena arising from dynamic interactions between the lower and upper plates of the Tyrrhenian-Ionian subduction system (e.g. subsidence and uplift events). Changes in depositional trends of sediments across the basin occur in response to variations in relative sea level and/or paleo-current circulation. Thus, the Paola Basin and the continental domain adjacent to its eastern part, the Northern Calabrian Arc have become areas of great interest to study the tectono-stratigraphic evolution of segments of the fore-arc region, and their relations with slab roll-back and steepening in a regime of overall convergence (e.g. Chiarabba et al., 2008; Faccenna et al., 2007).

Despite several studies conducted in the last decades (Argnani & Trincardi, 1988; Gamberi & Rovere, 2010; Guarnieri, 2006; Loreto et al., 2013; Milia et al., 2009; Pepe et al., 2010), the tectono-stratigraphic evolution, the main 3D geomorphic and depositional settings of the Paola Basin, the source areas of sediments, and the process responsible for the sediment transport are still poorly

known. Furthermore, the role of contractional, extensional and strike-slip tectonics, inside and along the flanks of the basin, is poorly understood and debated. According to Guarnieri (2006) and Milia et al. (2009), the Paola Basin segment has experienced extension during the Plio-Quaternary. In contrast, Argnani & Trincardi (1988) and Pepe et al. (2010), suggest that the subsidence of the Paola Basin is a consequence of the crustal shortening.

In our contribution, we focus on a crucial segment of the fore-arc region of the Tyrrhenian-Ionian subduction system: the Paola Basin and its western flank, the Paola Ridge. To do this, we analyze an unpublished grid of multi-channel seismic profiles and bathymetry data. Data and interpretation allow us to: a) reconstruct the 3D stratigraphic architecture and the Plio-Quaternary evolution of the basin; b) constrain the geometry and kinematics of fault systems inside the basin and along its flanks; c) quantify the vertical movements experienced by different sectors of the basin.

Integrating our results with the literature knowledge on the horizontal and vertical movements experienced by the Northern Calabrian Arc, we provide new insights in the long-term deformation processes of the fore-arc region of the Tyrrhenian-Ionian subduction zone. In addition, we define the role of a strike-slip fault zone formed along the western Calabrian margin in response to an oblique subduction. Finally, our data provide geological constrains on the evolution of "*Neutral Accretionary Type*" fore-arc basins (*sensu* Noda, 2016).

2.0 Geological background

2.1. Lithospheric Structure

Tomographic images reveal that the deep subsurface of the Tyrrhenian-Ionian subduction system is represented by the Ionian slab dipping ∼70 – 80° north-westward (Chiarabba et al., 2008; Piromallo & Morelli, 2003; Wortel & Spakman, 2000). In addition, a nearly detached subducting lithosphere is inferred beneath the north-eastern Sicily and northern Calabria may reach a depth of > 300 km (Neri et al., 2009). The Southern Tyrrhenian lithosphere is characterized by a thin mantle with very low Vs values (∼4.0–4.2 km/s) underneath the Marsili Basin (Panza et al., 2007; Frezzotti et al., 2009). On the contrary, moving toward the E and SE, the Adriatic-Ionian lithospheric mantle becomes thicker and acquires higher Vs values. Some authors (Gvirtzman & Nur, 2001) hypothesized a very thin to absent lithospheric mantle underneath the entire western Calabria continental margin. The lithosphere is ∼130 km thick in the Ionian area, (Pontevivo & Panza, 2006).

The information on the deep crustal structures refer to a deep seismic refraction profile recorded between Apulia (Salento Peninsula) and the Aeolian Islands (Morelli et al., 1975). The Tyrrhenian Moho results at ∼ 10 km depth below the Marsili Basin. It deepens eastwards from ∼ 27 km beneath the Paola Basin to ∼ 30 km beneath the Sila Massif. The Moho is at ∼ 40 km depth beneath the Apulia continental block (Salento).

2.2. The upper plate

The upper plate of the Tyrrhenian-Ionian subduction system includes the back-arc domain of the SE Tyrrhenian Sea (Marsili Basin), the Aeolian volcanic arc, the fore-arc region including the Calabrian-Peloritan Arc (CPA), and farther to the southeast the Calabrian accretionary wedge (CAW, Fig. 1a).

The Marsili Basin (MB in Fig.1a) is the youngest back-arc oceanic basin developed on the overriding plate of the subduction system during the Pleistocene (Kastens et al., 1988; Nicolosi et al., 2006). Domains of thinned continental crust (Sicilian and Calabrian continental margins) surround the spreading centre. Ring-shaped volcanoes of the Aeolian arc (AI) formed a few tens of kilometres towards east and southeast of the MB during the Quaternary (Beccaluva et al., 1985; Gillot, 1987; Santo & Clark, 1994, Fig. 1a). The calc-alkaline to shoshonitic and k-alkaline affinity of their volcanic products is related to the subduction of the Ionian slab beneath the Calabrian Arc region (Barberi et al., 1973; Beccaluva et al., 1985; Chiarabba et al., 2008; Ferrari & Manetti, 1993). The occurrence of intrusive and volcanic activity during the Pleistocene was also proved for the area between the Aeolian arc and the Capo Vaticano promontory (De Ritis et al., 2010; M. F. Loreto et al., 2015), as well as in correspondence of the northern limit of Ionian subducting slab (Cocchi et al., 2017).

The CPA is an arc-shaped segment of the Mediterranean mountain belt located between the NW-SE trending southern Apennines and the WSW-striking Maghrebian thrust belts (Fig. 1a). It is divided into two sectors consisting of different tectonic units and characterized by different tectonic evolution with opposite vertical axis rotations (clockwise and counter-clockwise rotations for the southern and northern sector, respectively) documented paleomagnetically for the Neogene to Early Pleistocene (Mattei et al., 2007). Such contrasting vertical axis rotations are not recorded by geodetic strain (GPS) with the whole CPA moving south-eastwards with velocities of 1.1–1.7 mm/yr in the Apulian reference frame (D'Agostino et al., 2011; Fig.1a).

The Quaternary uplift of the northern CPA was estimated of ~ 1 mm/yr (Carobene, 2003; Ferranti et al., 2006; 2009; Gliozzi, 1987; Molin et al., 2002), which is thought to result from dominant lithospheric process, with superposed effects of upper crustal faulting (Ferranti et al., 2006, 2007, 2010; Westaway, 1993). NW-SE trending, sinistral transpressional shear zones (Monaco et al., 1998; Spina et al., 2011; Tansi et al, 2007; Van Dijk et al., 2000) segment the northern CPA sector. Their offshore prolongations have been hypothesized both in the Tyrrhenian (Finetti, 2005; A. Milia et al., 2009) and Ionian seas (Del Ben et al., 2008; Ferranti et al., 2014). The northern CPA consists of the Coastal Chain, Sila Massif and a number of sedimentary basins both at its western (Paola and Amantea basins) and eastern sides (Sibari Plain, Crotone and Crotone-Spartivento basins; see paragraph 2.2.1). The Coastal Chain is a N-S elongated narrow mountain belt that lies between the Crati and Paola basins. The Sila Massif is a rectangular-shaped mountain range plateau up to ~1800 m high, bounded by straight flanks (Robustelli et al., 2009; Tansi et al., 2007). Apatite fission track

analysis suggests that its exhumation history is characterized by a rapid cooling of the crystalline basement rocks between 35 Ma and 15 Ma (Thomson et al., 1998; Thomson, 1994).

The Calabrian accretionary wedge is a few hundred kilometres long accretionary prism extending in the Ionian offshore and laterally confined by the WNW-ESE-trending Apulia and Malta escarpments. It is composed of a poorly resolved stack of mainly SE-verging thrust sheets with three recognized wedge portions: a pre-Messinian followed by a Messinian and finally by a Plio-Quaternary wedge (Minelli & Faccenna, 2010; Polonia et al., 2011; Bortoluzzi et al., 2017). The CAW wedge differ considerably in length, style of tectonic deformation and regional slope angle moving along the fore-arc region in the north- and south-east directions. A steep and narrow (40 - 60 km) wedge formed at the front of the Northern Calabrian Arc. On the contrary, a regular and broad (more than 250 km) wedge composed by a series of imbricate thrust slices developed at the front of the southern Calabrian Arc. The regional slope angle also decreases in the same direction.

2.2.1 Fore-arc basins

Fore-arc basins formed along the Tyrrhenian and Ionian margins of the Northern Calabrian Arc since the late Oligocene. The Paola Basin is a roughly NNW-SSE trending, ∼20 km wide asymmetric syncline developed on the Tyrrhenian side of the northern CPA sector from the Neogene to Recent times (Argnani & Trincardi, 1988; Guarnieri, 2006; Milia et al., 2009; Pepe et al., 2010). The eastern flank of the syncline coincides with the offshore prolongation of the Coastal Chain, while its western termination corresponds to the Paola Ridge, a NNW-SSE-trending morphological structure extending more than 70 km (PR in Fig. 1a). Oligocene to Quaternary sediments fill the basin (Pepe et al., 2010). Oligocene to lower Messinian deposits tend to fossilize pre-existing topography and reach, therefore, the largest thicknesses (∼1200 m) close to the (fault controlled) basement highs. On the contrary, Messinian evaporites are characterized by a constant thickness of ∼ 400 m along the whole western flank of the basin, and abruptly thicken to more than 1000 m westward to the depocenter of the Paola Basin. Plio-Quaternary deposits display substantial variations in thickness and tectonic style. They are < 800 m thick along the Paola Ridge, thicken up to 4.5 km in the depocenter of the Paola Basin, and decrease to ∼1.0 km thickness at the eastern termination of the basin (Fig. 1a). The structural evolution of the basin is controversial. Milia et al. (2009) suggested that the Paola Basin was controlled by E–W trending, normal faulting and by approximately N–S transfer faults during the Messinian–Early Pleistocene times. Folding associated with transcurrent tectonics along a NW-trending left lateral fault affected the basin during the Lower Pleistocene. Minor pull-apart basins subsequently opened during the Middle Pleistocene. Argnani and Trincardi, (1988) and more recently Pepe et al. (2010) highlight the importance of regional shortening in the development of the syncline. Generalized subsidence occurred from the Pleistocene to Recent times (Milia et al., 2009; Pepe et al., 2010). However, subsidence was not compensated by sufficient sediment input, leading to the development of the present-day bathymetry.

Few tens of km south-eastward from the Paola Basin, Upper Serravalian to Messinian deposits of the Amantea Basin are exposed along the southernmost part of the Coastal Chain (Mattei et al., 1999; 2002). The younger sequence filling these basins consists of a transgressive succession up to 80 m thick (middle Tortonian to Early Messinian).

The Crati Basin is a roughly N-S trending basin that hosted Upper Miocene to Holocene clastic marine and fluvial deposits (Fig. 1a and b). The thickness of Messinian and Lower Pliocene deposits decreases moving eastwards of the Coastal Chain, while Upper Pliocene to Quaternary deposits thicken (Colella, 1988; Spina et al., 2011). A 60-km long east-dipping normal fault controlled the evolution of the Crati Basin according to Brozzetti et al. (2017). Persistent seismic activity with medium-grade seismicity ($5.5 < M < 6$; Galli & Bosi, 2003; Spina et al., 2009) and focal mechanisms (Jacques et al, 2001; Orecchio et al., 2015; Tortorici et al., 1995; Totaro et al., 2016) agree with an extensional origin of the basin. On the other hand, Spina et al. (2011) highlight the importance of NW–SE trending left-lateral strike-slip faults active during the middle Miocene to middle Pleistocene tectonic evolution of the Crati Basin. The Sibari Plain represents the northernmost sector of the Crati Basin. Well data show that the Sibari Plain accumulated Miocene to Pleistocene deposits (Spina et al., 2011; Fig. 1b).

The Crotone Basin and its offshore prolongation, the Spartivento Basin, developed between the Serravalian and Tortonian times (Bonardi et al., 2001; Cavazza & DeCelles, 1998). The Plio-Pleistocene part of the Crotone Basin succession consists of continental, paralic, shallow-marine and deep-marine deposits organized to form unconformity-bounded strata units that in turn correspond to two main tectono-stratigraphic cycles (Zecchin et al., 2012 and references therein).

3.0 Data and methods

We based our study on the integration of geophysical datasets including a) EMODnet bathymetry data, and b) a grid of high-penetration, multi-channel seismic-reflection data (Fig. 1b).

3.1 Multibeam bathymetry

The high-resolution grid Digital Terrain Model (DTM) with cell size of ~ 200 m is a part of the EMODnet Bathymetry dataset for the European sea regions. The hill-shaded and slope gradients GeoTIFF images of the bathymetry dataset was created within GeoSuite AllWorks and Global Mapper software. The color ramp for the GeoTIFF of the marine area was scaled between the sea level and the maximum measured water depth: ambient lighting from NE (45°) at 45° above the horizon, vertical exaggeration 5.0 x.

3.2 High-penetration seismic-reflection data acquisition and processing

The seismic data used in the study area consist of eleven (~ 600 km in length) high-penetration, multi-channel seismic reflection data acquired in an E-W and NNW-SSE directions (Fig. 1b). The

Osservatorio Geofisico Sperimentale (OGS) of Trieste (Italy) with the DINMA - Univ. of Trieste and IPGP - Paris recorded the reflection seismic data in the frame of the project SINBUS. A 2975 m streamer long with 120 active channels recorded signals generated by a standard tuned air guns array totalling 60 liters. A shooting interval of 25 m allowed a 6000% coverage with 8 s records length and 2 ms sampling interval. Further comparison data have been acquired shooting a single-bubble mode operated array (Avedik et al., 1996, 1995) with 26 small standard guns accurately chosen and two GI guns (total volume: 37 liters). This arrangement directed the acquisition both to a high-frequency signature suitable for a good resolution of shallow horizons and to deep penetration (10 s the recording length with a sample rate of 4 ms). The streamer length used to acquire the single-bubble comparison data was of 3600 m including 144 active channels and a 7200% coverage after a shooting interval of 25 m.

The adopted processing sequence included the application of the following operators: amplitude recovery and signature conversion to minimum phase, spike deconvolution, velocity analysis every 1.5 km; normal move out correction; mute and 60 or 72 fold stack; wavelet shaping to zero phase. Post-stack processing utilized an FK filter; wave equation migration, time-variant filter and dynamic trace equalization. The seismic sections were converted from raster to SEG-Y format using the GeoSuite AllWorks software.

Seismo- and sequence-stratigraphic based analysis facilitated the reconstruction of the depositional architecture of seismic-stratigraphic units as well as the identification of volcanics. Following the analysis of acoustic facies, the thickness of sediment and volcanic features were derived from time to depth conversion using velocities of 1500 m/s and 2100 m/s for the water column and the Plio-Quaternary deposits, respectively. The latter value corresponds to seismic velocity analysis along the profiles and to sonic log data available for coeval deposits in wells drilled in similar offshore settings (see Pepe et al., 2010 for details).

Isopach maps of seismic units were obtained as difference between 2.5D contour maps computed from spatial interpolation of the time (ms) to depth (m) converted seismic horizons limiting at top and bottom each units.

4.0 Results

4.1 Seafloor morphology of the Paola Basin and surroundings

Almost all the tectonic structures identified on seismic profiles (see paragraph 4.4) have a bathymetric expression. Thus, the analysis of the DTM provides information on the prolongation of morpho-structures developed in the investigated area. The integration of these data with those obtained by analysing seismic profiles allows us to realize a structural-kinematic map of the Paola Basin and surrounding areas.

The Paola Basin is a NNW-SSE oriented depression that extends between the volcanic seamounts pertaining to the Ovidio volcanic field (OS) and the Santa Eufemia Gulf (SEG), bounded

to the West by the Paola Ridge (PRD) and to the East by the offshore prolongation of the Coastal Chain (Fig. 2a). Bathymetric data reveal a basin ~ 60 km long and ~ 15 km wide in the northern and central sectors to ~ 20 km to the South. The depth of the basin floor varies from ~ 400 m b.s.l. in the northern termination of the basin, to ~ 730 m b.s.l. West of the Paola village (PV and section 1 in Fig. 2b), to ~ 450 m b.s.l. in the Santa Eufemia Gulf (SEG in Fig. 2a). Here, a series of E-W oriented channels, formed along a gently (~ 3°) seaward-inclined slope, flow into the Angitola Canyon (Fig. 2a). The transition between continental shelf and slope occurs at ~ 125 m b.s.l., over a distance of ~ 5 km from the coastline (Fig. 2a and section 2 in Fig. 2b). The continental slope has an average angle of ~ 6°- 8° between the north-western edge of the Paola Basin and the Amantea village (AV in Fig. 2), while it increases up to 15° towards the South.

The Paola Ridge consists of a set of bathymetric highs (Sh in Fig. 2a) dissected by saddles and small- scale basins (sections 2 and 3 in Fig. 2b). One of these basins (PrB, Propeller Basin of Gamberi & Rovere, 2010) is NNW-SSE oriented. A flat top (Sh1) bathymetric high, which reaches 100 m b.s.l., formed on the northern sector of the PrB, gives a horseshoe shape to the basin. The PrB is surrounded by two narrow, elliptical-shape bathymetric highs, ~ 5-6 km long (Sh2 - Sh10 in Fig. 2a and profiles 2 and 3 in Fig. 2b). The highest of them (Sh2) rises ~ 500 m from the seafloor forming a steep escarpment to the North of the PrB (section 3 in Fig. 2b). A series of NW-SE oriented undulations of the seafloor are observed on top of the most of bathymetric highs. Several escarpments (es in Fig. 2a) dipping towards the West and South-West with values of 20°, 25° and 10° moving from North to South, are identified along the western part of the Paola Ridge.

4.2 Definition of seismic units

Three seismo-stratigraphic units, labelled MD, PQ and V from bottom to top (Fig. 3a and b), were identified by their bounding unconformities and described based on of their architecture and seismic characters (e.g. amplitude, lateral continuity and frequency of internal reflectors, according to Damuth, 1980).

Unit MD has subparallel, relatively continuous, medium frequency and high to moderate-amplitude reflections (Fig. 3a and b). It is bounded at the top by the well-defined, high-amplitude reflector “M” (in Fig. 3b, c and d), a horizon of regional importance associated with the top of evaporites deposited during the late Messinian salinity crisis and/or to an erosional unconformity formed during the late Messinian sea level fall (Malinverno et al., 1981, and references therein).

Unit PQ overlies the M horizon and is generally marked by layered, continuous medium to high frequency and moderate to high-amplitude reflections (Fig. 3a and b). It can be correlated with the Plio-Quaternary sedimentary succession widespread in the Tyrrhenian Sea. We have subdivided unit PQ in four subunits named PQ1–PQ4 from bottom to top, on the base of their internal geometry and unconformity surfaces recognized at top and bottom. The boundaries of these subunits are shown on the Line “Section-4” (Fig. 3c) that illustrate clearly the internal configuration and the external geometry of the subunits, as well as the eastwards reflector terminations onto against the M horizon.

Subunits PQ1–PQ4 have been identified in all seismic lines by correlating their top and bottom unconformities to the conformity surfaces.

Moderate to high-amplitude, well-defined laterally continuous reflectors characterize subunit PQ1 (Fig. 3c). An eastward progradational pattern typifies its internal structure. Onlap and downlap reflectors terminate onto the M horizon along the western and eastern side of the basin, respectively.

Moderate amplitude, continuous reflectors distinguish subunit PQ2. They slightly diverge toward the depocenter of the basin, and display a clinoform internal geometry with downlap terminations onto the subunit PQ1 (Fig. 3c). Subunits PQ1 and PQ2 are separated by an unconformity, which formed as a result of an eastwards shift of the offlap breaks of PQ2.

Subunit PQ3 shows discontinuous, moderate-amplitude reflections, which become continuous and with higher frequency content in the upper part (Fig. 3c). Subunit PQ3 consists of a series of clinoforms, which bottomsets converge towards the East and downlap the subunit PQ2 (Fig. 3e).

Subunit PQ4 is represented by sub-horizontal, discontinuous and low-amplitude reflections with parallel geometry and onlap terminations westward directed on top of subunit PQ3 (CDPs 9000-10500 Fig. 3c). It is limited upwards by the seafloor.

A stack of greatly discontinuous, medium to high-amplitude reflections (Fig. 3a and b) characterizes Unit V. The upper boundary corresponds to a high-amplitude, locally continuous reflector characterized by a rough morphology and numerous diffractions (CDPs 4500-6000, Fig. 3b). These figures can indicate the presence of volcanic rocks.

Seismic features LS are characterized by transparent to chaotic reflectors and exhibit a lens-shaped geometry. We interpret these features as mass transport deposits (CDPs 12000-14000, Fig. 3c).

4.3 3D architecture of the Paola Basin

The Paola Basin has the shape of an asymmetric syncline well-defined in the north and central sectors, from the offshore of Belvedere Marittimo to Amantea Village (BM and AV in Fig. 2). The syncline becomes more gentle southwards (Fig. 4a-d). The eastern and western flanks correspond to the offshore sector of the Coastal Chain and to a limb of a regional-scale anticline, here defined as Paola Anticline (Fig. 4a). The eastern flank varies in inclination from ~ 20° to the north (Fig. 4a) to ~ 24° in the offshore of Amantea Village (Fig. 4c) until ~10° to the South (Fig. 4d). The inclination of the western side of the basin decreases from ~ 18° in the north (Fig. 4a) to less than 4° in the Santa Eufemia Gulf (Fig. 4d).

The basin infill comprises Plio-Quaternary sediments up to 5.5 km thick, which rest above the M horizon (Fig. 4a-d). The depth of the M horizon has been estimated to vary between 1 and 2 km along the flanks of the basin, increasing in correspondence of the depocenter of the basin, where

it reaches ~ 5 - 6 km in the northern and central sectors (Fig. 4a, b and c) and ~ 3 km in the southern sector (Fig. 4d). Geometries, distributions and thicknesses of pre-Pliocene succession are less constrained by our seismic data. Thus, our research was focused on the reconstruction of the tectono-sedimentary evolution of the study area during the Plio-Quaternary time interval.

Reflectors of sub-units PQ1, PQ2 and PQ3 show an eastward-dipping clinoforms geometry with foreset steepness increasing northward up to ~20° (CDPs 7500-9000, Fig. 4a) in the central sector of the basin, and an aggradational stacking pattern in the area around the Paola Ridge (CDPs 4500-6000, Fig. 4a; 1-4500, Fig. 4b; 1-6000, Fig.4c). In the southern part of the basin, all subunits show an aggradational geometry with sub-horizontal reflectors (Fig. 4d). Along the eastern flank of the syncline, sub-units PQ1, PQ2 and PQ3 display onlap reflectors terminating onto the M horizon both in the northern (offshore of BM, Fig. 5a) and southern sectors (from offshore of AV southwards, CDPs 10500-13000, Fig. 4c; Fig. 5c). Conversely, sub-units PQ1, PQ2 and PQ3 show downlap reflectors terminating, respectively, onto the M horizon, top of PQ1 and top of PQ2, in the central sector of the basin, which corresponds to the offshore prolongation of the Coastal Chain (CDPs 10500-13500, Fig.4b; Fig.5b). Here, subunit PQ3 also displays an eastward convergent pattern of reflectors (Fig. 2e; CDPs 10500-13000, Fig. 4b).

Subunit PQ4 is characterized by parallel and sub-horizontal reflectors with onlap reflectors terminating on top of subunit PQ3 (CDPs 7500-8500, Fig. 4a; CDPs 9000-10000, Fig. 4b; CDPs 7500-9000, Fig. 4c). Submarine mass transport deposits (LS) occur in the eastern side of the basin within sub-units PQ3 and PQ4 (around CDP 12000, Fig. 4a; CDPs 10500-14000, Fig. 4b).

Along the western part of the study area, two erosional surfaces, named Ers1 and Ers2, are detected in the PQ succession. Ers1 corresponds to the top of PQ2 and extends from the western side of the Paola Ridge (CDPs 1-2500, Fig.4b) to western flank of the syncline, where cuts the clinoforms of PQ2 (CDPs 6000-7500 b in Fig.4). In addition, this surface truncates the oldest topsets of PQ3 (CDPs 7500-8000 Fig.4b). The upper erosional surface Ers2 is recognized inside the PQ3 in the western sector of the basin (CDPs 1-6500 Fig. 4b).

In the northwestern sector of the basin, Unit PQ is intruded by volcanics (Unit V) that locally reach the seafloor (CDPs 1-3000, Fig.4a; CDPs 1500-3000, Fig. 6b). Volcanic rocks have a mound-shape extending in E-W direction for about 7 km.

The isopach maps of subunits PQ1, PQ2 and PQ3 show an abruptly decreasing of thickness moving from the depocenter towards the eastern flank of the basin (Fig. 7 a, b and c). Here, the thickness of each subunit is less than ~200 m. The depocenter of the basin shifts from the western side, where PQ1 thickens up to ~1600 m (Fig. 7a), towards the North, where PQ2 reaches the thickness of ~1800 m (Fig. 7b) and, successively, towards the central sector of the basin where PQ3 shows a maximum thickness of ~2400 m. In particular, subunit PQ3 reaches the highest values of thickness, ranging between ~1800 m and ~2400 m, in a NNW-SSE elongated zone, which correspond to the offshore prolongation of the Coastal Chain (Fig. 7c). The subunit PQ4 presents a different

trend of the thickness distribution. In fact, the highest value of ~ 800 m was computed along the eastern flank of the basin (Fig. 7d), and the thickness decreases westwards reaching less than ~ 200 m in correspondence of the Paola Ridge (Fig. 7d; CDPs 45000, 6000-7000, Fig. 4a; CDPs 6000-8000, Fig. 4a).

4.4 Structural map

The Paola Basin has the shape of a wide syncline structure (Figs. 4a, b, c, 8a and b) bounded by the offshore sector of the Coastal Chain to the East and by the regional-scale Paola Anticline to the West. The basin has two axes oriented in the NNW-SSE and NE-SW directions. The Paola Anticline developed since the Late Neogene as a regional-scale NNW-SSE elongated ridge near or partly above the sea level. Evidences of kilometre scale, tectonic features, formed because of the Plio-Quaternary deformations, are observed on a ~ 60 km long, ~ 20 km wide zone corresponding to the hinge zone of the Paola Anticline. Here, seismic profiles show fault-propagating folds (Fig. 8), positive and negative flower structures, and normal faults (Fig. 9a, b, and c).

Positive flowers structures are associated with transpressive faults that offset MD and PQ deposits, and as a whole, depict a ~ 4-5 km wide anticline. Faults have tens to hundred meters offset, and typically converge at depth into high-angle faults (Figs. 7b, 7d and 9a). High-angle normal faults, dipping ~ 50°–60° to the East and West, offset PQ sediments in the maximum curvature zone of the positive flower structures (Fig. 9c). Most of them reach the seafloor. The convex upwards morphology of the seafloor above the positive flower structures, and the divergent pattern of reflectors inside PQ4 deposits close to them (Fig. 9a), suggest that these tectonic features are still active.

Negative flower structures are associated with transtensive faults forming kilometres scale, graben-like structures. They developed in the surroundings of the positive flower structures (Fig. 9b; around CDP 6000 in Fig. 4a; CDPs 1500-5000 in Fig. 4b; CDPs 9000-10500 in Fig. 7b). One of them consists of several normal faults, dipping ~ 50°- 60° inwards of the graben, which corresponds to the southern limb of the Propeller basin (Fig. 9b). Overall, positive and negative flower structures produce a series of bathymetric highs (Shs in Fig. 2a) and lows on the seafloor along the Paola Ridge (Fig. 9).

Opposite fault-propagation folds, dipping towards the SE are detected in the north-eastern side of the Paola Ridge (Fig. 8). These faults cut the PQ deposits at different levels, and form ramps with a dip in the range of ~ 20 - 50°. Above the N-dipping, ramp upper tips some high-angle (~ 70°) normal faults formed.

Normal faults dipping ~ 60° to the West and South-West, offset MD and PQ deposits, with displacements ranging from ~ 200 m to ~ 600 m (around CDP 1500 in Fig. 4d; Fig. 9c), along the south-western side of the Paola Ridge.

A structural-kinematic map of the investigated area obtained from correlation of tectonic features inferred on seismic profiles and morpho-structures recognized on the DTM is shown in Fig. 9d. The map highlights the positive flowers structures, which are mainly elongated in the range from N115° and N145°. The fault-propagation folds are verging in the ~ N315° direction, which is approximatively perpendicular to the direction of most of normal faults. Overall, they developed over the hinge zone of the Paola Anticline, defining the so-called Paola Ridge. The formation of such structures is compatible with a NW-SE oriented maximum stress axis (Fig. 9e).

4.5 Plio-Quaternary evolution of the Paola Basin and adjacent segments of the fore-arc region

A model for the evolution of the Paola Basin from the Pliocene to Recent was reconstructed based on of the architecture of the basin and on the stratigraphic and paleo bathymetric interpretation inferred from the analysis of seismic facies. The evolution is summarized in four cross-sections displaying geometries and thickness of the Plio-Quaternary deposits inside the Paola Basin soon after the beginning of the Messinian stage (Fig. 10a) and at moments corresponding to the top of PQ2, PQ3 and PQ4 (Fig. 10b, c and d). To represent the sections, we have: (1) removed the sediments younger than the time step; (2) predicted the paleobathymetry; (3) "hanged" to the paleobathymetric profile the underlying part of the section inclusive of thicknesses of sedimentary bodies and their internal geometry.

The stratigraphic age of the unconformities bounding the PQ subunits is unknown for the lack of direct information, such as wells. However, an attempt to infer the age for the top of subunit PQ3 can be done by correlating the Ers1 and Ers2 erosional surfaces to the lowstand of the sea-level calibrated at 3.75 to 3.5 Ma, and 2.85 to 2.6 Ma, respectively (Fig. 10e: see Capozzi & Picotti, 2003 for details). A further assumption considers that the sedimentation rate should not fluctuate trough time, at the scale of hundreds kyr. Because of the lack of density and lithology data, sediments thicknesses have not been corrected for compaction. The measure of the sedimentation rate for PQ2 subunit from 3.5 to 2.85 Ma, in the depocenter gives a value of ~ 0.5 mm/yr, similar to other Pliocene settings of the Mediterranean (e.g. Capozzi and Picotti, 2003). Applying the same rate to the subunit PQ3, we provide an age for the bottom of the subunit PQ4 of ~ 2.2 Ma.

Based on the reconstruction of the 3D architecture of the basin, and integrated with stratigraphic and geomorphologic data available in literature, we propose a model for the Plio-Quaternary evolution of the fore-arc region of interest. The evolution is summarized in three paleogeographic maps representing the geological setting at the ages of the top of PQ2 (Fig. 11a), of PQ3 (Fig. 11b), and of PQ4 (Fig. 11c).

4.5.1 Plio-Quaternary evolution of the Paola Basin and adjacent segments

The Early Pliocene development of the Paola Basin sea-floor morphology is not well constrained. We assume a generally flat sea bottom in the central and eastern sectors of the proto Paola Basin, based on the rather constant thickness of Messinian sediments, and the lack of major erosional and deformational features. At that time, the proto Paola Basin extended from the Paola Anticline until the western flank of the Sila Massif, including the area of the present-day Coastal Chain and the Crati Basin that represented the distal part of the Paola Basin progradational system (Fig. 10a). The eastward thinning of these sediments in the Crati Basin (Spina et al., 2011) agrees with this hypothesis. In our paleogeographic reconstruction the water depth increases from the Paola Anticline eastwards (Fig. 10a).

Starting from the Messinian, a generalized subsidence created the accommodation space necessary for the deposition of a series of east-dipping clinoforms of subunits PQ1 and PQ2, with their foreset-strike parallel to the paleo-coastline along the Paola Anticline, formed over tens of kilometres (Fig. 10b). The prograding system was confined between the offshore of the Southern Apennines and West the Amantea Basin (Fig. 11a). The latter sectors were uplifted during this time interval (Fig. 11a) as documented by the PQ1 and PQ2 reflectors onlapping onto the M horizon (Figs. 5a and c). This scenario agrees with apatite fission track data that indicate a late Miocene (<10 Ma) onset of exhumation of previously deeply buried rocks in the southern Apennines (Mazzoli et al., 2008 and references therein) and with the end of extensional tectonics in the Amantea Basin during the Early Pliocene (Mattei et al., 2002). Conversely, in the basinal area between the Southern Apennines and Amantea, reflectors of units PQ1 and PQ2 display tilted downlap terminations (Fig. 5b), suggesting that this sector was still not uplifted at this stage (Figs. 10b, 11a). To the West, the Paola Ridge started to develop as an elongated ridge associated with strike-slip tectonics. Left-lateral strike slip fault systems were active to the East, in the area of the present Northern Calabrian Arc and surroundings (Fig. 11a).

The western flank of the Paola Basin remains above sea level during the falling stage and lowstand of sea level occurred from 3.75 and 3.5 Ma. The deposition of eastward prograding sediments continued in the central sector of the basin and formed the clinoforms of the unit PQ3 (Fig. 10c). An erosional surface developed on the uppermost part of the PQ2 as well as on the oldest clinoform topsets of PQ3 (Ers 1 in Fig. 10c). During the formation of PQ3, the amount of subsidence increased in the central sector of the proto Paola Basin (Fig. 6c). The convergent pattern of PQ3 reflectors towards the East suggests that its deposition occurred during the uplift of the eastern flank of the basin (Figs. 10c, 11b). Therefore, the uplift of the Coastal Chain is slightly older than 3.5 Ma. The growth of the Coastal Chain led to the separation of the proto Paola Basin into two sectors corresponding to the Paola and Crati basins (Figs. 10c and 11b). The eroded Coastal Chain became the source area supplying sediments to the Crati and Paola basins. Likewise, the uplift rate of the Sila Massif increased during the Late Pliocene (Olivetti et al., 2012). Consequently, the Northern

Calabrian Arc formed as we presently see and normal faults grew along the flanks of the Crati Basin (Fig. 11b).

The deposition of sediments pertaining to the subunit PQ4, which is characterized by an aggradational geometry in the whole area (Figs. 4a-d and 11c), started at ~ 2.20 Ma (Figs. 10d and 11c). The sediments were supplied by the Coastal Chain, as indicated by the westward decrease in thickness of subunit PQ4 (Fig. 6d). During this time interval the Paola Anticline deepened as consequence of the generalized subsidence that affected the western sector of the continental margin in the final evolutionary stage of the Tyrrhenian Sea, likewise due to oceanic crust cooling in the Marsili Basin (Pepe, Bertotti, & Cloetingh, 2004, and references therein). Differential subsidence was locally accounted by the formation of normal faults to the West of the Paola Ridge, predominantly dipping ~ 60° to the West and South-west (around CDP 1500 in Fig. 4d and Fig. 9c).

Finally, submarine volcanoes (V in Figs. 3b and 4a) formed in the north-western sector of the Paola Basin, in correspondence of an E-W striking tear faults delimiting the northern side of the Ionian Sea-Calabrian Arc subduction (Cocchi et al., 2017b).

4.6 Role of sediment loading and tectonic subsidence

Part of the subsidence that created the Paola Basin is due to the load exerted by the sediments deposited in the area. Using standard equations (Allen & Allen, 1990) with the following parameters: ρ_{Mantle}=3.3 g/cm^3, ρ_{Crust}=2.8 g/cm^3, $\rho_{Sediments}$=2.253 g/cm^3, ρ_{Water}=1.03 g/cm^3, and a local isostatic compensation approximation, we have calculated the position of the M reflection in the absence of sediments of the unit PQ, which is in a water-loaded. This method allowed us to separate the sedimentary loading and the tectonic subsidence from the total subsidence. In our analysis, the total subsidence was computed from the present-day depth of the M reflection, with the sedimentary load and water column, by assuming that most of the area presently corresponding to the Paola Basin and its western prolongation was at shallow water or emerged during the Messinian time. We also consider that in the depocenter of the proto Paola Basin the maximum water depth was of about 500 m during this time interval (see previous section). This assumption implies that the computed values of the tectonic subsidence are the highest that can be reached in the whole area, but it has no consequences in the computation of the Plio-Quaternary sedimentary loading because it was quantified by subtracting the depth values of the M reflector calculated in the absence of sediments from those presently measured. Finally, the values representing the total, sedimentary and tectonic subsidence were interpolated onto 2000-m-spaced cells, using the kriging gridding method.

The plot of Figure 12a, shows that in the Paola Basin the higher subsidence is restricted within an area oriented NNW-SSE. In particular, the highest value of ~ 3.9 km is reached in the depocenter of the basin, while it decreases west- and east-wards toward the flanks of the basin. Within the same area, the highest sedimentary subsidence due to the load exerted by the Plio-Quaternary sediments is of ~ 2.0 km (Figure 12b). Thus, tectonic processes are needed to cause differential

vertical movements in the Paola Basin and surrounding area, varying from few hundred meters in the flanks of the basin to > 2.2 km in the depocenter of the basin (Figure 12c).

5.0 Discussion

5.1. Sediment provenance and transport

The prograding systems developed within the Paola Basin during the Pliocene and the early Pleistocene suggests that a local counterclockwise pattern of longshore currents should have developed in the restricted gulf among the Sila and the Paola anticline, and the Apennines to the North (Fig. 11a). In our paleogeographic reconstruction, the Pliocene and Early Pleistocene Paola Anticline was integrated with the Southern Apennines and maybe the Sila shelves, protruding into the Tyrrhenian sea and allowing longshore currents to disperse sediments southward, supplied from unknown Apennine/Sila entry points. Thus, the eastward dipping clinoforms, bordering to the east the Paola Ridge, represent the basinward progradation of the shelfal system supplied by locally south-flowing longshore currents. Conversely, in the southern part of the proto-Paola Basin, where the Paola Ridge ended, clinoforms did not form and sediments deposited with an aggradational internal pattern (Fig. 4d). The sinking of the Paola Ridge ended the local anticlockwise gyre of longshore currents and, as a consequence, the dispersal of sediment from the north to form the eastward progradation (Fig. 11c). The formation of clinoforms on shelf margins far from the main entry points can be associated with sediment transport dominantly subparallel to the coastline (e.g. Cattaneo et al., 2003). A similar progradational pattern of the shelf deposits, perpendicular to the effective direction of the current, was documented for the western Adriatic shelf (Cattaneo et al., 2003; 2007), the western Yellow Sea (Liu et al., 2007; Qiu et al., 2014), the Guadix Basin, southern Spain (Puga-Bernabéu, 2010) and the Western Interior Seaway of North America (Li & Schieber, 2018; Slingerland & Keen, 1999).

5.2. On the crustal folding of the fore-arc region

The previous results integrated with data derived from the published Crop M27 profile (Pepe et al., 2010, Fig. 13b) show the Paola Basin as a deforming synform, bounded to the West by the NNW-SSE elongated Paola Anticline (Fig. 13a). On land, East of the Paola Basin, the Digital Elevation Model shows that the Sila Massif is a convex-upward, regional-scale, topographic high, with long axis oriented in the same direction of the Paola Anticline (Fig. 13a).

Messinian to early Pleistocene extensional regime controls the subsidence history of the Paola Basin according to Guarnieri et al. (2006) and Milia et al. (2009). However, extension is an unlikely mechanism for the formation of the basin because divergent geometry and large normal faults, usually associated with extension and crustal thinning, are not observed in our data set. Thus, other processes are required to explain the formation and evolution of the basin during the Plio-Quaternary interval. Lithosphere folding or buckling resulting from shortening is a potential

alternative mechanism (Burg & Podladchikov, 2000; Cloetingh & Burov, 2011; Lambeck, 1983; Stephenson & Cloetingh, 1991). Short wavelength (~ 80 km, Fig. 13c) lithospheric buckling, resulting from ENE-WSW-oriented compressive stress field, can explain: a) the lack of significant normal faults bordering the basin; b) the development of ridges (Paola Anticline and Sila Massif) and deep basin (Paola Basin) with parallel long axes; c) the preservation of their relative positions that do not change over time. Buckling of the lithosphere is expected to exert first-order control on basin formation and tectonic subsidence, which is about the 50% of the total subsidence recorded within the basin (see paragraph 4.6), as well as for a component of uplift experienced by the Sila Massif since the Neogene time.

To initiate buckling of the lithosphere, in-plane compressional stresses and a higher degree of interplate coupling are required (Cloetingh & Burov, 2011 and references therein). In the region of interest, high level of stress can be induced by the frontal accretion and retreat of the Apulian-Ionian domains. Thus, the orientation of the maximum compressional stress had to be approximatively orthogonal to the trench as suggested by the parallel long axis of Paola Anticline, Paola Basin and Sila Massif (Fig. 9f) and the present-day N130E-oriented trench inferred from seismic data (Doglioni et al., 1999).

The undulation of the M horizon (Fig. 13e) suggests a lithosphere folding active since the Miocene times. Large-scale folds with long-axes oriented in the same direction of the ridges and basins also developed in the central and southern Adriatic domains during the same time interval (Bertotti et al., 2001). Therefore, lithosphere folding can be considered a mechanism responsible for the crustal folding in a large sector of the fore-arc region of the Tyrrhenian-Ionian subduction system.

5.3. Regional stress variation during the Plio-Quaternary

In the region of interest, lithospheric buckling resulting from ENE-WSW oriented compressive stress field resulting from trench orthogonal compression. Instead, the orientation of the tectonic features associated with strike-slip restraining and releasing bends defining the Paola Ridge suggests that the maximum horizontal stress responsible for their formation was approximately oriented in the NW-SE direction (Fig. 9d and e). Furthermore, GPS velocity fields in the Apulian plate reference frame indicate that the Calabrian Arc moves in the N110E direction with velocities of 1.1–1.7 mm/yr (D'Agostino et al., 2011). Therefore, these data coherently indicate that the orientation of the regional intraplate stress field in the upper plate of the Tyrrhenian-Ionian subduction system varies through time. Change in direction and magnitude of the stress field in the fore-arc region of interest can result from the transition from orthogonal to oblique subduction resulting in the partitioning of strain into trench-parallel and trench-normal tectonics (insets in Fig. 13c). Thus, we propose that trench-parallel tectonics was responsible for: i) the formation of the NNW-SSE strike-slip zone (Paola Ridge) on the hinge zone of the Paola Anticline; ii) the syncline within the Paola Basin with axis oriented in the NE-SW direction; iii) the NW-SE trending zones of strike-slip deformation in the Northern

Calabrian Arc (e.g. Tansi et al., 2007; Van Dijk et al., 2000), as well as in the Gulf of Taranto along the Amendolara Ridge (Ferranti et al., 2014).

5.4. On the Quaternary uplift of the Northern Calabria Arc

The Quaternary uplift of the Northern Calabria Arc was estimated of ~ 1 mm/yr (Luigi Ferranti et al., 2006 and references therein). By considering that buckling of the lithosphere is not expected to produce the total vertical movement experienced by the Northern Calabrian Arc during the Quaternary, other processes must be invoked. Analogue experiments of material transfer in accretionary wedge have demonstrate that high basal friction produces a cyclic behaviour of alternating frontal accretion and underthrusting of lower plate material underplating beneath the backstop (Gutscher et al., 1998). The SW–NE cross-section constructed across the back- and fore-arc region of the Tyrrhenian-Ionian subduction system (Fig. 13d) shows that the thickness of the crust beneath the Northern Calabria Arc increases moving to the East of the Paola Basin and it reaches the maximum value beneath the Sila massif (Fig. 13d). A comparison of high basal friction analogue experiments (Kukowski et al., 2002) with this segment of the fore-arc region lead us finding geometric similarities. Thus, we propose that overriding plate experienced periods of high basal friction producing an alternation of frontal accretion and underthrusting of lower plate material underplating beneath Northern Calabrian Arc.

The thickening of the crust implies deviation from isostatic equilibrium and consequent vertical adjustment. Furthermore, seismic tomography and deep earthquake distribution indicate that beneath the N-Calabrian Arc the slab is detached from its upper part also causing isostatic rebound (Westaway, 1993; Wortel & Spakman, 2000). Therefore, three independent processes act at regional scale during the Plio-Quaternary with variable rates to control deformation and uplift of the N-Calabrian Arc, respectively: buckling of the lithosphere, underplating/underthrusting, and isostatic rebound.

5.5. Tensile stress induced by long-wavelength folding of the lithosphere

To discuss the tensile stress induced by long-wavelength folding of the lithosphere across the Northern Calabria Arc, we constructed an upper crustal cross-section (Fig.13e). It shows the geometries and thickness of the Plio-Quaternary deposits inside the Paola and Crati basins, the main transcurrent fault zones and the normal faults bordering the Crati Basin (Brozzetti et al., 2017; Spina et al., 2011 and references therein). To visualize the Plio-Quaternary vertical movements of this fore-arc region the M horizon is used as reference. It is plotted at the Messinian and at Present times by considering the topography of the Calabrian Arc and flexure modelling results derived by applying a horizontal load to a beam. Results suggest that extensional fiber stresses are expected in the extrados above the middle-plane of the beam. The tectonic interpretation of flexure experiments is that the continental crust the Northern Calabria Arc in the extrados of the large anticlines is bent

enough to cause faulting. Thus, we consider the N-S trending normal faults flanking the Crati Basin as an effect of these bending stresses.

In the hinge zone of the Calabrian Arc, normal faults activity started during the Top PQ3 time interval (Fig. 11c), and persisted through the Top PQ4 time interval (Fig. 11d) allowing the Crati Basin deepening and widening eastward. Field and seismological data coherently indicate that this fault system is still active (Brozzetti et al., 2017; Cianflone & Calabria, 2015; Orecchio et al., 2015; Spina et al., 2011; Tortorici et al., 1995).

5.6 The Paola Basin in the new classification scheme for fore-arc basins

Strike-slip deformation systems develop only along the hinge zone of the Paola Anticline and over the N-Calabrian Arc (Fig. 13e). On the contrary, the Plio-Quaternary sedimentary infill of the Paola Basin shows weak deformation (Figs. 4, 7 and 8) as suggested by the less than 5×10^{-2} compressional strain computed by applying the constant line length restoration method at the M horizon (Table 1). Similar structural setting was documented for fore-arc basins developed in oblique subduction systems, such as the Tofino and Eel River basins along the Cascadia margin (Gulick et al., 2002; Spence et al., 1991), the Atka basin along the Aleutian arc (Ryan et al., 2013), the Valparaiso basin along the central Chile margin (Laursen et al., 2002) and the Simeulue basin along the Northern Sumatra arc (Shulgin et al., 2013). According to Noda (2016), oblique subduction may lengthen rather than widen the basin along the outer-arc high, which represents the uplift sector of the outer wedge. The occurrence of this process is indicated by the migration of the depocenter of the basin. Our data shows that the depocenter of the Paola Basin tends to keep its cross-sectional position (Fig. 4a, b and c), but shifts parallel to the Coastal chain (Fig. 6a, b and c). A similar evolution was documented for the Sumatra and Valparaiso arc fore-arc basins (Noda, 2013; Laursen et al., 2002). Therefore, we propose that the Paola Basin can be classified as a "Neutral Accretionary-type" fore-arc basin (*sensu* Noda, 2016) on the basis of the oblique subduction, of the major strike-slip faults found in the areas adjacent the basin, and of the weak deformation of sedimentary infill.

6.0 Conclusions

The interpretation of a grid of high-penetration reflection seismic profiles provides new insights into the 3D architecture and the Plio-Quaternary evolution of the Paola Basin. Our results, integrated with data derived from the literature are relevant for the understanding of the long-term deformation processes of the fore-arc region of the Tyrrhenian-Ionian Subduction System. The main outcomes can be summarized as follows:

1) The Paola Basin is a NNW-SSE trending asymmetric syncline developed in the fore-arc region of the Tyrrhenian-Ionian subduction system. In the Early Pliocene the proto Paola Basin extended from the regional-scale Paola Anticline until the western flank of the Sila Massif. Since 3.5 Ma, the uplift of the Coastal Chain led to the separation of the proto Paola Basin into two

subsiding sectors corresponding to the Paola and Crati basins. Presently, the eastern and western flanks of the Paola Basin correspond to the offshore sector of the Coastal Chain and the eastern limb of the Paola Anticline, respectively.

2) The Paola Basin consist of up to 5.5 km thick Plio-Quaternary deposits, most of them (sub-units PQ1, PQ2 and PQ3) showing an eastward-dipping clinoforms geometry. The prograding systems suggest that a local counterclockwise pattern of longshore currents should have developed in the restricted gulf between the Sila Massif and the Paola Anticline, and the Apennines to the north. Until ~ 2.2 Ma, the south-flowing longshore currents were responsible for dispersing sediments, supplied from unknown Apennine/Sila entry points. Subsequently, the Coastal chain provided sediments to the basin as indicated by the aggradational internal geometry of the uppermost deposits (sub-unit PQ4).
3) Short wavelength (~ 80 km) lithospheric buckling, resulting from ENE-WSW-oriented compressive paleostress, is the mechanism that better explain the tectonic subsidence of the Paola Basin as well as the uplift of the Paola Anticline since the Miocene. Furthermore, this mechanism exerts a first-order control on the uplift of the Sila Massif.
4) Tensile stress from uplift of the Northern Calabrian Arc was responsible for the formation of N-S trending normal faults along the extrados of the Sila Massif anticline. These faults bound the Crati Basin and allow its widening through time.
5) Kilometre scale, flower structures, fault-propagation folds and normal faults formed along the hinge zone of the Paola Anticline, defining the Paola Ridge. The formation of such structures is compatible with a NW-SE oriented maximum stress axis, which is parallel to the present-day trench direction in the eastern offshore of the Northern Calabrian Arc. The change in direction of the maximum stress axis from ENE-WSW to NW-SE is a consequence of the transition from orthogonal to oblique subduction resulting in the partitioning of strain.
6) Given the weak deformation of the sedimentary infill and the strike-slip deformation of its boundaries, associated with oblique component of subduction, the Paola Basin can be defined as a “Neutral Accretionary-type” fore-arc basin (*sensu* Noda, 2016).

Captions

Figure 1. (a) Schematic tectonic map of the Tyrrhenian-Ionian subduction system. AEFS: Alfeo-Etna Fault System; AI: Aeolian Islands; AP: Apulian block; CAW: Calabrian accretionary wedge; CrSB, Crotone-Spartivento Basin; HB: Hyblean block; MB: Marsili Basin; N-CPA: Northern Calabria Arc; Os: Ovidio seamounts; PR: Paola Ridge; Ps: Palinuro seamounts; SCA: southern Calabria Arc; SEG: Santa Eufemia Gulf; SFS: Sangineto fault system; TG, Taranto Gulf; TL: Tindari-Letojanni fault. Inset shows the location of the area. (b) Geological sketch map of the Northern Calabrian Arc (after Monaco et al., 1998; Van Dijk et al., 2000, and Tansi et al., 2007) with location of the seismic dataset used in this study. 1: Continental and marine deposits (Holocene-upper Pleistocene); 2: Terrigenous marine deposits (Pleistocene-upper Pliocene); 3: Marine deposits and calcarenites (lower Pliocene); 4: Marine deposits: clays, sandstone and evaporites (Messinian-upper Tortonian); 5: Apennines carbonate units; 6: Igneous and continental-derived metamorphic units; 7: Ophiolitic units; 8: Longobucco cover and Paludi Formation (Paleogene-Mesozoic).

Figure 2. (a) Morpho-bathymetric map of the Paola Basin and surroundings. AV: Amantea Village; BM: Belvedere Marittimo Village; es: escarpment; PrB: Propeller basin; PRD: Paola Ridge; PV: Paola Village; SEG: Santa Eufemia Gulf; Sh: Structural high. (b) Bathymetric profiles across the Paola Basin. ICS: inner continental shelf; ICSB: inner continental shelf break; VE: vertical exaggeration.

Figure 3. (a), (b) and (c) Seismo-stratigraphic units (MD, PQ and V), and subunits (PQ1, PQ2, PQ3 and PQ4) recognized on seismic profiles. Insets show the location of the profiles. LS, Landslide. (d) and (e) display parts of the Section 4 at small scale.

Figure 4. Depth-converted EW profiles and their interpretation. MD, Upper Miocene deposits; PQ, Plio Quaternary deposits, PQ1, PQ2, PQ3 and PQ4 subunits recognized on seismic profiles; V, Volcanics; Ers1 and Ers2: erosional surfaces. Insets show the location of the profiles. Grey pins indicate the restoration pin lines.

Figure 5. Lateral terminations of the Plio-Quaternary deposits onto the eastern flank of the Paola Basin. BM: Belvedere Marittimo village; PV: Paola Village; AV: Amantea Village. See Figs. 3b, 4b and 4d for location of box a, b and c, respectively. Vertical exaggeration 1:2.

Figure 6. Depth-converted "Section-11" profile and its interpretation. PQ1, PQ2, PQ3 and PQ4: subunits recognized on seismic profiles. Inset shows the location of the profile. Vertical exaggeration 1:2.

Figure 7. (a), (b), (c), and (d) Isopach maps of subunits PQ1, PQ2, PQ3 and PQ4. PV: Paola Village; AV: Amantea Village.

Figure 8. Depth-converted profiles “Section-9” and “Section-10” and their interpretation. PQ1, PQ2, PQ3 and PQ4 subunits recognized on seismic profiles. Insets show the location of the profiles. No vertical exaggeration.

Figure 9. Morpho-structural map of the Paola Basin and surroundings. PRD: Paola Ridge; PV: Paola village; AV: Amantea village. Transpressive, transtensive and normal faults that, overall, form the Paola Ridge are shown in the boxes (a), (b) and (c), respectively. (e) and (f) Orientation diagrams of principal stress axes as derived from structural and kinematic data. PDZ, Principal displacement zone; VE: vertical exaggeration.

Figure 10. (a) Sketch of the proto Paola Basin at the end of the Messinian (Late Miocene). (b), (c) and (d) Stages of the Plio-Quaternary evolution of the Paola Basin corresponding to the deposition of subunits PQ2; PQ3, and PQ4. LS, Landslide; Ers1 and Ers2: erosional surfaces; sl, sea level. See Fig. 11a, b and c for location of sections b, c and d, respectively. No vertical exaggeration. (e) Schematic accumulation rate (AR) plot for the subunits PQ1- PQ4 derived from their thickness and ages assumed for the erosional surfaces (Ers). Inferred age of the top of subunit PQ3 is also reported. The circle in the inset indicates the location.

Figure 11. Plan view evolutionary model of the interest fore-arc region at the ages of the top of PQ2 (box a), PQ3 (box b), and PQ4 (box c).

Figure 12. Plio-Quaternary (a) total, (b) sediment loading and (c) tectonic subsidence map of the M horizon in the Paola Basin.

Figure 13. (a) Schematic tectonic map showing the northern trench, the accretionary wedge (CAW) of the Tyrrhenian-Ionian subduction system and the axis directions of the Paola anticline (PA), Sila Massif (SM) and Paola synclines. The contour level curves from 1300 a.s.l up to 1700 a.s.l of the Sila Massif are shown in inset 1. (b) Crop M27 profile showing the regional-scale Paola Anticline (modified from Pepe et al., 2010). (c) Sketches of the effects of lithospheric buckling and shearing in the early and late stages of deformation of the proto Paola Basin and surroundings. Insets show the direction of the Tyrrhenian plate (TP) motion vector. (d) Schematic cross-section showing the lithospheric structure across the back- and fore-arc regions of the Tyrrhenian-Ionian subduction system. Structure of the crust based on the results of the DSS seismic refraction data (Morelli, 1975), and the time to depth converted and gravity modelled Crop M27 profile (modified from Pepe et al., 2010). Abbreviations: MB, Marsili Basin; COB, Continent oceanic boundary; VA, Volcanic Arc; PA, Paola anticline; PB, Paola Basin; CB, Crati Basin; oc, Oceanic crust; cc, continental crust. (e) The position of the reference M horizon along the Paola Basin and Northern Calabrian Arc at the Messinian time and at the present-day. Data were derived from the Line Section 4 and by Spina et

al., 2011. The positions of the main transcurrent fault zone are also shown. V.E., Vertical exaggeration. Location of sections (d) and (e) are shown in box (a).

Table 1. Crustal shortening across the Paola Basin based on the M horizon recognized of seismic profiles. Lprd, pre-defromation length of the M horizon; Lpd, post-deformation length of the M horizon; S, Shortening percentage.

Acknowledges

Interpretation of seismic profiles and isopach maps of seismic units were performed within the GeoSuite AllWork software package. This study has been partly funded by the Ministero degli Affari Esteri e della Cooperazione Internazionale (Italy), in the frame of EPAF Project.

References

Acocella, V. (2008). Activating and reactivating pairs of nested collapses during calderaforming eruptions: Campi Flegrei (Italy). *Geophysical Research Letters*, *35*(17), 1–5. https://doi.org/10.1029/2008GL035078

Acocella, V. (2010). Evaluating fracture patterns within a resurgent caldera: Campi Flegrei, Italy. *Bulletin of Volcanology*, *72*(5), 623–638. https://doi.org/10.1007/s00445-010-0347-x

Acocella, V., Cifelli, F., & Funiciello, R. (2000). <Acocella et al. Analogue models of collapse calderas and resurgent domes.pdf>, *104*, 81–96. https://doi.org/10.1016/S0377-0273(00)00201-8

Acocella, V., & Funiciello, R. (1999). The interaction between regional and local tectonics during resurgent doming: the case of the island of Ischia, Italy. *Journal of Volcanology and Geothermal Research*, *88*(1–2), 109–123. https://doi.org/10.1016/S0377-0273(98)00109-7

Acocella, V., Funiciello, R., Marotta, E., Orsi, G., & De Vita, S. (2004). The role of extensional structures on experimental calderas and resurgence. *Journal of Volcanology and Geothermal Research*, *129*(1–3), 199–217.

Allen, P. A., & Allen, J. R. (1990). Basin analysis: principles & applications: Blackwell Science. Oxford, UK.

Argnani, A., & Savelli, C. (1999). Cenozoic volcanism and tectonics in the southern Tyrrhenian sea: Space-time distribution and geodynamic significance. *Journal of Geodynamics*, *27*(4–5), 409–432. https://doi.org/10.1016/S0264-3707(98)00025-8

Argnani, A., & Trincardi, F. (1988). Paola slope basin: evidence of regional contraction on the eastern Tyrrhenian margin. *Memorie Della Società Geologica Italiana*, *44*, 93–105.

Avedik, F., Hirn, A., Renard, V., Nicolich, R., Olivet, J. L., & Sachpazi, M. (1996). "Single-bubble" marine source offers new perspectives for lithospheric exploration. *Tectonophysics*, *267*(1–4), 57–71.

Avedik, F., Nicolich, R., Hirn, A., Maltezou, F., McBride, J., & Cernobori, L. (1995). Appraisal of a new, high-energy and low-frequency seismic pulse generating method on a deep seismic reflection profile in the Central Mediterranean Sea. *First Break*, *13*(7), 277–290.

Barberi, F., Gasparini, P., Innocenti, F., & Villari, L. (1973). Volcanism of the southern Tyrrhenian Sea and its geodynamic implications. *Journal of Geophysical Research*, *78*(23), 5221–5232.

Battaglia, M., Troise, C., Obrizzo, F., Pingue, F., & De Natale, G. (2006). Evidence for fluid migration as the source of deformation at Campi Flegrei caldera (Italy). *Geophysical Research Letters*, *33*(1).

Beccaluva, L., Gabbianelli, G., Lucchini, F., Rossi, P. L., & Savelli, C. (1985). Petrology and K/Ar ages of volcanics dredged from the Eolian seamounts: implications for geodynamic evolution of the southern Tyrrhenian basin. *Earth and Planetary Science Letters*, *74*(2–3), 187–208.

Bellucci, F., Woo, J., Kilburn, C. R. J., & Rolandi, G. (2006). Ground deformation at Campi Flegrei, Italy: implications for hazard assessment. *Geological Society, London, Special Publications*, *269*(1), 141–157.

Berardino, P., Fornaro, G., Lanari, R., & Sansosti, E. (2002). A new algorithm for surface deformation monitoring based on small baseline differential SAR interferograms. *IEEE Transactions on Geoscience and Remote Sensing*, *40*(11), 2375–2383.

Bertotti, G., Picotti, V., Chilovi, C., Fantoni, R., Merlini, S., & Mosconi, A. (2001). Neogene to quaternary sedimentary basins in the South Adriatic (Central Mediterranean): Foredeeps and lithospheric buckling. *Tectonics*, *20*(5), 771–787. https://doi.org/10.1029/2001TC900012

Bigi, G., Castellarin, A., Catalano, R., Coli, M., Cosentino, D., Dal Piaz, G. V, … Praturlon, A. (1989). Synthetic structural-kinematic map of Italy, scale 1: 2.000. 000. *CNR, Progetto Finalizzato Geodinamica, Roma*.

Bonardi, G., Cavazza, W., Perrone, V., & Rossi, S. (2001). Calabria-Peloritani terrane and northern Ionian sea. In *Anatomy of an orogen: The Apennines and adjacent Mediterranean basins* (pp. 287–306). Springer.

Bortoluzzi, G., Polonia, A., Torelli, L., Artoni, A., Carlini, M., Carone, S., … Stanghellini, G. (2017). Styles and rates of deformation in the frontal accretionary wedge of the Calabrian Arc (Ionian Sea): Controls exerted by the structure of the lower African plate. *Italian Journal of Geosciences*, *136*(3), 347–364. https://doi.org/10.3301/IJG.2016.11

Bottiglieri, M., Falanga, M., Tammaro, U., De Martino, P., Obrizzo, F., Godano, C., & Pingue, F. (2010). Characterization of GPS time series at the Neapolitan volcanic area by statistical analysis. *Journal of Geophysical Research: Solid Earth*, *115*(B10).

Branney, M. J., & Kokelaar, P. (1994). Volcanotectonic faulting, soft-state deformation, and rheomorphism of tuffs during development of a piecemeal caldera, English Lake District. *Geological Society of America Bulletin*, *106*(4), 507–530.

Brothelande, E., Peltier, A., Got, J. L., Merle, O., Lardy, M., & Garaebiti, E. (2016). Constraints on the source of resurgent doming inferred from analogue and numerical modeling — Implications on the current feeding system of the Yenkahe dome–Yasur volcano complex (Vanuatu). *Journal of Volcanology and Geothermal Research*, *322*(December 2015), 225–240. https://doi.org/10.1016/j.jvolgeores.2015.11.023

Brozzetti, F., Cirillo, D., Liberi, F., Piluso, E., Faraca, E., De Nardis, R., & Lavecchia, G. (2017). Structural style of Quaternary extension in the Crati Valley (Calabrian Arc): Evidence in support of an east-dipping detachment fault. *Italian Journal of Geosciences*, *136*(3), 434–453. https://doi.org/10.3301/IJG.2017.11

Bruno, P. P. (2004). Structure and evolution of the Bay of Pozzuoli (Italy) using marine seismic reflection data: implications for collapse of the Campi Flegrei caldera. *Bulletin of Volcanology*, *66*(4), 342–355.

Burg, J.-P., & Podladchikov, Y. (2000). From buckling to asymmetric folding of the continental lithosphere: Numerical modelling and application to the Himalayan syntaxes. *Geological Society, London, Special Publications*, *170*(1), 219–236.

Capozzi, R., & Picotti, V. (2003). Pliocene sequence stratigraphy, climatic trends and sapropel formation in the Northern Apennines (Italy). *Palaeogeography, Palaeoclimatology, Palaeoecology*, *190*, 349–371. https://doi.org/10.1016/S0031-0182(02)00614-4

Carminati, E., Cavazza, W., Roure, F., Spakman, W., Stampfli, G. M., & Ziegler, P. A. (2004). TRANSMED Transect III: Massif Central-Provence-Gulf of Lion-Provençal Basin-Sardinia-Tyrrhenian Basin-Southern Apennines-Apulia-Adriatic Sea-Albanides-Balkans-Moesian Platform. *Cavazza, W., Roure, F., Spakman, Stampfli, GM and Ziegler, PA, Eds., The TRANSMED Atlas: The Mediterranean Region from Crust to Mantle: Heidelberg, Springer-Verlag*.

Carminati, E., & Doglioni, C. (2005). EUROPE| Mediterranean Tectonics.

Carminati, E., Wortel, M. J. R., Spakman, W., & Sabadini, R. (1998). The role of slab detachment processes in the opening of the western–central Mediterranean basins: some geological and geophysical evidence. *Earth and Planetary Science Letters*, *160*(3–4), 651–665.

Carmisciano, C., Grassi, M., Cocchi, L., Masetti, G., Filippone, M., Ricci, E., … Berrino, G. (2013). RICAMAR2013-RIlievi per la Caratterizzazione dell'Ambiente MARino nel Golfo di Pozzuoli.

Carobene, L. (2003). Genesi, età, sollevamento ed erosione dei terrazzi marini di Crosia-Calopezzati (Costa ionica della Calabria-Italia). *Il Quaternario*, *16*(1), 43–90.

Casu, F., Manzo, M., & Lanari, R. (2006). A quantitative assessment of the SBAS algorithm performance for surface deformation retrieval from DInSAR data. *Remote Sensing of Environment*, *102*(3–4), 195–210.

Cattaneo, A., Correggiari, A., Langone, L., & Trincardi, F. (2003). The late-Holocene Gargano subaqueous delta, Adriatic shelf: sediment pathways and supply fluctuations. *Marine Geology*, *193*(1–2), 61–91.

Cattaneo, A., Trincardi, F., Asioli, A., & Correggiari, A. (2007). The Western Adriatic shelf clinoform: energy-limited bottomset. *Continental Shelf Research*, *27*(3–4), 506–525. https://doi.org/10.1016/j.csr.2006.11.013

Cavazza, W., & DeCelles, P. G. (1998). Upper Messinian siliciclastic rocks in southeastern Calabria (southern Italy): palaeotectonic and eustatic implications for the evolution of the central Mediterranean region. *Tectonophysics*, *298*(1–3), 223–241.

Chiarabba, C., De Gori, P., & Speranza, F. (2008). The southern Tyrrhenian subduction zone: deep geometry, magmatism and Plio-Pleistocene evolution. *Earth and Planetary Science Letters*, *268*(3–4), 408–423.

Cianflone, G., & Calabria, U. (2015). Preliminary study of the surface ground displacements in the Crati Valley (Calabria) by means of InSAR data, (November).

Cinque_1985.pdf. (n.d.).

Cinque, A., Rolandi, G. t, & Zamparelli, V. (1985). L'estensione dei depositi marini olocenici nei Campi Flegrei in relazione alla vulcano-tettonica. *Bollettino Della Società Geologica Italiana*, *104*(2), 327–348.

Cloetingh, S., & Burov, E. (2011). Lithospheric folding and sedimentary basin evolution: a review and analysis of formation mechanisms. *Basin Research*, *23*(3), 257–290.

Cocchi, L., Passaro, S., Tontini, F. C., & Ventura, G. (2017a). Volcanism in slab tear faults is larger than in island-arcs and back-arcs. *Nature Communications*, *8*(1). https://doi.org/10.1038/s41467-017-01626-w

Cocchi, L., Passaro, S., Tontini, F. C., & Ventura, G. (2017b). Volcanism in slab tear faults is larger than in island-arcs and back-arcs. *Nature Communications*, *8*(1), 1451. https://doi.org/10.1038/s41467-017-01626-w

Cole, J. W., Milner, D. M., & Spinks, K. D. (2005). Calderas and caldera structures: A review. *Earth-Science Reviews*, *69*(1–2), 1–26. https://doi.org/10.1016/j.earscirev.2004.06.004

Colella, A. (1988). Fault-controlled marine Gilbert-type fan deltas. *Geology*, *16*(11), 1031–1034. Retrieved from http://dx.doi.org/10.1130/0091-7613(1988)016%3C1031:FCMGTF%3E2.3.CO

D'Agostino, N., D'Anastasio, E., Gervasi, A., Guerra, I., Nedimović, M. R., Seeber, L., & Steckler, M. (2011). Forearc extension and slow rollback of the Calabrian Arc from GPS measurements. *Geophysical Research Letters*, *38*(17), 1–6. https://doi.org/10.1029/2011GL048270

D'Antonio, M., Civetta, L., Orsi, G., Pappalardo, L., Piochi, M., Carandente, A., … Isaia, R. (1999). The present state of the magmatic system of the Campi Flegrei caldera based on a reconstruction of its behavior in the past 12 ka. *Journal of Volcanology and Geothermal Research*, *91*(2), 247–268.

D'Auria, L., Pepe, S., Castaldo, R., Giudicepietro, F., Macedonio, G., Ricciolino, P., … Zinno, I. (2015). Magma injection beneath the urban area of Naples: A new mechanism for the 2012-2013 volcanic unrest at Campi Flegrei caldera. *Scientific Reports*, *5*(August), 1–11. https://doi.org/10.1038/srep13100

Damuth, J. E. (1980). Use of high-frequency (3.5–12 kHz) echograms in the study of near-bottom sedimentation processes in the deep-sea: a review. *Marine Geology*, *38*(1–3), 51–75.

De Martino, P., Guardato, S., Tammaro, U., Vassallo, M., & Iannaccone, G. (2014). A first GPS measurement of vertical seafloor displacement in the Campi Flegrei caldera (Italy). *Journal of Volcanology and Geothermal Research*, *276*, 145–151. https://doi.org/10.1016/j.jvolgeores.2014.03.003

De Natale, G., & Pingue, F. (1993). Ground deformations in collapsed caldera structures. *Journal of Volcanology and Geothermal Research*, *57*(1–2), 19–38.

De Natale, G., Troise, C., Pingue, F., Mastrolorenzo, G., Pappalardo, L., Battaglia, M., & Boschi, E. (2006). The Campi Flegrei caldera: unrest mechanisms and hazards. *Geological Society, London, Special Publications*, *269*(1), 25–45. https://doi.org/10.1144/GSL.SP.2006.269.01.03

De Ritis, R., Dominici, R., Ventura, G., Nicolosi, I., Chiappini, M., Speranza, F., … Sonnino, M. (2010). A buried volcano in the Calabrian Arc (Italy) revealed by high-resolution aeromagnetic data. *Journal of Geophysical Research: Solid Earth*, *115*(11), 1–18. https://doi.org/10.1029/2009JB007171

Deino, A. L., Orsi, G., de Vita, S., & Piochi, M. (2004). The age of the Neapolitan Yellow Tuff caldera-forming eruption (Campi Flegrei caldera–Italy) assessed by 40 Ar/39 Ar dating method. *Journal of Volcanology and Geothermal Research*, *133*(1), 157–170.

Del Ben, A., Barnaba, C., & Taboga, A. (2008). Strike-slip systems as the main tectonic features in the Plio-Quaternary kinematics of the Calabrian Arc. *Marine Geophysical Researches*, *29*(1), 1–12. https://doi.org/10.1007/s11001-007-9041-6

Del Gaudio, C., Aquino, I., Ricciardi, G. P., Ricco, C., & Scandone, R. (2010). Unrest episodes at Campi Flegrei: A reconstruction of vertical ground movements during 1905-2009. *Journal of Volcanology and Geothermal Research*, *195*(1), 48–56. https://doi.org/10.1016/j.jvolgeores.2010.05.014

Dello Iacono, D., Zollo, A., Vassallo, M., Vanorio, T., & Judenherc, S. (2009). Seismic images and rock properties of the very shallow structure of Campi Flegrei caldera (southern Italy). *Bulletin of Volcanology*, *71*(3), 275–284. https://doi.org/10.1007/s00445-008-0222-1

Di Renzo, V., Arienzo, I., Civetta, L., D'Antonio, M., Tonarini, S., Di Vito, M. A., & Orsi, G. (2011). The magmatic feeding system of the Campi Flegrei caldera: architecture and temporal evolution. *Chemical Geology*, *281*(3), 227–241.

Di Vito, M. A., Isaia, R., Orsi, G., Southon, J. d, De Vita, S., d'Antonio, M., … Piochi, M. (1999). Volcanism and deformation since 12,000 years at the Campi Flegrei caldera (Italy). *Journal of Volcanology and Geothermal Research*, *91*(2–4), 221–246.

Dickinson, W. R., & Seely, D. R. (1979). Structure and stratigraphy of forearc regions. *AAPG Bulletin*, *63*(1), 2–31.

Doglioni, C., Gueguen, E., Harabaglia, P., & Mongelli, F. (1999). On the origin of west-directed subduction zones and applications to the western Mediterranean. *Geological Society, London, Special Publications*, *156*(1), 541–561.

du Bray, E. A., & Pallister, J. S. (1999). Recrystallization and anatexis along the plutonic-volcanic contact of the Turkey Creek caldera, Arizona. *Geological Society of America Bulletin*, *111*(1), 143–153.

Dvorak, J. J., & Berrino, G. (1991). Recent ground movement and seismic activity in Campi Flegrei, southern Italy: Episodic growth of a resurgent dome. *Journal of Geophysical Research: Solid Earth*, *96*(B2), 2309–2323.

Dvorak, J. J., & Mastrolorenzo, G. (1991). *The mechanisms of recent vertical crustal movements in Campi Flegrei caldera, southern Italy* (Vol. 263). Geological Society of America.

Faccenna, C., Becker, T. W., Lucente, F. P., Jolivet, L., & Rossetti, F. (2001). History of subduction and back arc extension in the Central Mediterranean. *Geophysical Journal International*, *145*(3), 809–820.

Faccenna, C., Funiciello, F., Civetta, L., D Antonio, M., Moroni, M., & Piromallo, C. (2007). Slab disruption, mantle circulation, and the opening of the Tyrrhenian basins. *SPECIAL PAPERS-GEOLOGICAL SOCIETY OF AMERICA*, *418*, 153.

Fedele, L., Insinga, D. D., Calvert, A. T., Morra, V., Perrotta, A., & Scarpati, C. (2011). 40 Ar/39 Ar dating of tuff vents in the Campi Flegrei caldera (southern Italy): toward a new chronostratigraphic reconstruction of the Holocene volcanic activity. *Bulletin of Volcanology*, *73*(9), 1323–1336.

Ferranti, L., Antonioli, F., Mauz, B., Amorosi, A., Dai Pra, G., Mastronuzzi, G., … Verrubbi, V. (2006). Markers of the last interglacial sea-level high stand along the coast of Italy: Tectonic implications. *Quaternary International*, *145–146*, 30–54. https://doi.org/10.1016/j.quaint.2005.07.009

Ferranti, L., Burrato, P., Pepe, F., Santoro, E., Mazzella, M. E., Morelli, D., … Vannucci, G. (2014). An active oblique-contractional belt at the transition between the Southern Apennines and Calabrian Arc: The Amendolara Ridge, Ionian Sea, Italy. *Tectonics*, *33*(11), 2169–2194. https://doi.org/10.1002/2014TC003624

Ferranti, L., Monaco, C., Antonioli, F., Maschio, L., Kershaw, S., & Verrubbi, V. (2007). The contribution of regional uplift and coseismic slip to the vertical crustal motion in the Messina Straits, southern Italy: Evidence from raised Late Holocene shorelines. *Journal of Geophysical Research: Solid Earth*, *112*(6). https://doi.org/10.1029/2006JB004473

Ferranti, L., Santoro, E., Mazzella, M. E., Monaco, C., & Morelli, D. (2009). Active transpression in the northern Calabria Apennines, southern Italy. *Tectonophysics*, *476*(1–2), 226–251. https://doi.org/10.1016/j.tecto.2008.11.010

Ferrari, L., & Manetti, P. (1993). Geodynamic framework of the Tyrrhenian volcanism: a review. *Acta Vulcanol*, *3*, 1–10.

Finetti, I. R. (2005). *CROP project: deep seismic exploration of the central Mediterranean and Italy* (Vol. 1). Elsevier.

Florio, G., Fedi, M., Cella, F., & Rapolla, A. (1999). The Campanian Plain and Phlegrean Fields: structural setting from potential field data. *Journal of Volcanology and Geothermal Research*, *91*(2–4), 361–379.

Folch, A., & Gottsmann, J. (2006). Faults and ground uplift at active calderas. *Geological Society, London, Special Publications*, *269*(1), 109–120. https://doi.org/10.1144/GSL.SP.2006.269.01.07

Frezzotti, M. L., Peccerillo, A., & Panza, G. (2009). Carbonate metasomatism and CO2 lithosphere–asthenosphere degassing beneath the Western Mediterranean: an integrated model arising from petrological and geophysical data. *Chemical Geology*, *262*(1–2), 108–120.

Galli, P., & Bosi, V. (2003). Catastrophic 1638 earthquakes in Calabria (southern Italy): New insights from paleoseismological investigation. *Journal of Geophysical Research: Solid Earth*, *108*(B1).

Gamberi, F., & Rovere, M. (2010). Mud diapirs, mud volcanoes and fluid flow in the rear of the Calabrian Arc Orogenic Wedge (southeastern Tyrrhenian sea). *Basin Research*, *22*(4), 452–464.

Gazis, C. A., Lanphere, M., Taylor Jr, H. P., & Gurbanov, A. (1995). 40Ar/39Ar and 18O/16O studies of the Chegem ash-flow caldera and the Eldjurta Granite: Cooling of two late Pliocene igneous bodies in the Greater Caucasus Mountains, Russia. *Earth and Planetary Science Letters*, *134*(3–4), 377–391.

Gillot, P. Y. (1987). Histoire volcanique des Iles Eoliennes: arc insulaire ou complexe orogénique anulaire. *Doc. Trav. IGAL*, *11*, 35–42.

Giudicepietro, F. (1993). La dinamica recente dell'area vulcanica flegrea. Ph. D. thesis, 179 pp., Univ. of Naples, Naples, Italy.

Gliozzi, E. (1987). I terrazzi delpleistocene superiore della peninsola do Crotone (Calabria). *Geologica Romana*, *26*, 17–49.

Guarnieri, P. (2006). Plio-Quaternary segmentation of the south Tyrrhenian forearc basin. *International Journal of Earth Sciences*, *95*(1), 107–118. https://doi.org/10.1007/s00531-005-0005-2

Gueguen, E., Doglioni, C., & Fernandez, M. (1998). On the post-25 Ma geodynamic evolution of the western Mediterranean. *Tectonophysics*, *298*(1–3), 259–269.

Gulick, S. P. S., Meltzer, A. S., & Clarke Jr, S. H. (2002). Effect of the northward-migrating Mendocino triple junction on the Eel River forearc basin, California: Stratigraphic development. *Geological Society of America Bulletin*, *114*(2), 178–191.

Gutscher, M., Kukowski, N., Malavieille, J., & Lallemand, S. (1998). Episodic imbricate thrusting and underthrusting: Analog experiments and mechanical analysis applied to the Alaskan accretionary wedge. *Journal of Geophysical Research: Solid Earth*, *103*(B5), 10161–10176.

Gvirtzman, Z., & Nur, A. (2001). Residual topography, lithospheric structure and sunken slabs in the central Mediterranean. *Earth and Planetary Science Letters*, *187*(1–2), 117–130.

Holohan, E. P., Troll, V. R., Walter, T. R., Münn, S., McDonnell, S., & Shipton, Z. K. (2005). Elliptical calderas in active tectonic settings: An experimental approach. *Journal of*

Volcanology and Geothermal Research, *144*(1–4 SPEC. ISS.), 119–136. https://doi.org/10.1016/j.jvolgeores.2004.11.020

Hon, K. (1987). Geologic and petrologic evolution of the Lake city caldera, San Juan Mountains, Colorado. University of Colorado.

Isaia, R., Marianelli, P., & Sbrana, A. (2009). Caldera unrest prior to intense volcanism in Campi Flegrei (Italy) at 4.0 ka BP: Implications for caldera dynamics and future eruptive scenarios. *Geophysical Research Letters*, *36*(21).

Iuliano, S., Matano, F., Caccavale, M., & Sacchi, M. (2015). Annual rates of ground deformation (1993–2010) at Campi Flegrei, Italy, revealed by Persistent Scatterer Pair (PSP) – SAR interferometry. *International Journal of Remote Sensing*, *36*(24), 6160–6191. https://doi.org/10.1080/01431161.2015.1111541

Jacques, E., Monaco, C., Tapponnier, P., Tortorici, L., & Winter, T. (2001). Faulting and earthquake triggering during the 1783 Calabria seismic sequence. *Geophysical Journal International*, *147*(3), 499–516.

Judenherc, S., & Zollo, A. (2004). The Bay of Naples (southern Italy): Constraints on the volcanic structures inferred from a dense seismic survey. *Journal of Geophysical Research: Solid Earth*, *109*(B10).

Kastens, K., Mascle, J., Auroux, C., Bonatti, E., Broglia, C., Channell, J., … Hasegawa, S. (1988). ODP Leg 107 in the Tyrrhenian Sea: Insights into passive margin and back-arc basin evolution. *Geological Society of America Bulletin*, *100*(7), 1140–1156.

Kennedy, B., Stix, J., Vallance, J. W., Lavallée, Y., & Longpré, M. A. (2004). Controls on caldera structure: Results from analogue sandbox modeling. *Bulletin of the Geological Society of America*, *116*(5–6), 515–524. https://doi.org/10.1130/B25228.1

Kennedy, B., Wilcock, J., & Stix, J. (2012). Caldera resurgence during magma replenishment and rejuvenation at Valles and Lake City calderas. *Bulletin of Volcanology*, *74*(8), 1833–1847. https://doi.org/10.1007/s00445-012-0641-x

Kukowski, N., Lallemand, S. E., Malavieille, J., Gutscher, M.-A., & Reston, T. J. (2002). Mechanical decoupling and basal duplex formation observed in sandbox experiments with application to the Western Mediterranean Ridge accretionary complex. *Marine Geology*, *186*(1–2), 29–42.

Lambeck, K. (1983). The role of compressive forces in intracratonic basin formation and mid-plate orogenies. *Geophysical Research Letters*, *10*(9), 845–848.

Laursen, J., Scholl, D. W., & von Huene, R. (2002). Neotectonic deformation of the central Chile margin: Deepwater forearc basin formation in response to hot spot ridge and seamount subduction. *Tectonics*, *21*(5), 2-1-2–27. https://doi.org/10.1029/2001TC901023

Li, Z., & Schieber, J. (2018). Detailed facies analysis of the Upper Cretaceous Tununk Shale Member, Henry Mountains Region, Utah: Implications for mudstone depositional models in epicontinental seas. *Sedimentary Geology*, *364*(May), 141–159. https://doi.org/10.1016/j.sedgeo.2017.12.015

Lipman, P. W. (1984). The roots of ash flow calderas in western North America: windows into the tops of granitic batholiths. *Journal of Geophysical Research: Solid Earth*, *89*(B10), 8801–8841.

Lipman, P. W. (2000). Central San Juan caldera cluster: Regional volcanic framework. *SPECIAL*

PAPERS-GEOLOGICAL SOCIETY OF AMERICA, 9–70.

Liu, J. P., Xu, K. H., Li, A. C., Milliman, J. D., Velozzi, D. M., Xiao, S. B., & Yang, Z. S. (2007). Flux and fate of Yangtze River sediment delivered to the East China Sea. *Geomorphology*, *85*(3–4), 208–224. https://doi.org/10.1016/j.geomorph.2006.03.023

Locardi, E. (1993). Dynamics of deep structures in the Tyrrhenian-Apennines area and its relation to neotectonics. *Il Quaternario*, *6*, 59–66.

Loreto, M. F., Fracassi, U., Franzo, A., Del Negro, P., Zgur, F., & Facchin, L. (2013). Approaching the seismogenic source of the Calabria 8 September 1905 earthquake: New geophysical, geological and biochemical data from the S. Eufemia Gulf (S Italy). *Marine Geology*, *343*(September 1905), 62–75. https://doi.org/10.1016/j.margeo.2013.06.016

Loreto, M. F., Pepe, F., De Ritis, R., Ventura, G., Ferrante, V., Speranza, F., … Sacchi, M. (2015). Geophysical investigation of Pleistocene volcanism and tectonics offshore Capo Vaticano (Calabria, southeastern Tyrrhenian Sea). *Journal of Geodynamics*, *90*, 71–86. https://doi.org/10.1016/j.jog.2015.07.005

Lundgren, P., Usai, S., Sansosti, E., Lanari, R., Tesauro, M., Fornaro, G., & Berardino, P. (2001). Modeling surface deformation observed with synthetic aperture radar interferometry at Campi Flegrei caldera. *Journal of Geophysical Research: Solid Earth*, *106*(B9), 19355–19366.

Maesano, F. E., Tiberti, M. M., & Basili, R. (2017). The Calabrian Arc: Three-dimensional modelling of the subduction interface. *Scientific Reports*, *7*(1), 1–15. https://doi.org/10.1038/s41598-017-09074-8

Malinverno, A., Cafiero, M., Ryan, W. B. F., & Cita, M. B. (1981). Distribution of messinian sediments and erosional surfaces beneath the tyrrhenian sea-geodynamic implications. *Oceanologica Acta*, *4*(4), 489–495.

Mandl, G. (1988). *Mechanics of tectonic faulting*. Elsevier Amsterdam.

MARSH, B. D. (1984). Mechanics and energetics of magma formation and ascension. *Studies in Geophysics. Explosive Volcanism: Inception, Evolution, and Hazards*, 67–83.

Mattei, M., Cifelli, F., & D'Agostino, N. (2007). The evolution of the Calabrian Arc: Evidence from paleomagnetic and GPS observations. *Earth and Planetary Science Letters*, *263*(3–4), 259–274. https://doi.org/10.1016/j.epsl.2007.08.034

Mattei, M., Cipollari, P., Cosentino, D., Argentieri, A., Rossetti, F., Speranza, F., & Di Bella, L. (2002). The Miocene tectono-sedimentary evolution of the southern Tyrrhenian Sea: Stratigraphy, structural and palaeomagnetic data from the on-shore Amantea basin (Calabrian Arc, Italy). *Basin Research*, *14*(2), 147–168. https://doi.org/10.1046/j.1365-2117.2002.00173.x

Mattei, M., Speranza, F., Argentieri, A., Rossetti, F., Sagnotti, L., & Funiciello, R. (1999). Extensional tectonics in the Amantea basin (Calabria, Italy): A comparison between structural and magnetic anisotropy data. *Tectonophysics*, *307*(1–2), 33–49. https://doi.org/10.1016/S0040-1951(99)00117-1

Mazzoli, S., D'Errico, M., Aldega, L., Corrado, S., Invernizzi, C., Shiner, P., & Zattin, M. (2008). Tectonic burial and "young" (<10 Ma) exhumation in the southern Apennines fold-and-thrust belt (Italy). *Geology*, *36*(3), 243–246. https://doi.org/10.1130/G24344A.1

Milia, A., & Giordano, F. (2002). Holocene stratigraphy and depositional architecture of eastern Pozzuoli Bay (eastern Tyrrhenian sea margin, Italy): the influence of tectonics and wave-

induced currents. *Geo-Marine Letters*, *22*(1), 42–50.

Milia, A., Torrente, M. M., Russo, M., & Zuppetta, A. (2003). Tectonics and crustal structure of the Campania continental margin: relationships with volcanism. *Mineralogy and Petrology*, *79*(1–2), 33–47.

Milia, A., Turco, E., Pierantoni, P. P., & Schettino, A. (2009). Four-dimensional tectono-stratigraphic evolution of the Southeastern peri-Tyrrhenian basins (Margin of Calabria, Italy). *Tectonophysics*, *476*(1–2), 41–56. https://doi.org/10.1016/j.tecto.2009.02.030

Minelli, L., & Faccenna, C. (2010). Evolution of the Calabrian accretionary wedge (central Mediterranean). *Tectonics*, *29*(4).

Molin, P., Dramis, F., & Palmieri, E. (2002). The Pliocene-Quaternary uplift of the Ionian northern Calabria coastal belt between Corigliano Calabro and Capo Trionto. *Studi Geologici Camerti, Vol. Spec.*, 135–145.

Monaco, C., Tortorici, L., & Paltrinieri, W. (1998). Structural evolution of the Lucanian Apennines, southern Italy. *Journal of Structural Geology*, *20*(5), 617–638.

Moore, I., & Kokelaar, P. (1998). Tectonically controlled piecemeal caldera collapse: A case study of Glencoe volcano, Scotland. *Geological Society of America Bulletin*, *110*(11), 1448–1466.

Morán-Zenteno, D. J., Alba-Aldave, L. A., Solé, J., & Iriondo, A. (2004). A major resurgent caldera in southern Mexico: The source of the late Eocene Tilzapotla ignimbrite. *Journal of Volcanology and Geothermal Research*, *136*(1–2), 97–119. https://doi.org/10.1016/j.jvolgeores.2004.04.002

Morelli, C., Giese, P., Cassinis, R., Colombi, B., Guerra, I., Luongo, G., … Schutte, K. G. (1975). Crustal structure of Southern Italy. A seismic refraction profile between Puglia-Calabria-Sicily. *Boll. Geofis. Teor. Appl*, *18*, 183–210.

Natale, D., & Petrazzuoli, M. (1997). of the crest chamber I ...., *24*(13), 1555–1558.

Neri, G., Orecchio, B., Totaro, C., Falcone, G., & Presti, D. (2009). Subduction beneath southern Italy close the ending: Results from seismic tomography. *Seismological Research Letters*, *80*(1), 63–70.

Nicolosi, I., Speranza, F., & Chiappini, M. (2006). Ultrafast oceanic spreading of the Marsili Basin, southern Tyrrhenian Sea: Evidence from magnetic anomaly analysis. *Geology*, *34*(9), 717–720.

Noda, A. (2016). Forearc basins: Types, geometries, and relationships to subduction zone dynamics. *Bulletin of the Geological Society of America*, *128*(5–6), 879–895. https://doi.org/10.1130/B31345.1

Olivetti, V., Cyr, A. J., Molin, P., Faccenna, C., & Granger, D. E. (2012). Uplift history of the Sila Massif, southern Italy, deciphered from cosmogenic ^{10}Be erosion rates and river longitudinal profile analysis. *Tectonics*, *31*(3), 1–19. https://doi.org/10.1029/2011TC003037

Orecchio, B., Presti, D., Totaro, C., D'Amico, S., & Neri, G. (2015). Investigating slab edge kinematics through seismological data: The northern boundary of the Ionian subduction system (south Italy). *Journal of Geodynamics*, *88*, 23–35. https://doi.org/10.1016/j.jog.2015.04.003

Orsi, G., Civetta, L., Del Gaudio, C., De Vita, S., Di Vito, M. A., Isaia, R., … Ricco, C. (1999). Short-term ground deformations and seismicity in the resurgent Campi Flegrei caldera (Italy):

An example of active block-resurgence in a densely populated area. *Journal of Volcanology and Geothermal Research*, *91*(2–4), 415–451. https://doi.org/10.1016/S0377-0273(99)00050-5

Orsi, G., De Vita, S., & Di Vito, M. (1996). The restless, resurgent Campi Flegrei nested caldera (Italy): Constraints on its evolution and configuration. *Journal of Volcanology and Geothermal Research*, *74*(3–4), 179–214. https://doi.org/10.1016/S0377-0273(96)00063-7

Orsi, G., Gallo, G., & Zanchi, A. (1991). Simple-shearing block resurgence in caldera depressions. A model from Pantelleria and Ischia. *Journal of Volcanology and Geothermal Research*, *47*(1–2), 1–11. https://doi.org/10.1016/0377-0273(91)90097-J

Panza, G. F., Peccerillo, A., Aoudia, A., & Farina, B. (2007). Geophysical and petrological modelling of the structure and composition of the crust and upper mantle in complex geodynamic settings: the Tyrrhenian Sea and surroundings. *Earth-Science Reviews*, *80*(1–2), 1–46.

Parascandola, A. (1947). *I fenomeni bradisismici del Serapeo di Pozzuoli*. Stabilmento tipografico G. Genovese.

Passaro, S., Barra, M., Saggiomo, R., Di Giacomo, S., Leotta, A., Uhlen, H., & Mazzola, S. (2013). Multi-resolution morpho-bathymetric survey results at the Pozzuoli–Baia underwater archaeological site (Naples, Italy). *Journal of Archaeological Science*, *40*(2), 1268–1278.

Pepe, F., Bertotti, G., & Cloetingh, S. (2004). Tectono-stratigraphic modelling of the North Sicily continental margin (southern Tyrrhenian Sea). *Tectonophysics*, *384*(1–4), 257–273.

Pepe, F., Sulli, A., Bertotti, G., & Cella, F. (2010). Architecture and Neogene to Recent evolution of the western Calabrian continental margin: An upper plate perspective to the Ionian subduction system, central Mediterranean. *Tectonics*, *29*(3), 1–24. https://doi.org/10.1029/2009TC002599

Petrinovic, I. A., Martí, J., Aguirre-Díaz, G. J., Guzmán, S., Geyer, A., & Paz, N. S. (2010). The Cerro Aguas Calientes caldera, NW Argentina: An example of a tectonically controlled, polygenetic collapse caldera, and its regional significance. *Journal of Volcanology and Geothermal Research*, *194*(1–3), 15–26. https://doi.org/10.1016/j.jvolgeores.2010.04.012

Phillips, W. J. (1974). The dynamic emplacement of cone sheets. *Tectonophysics*, *24*(1–2), 69–84.

Piromallo, C., & Morelli, A. (2003). P wave tomography of the mantle under the Alpine-Mediterranean area. *Journal of Geophysical Research: Solid Earth*, *108*(B2).

Polonia, A., Torelli, L., Mussoni, P., Gasperini, L., Artoni, A., & Klaeschen, D. (2011). The Calabrian Arc subduction complex in the Ionian Sea: Regional architecture, active deformation, and seismic hazard. *Tectonics*, *30*(5).

Pontevivo, A., & Panza, G. F. (2006). The lithosphere-asthenosphere system in the Calabrian Arc and surrounding seas–Southern Italy. *Pure and Applied Geophysics*, *163*(8), 1617–1659.

Puga-Bernabéu, Á., Martín, J. M., Braga, J. C., & Sánchez-Almazo, I. M. (2010). Downslope-migrating sandwaves and platform-margin clinoforms in a current-dominated, distally steepened temperate-carbonate ramp Guadix Basin, Southern Spain. *Sedimentology*, *57*(2), 293–311. https://doi.org/10.1111/j.1365-3091.2009.01079.x

Qiu, J., Liu, J., Saito, Y., Yang, Z., Yue, B., Wang, H., & Kong, X. (2014). Sedimentary evolution of the Holocene subaqueous clinoform off the southern Shandong Peninsula in the Western South Yellow Sea. *Journal of Ocean University of China*, *13*(5), 747–760.

https://doi.org/10.1007/s11802-014-2227-z

Rehault, J. P., Moussat, E., & Fabbri, A. (1987). Structural evolution of the Tyrrhenian back-arc basin. *Marine Geology*, *74*(1–2), 123–150.

Robustelli, G., Lucà, F., Corbi, F., Pelle, T., Dramis, F., Fubelli, G., … Cugliari, D. (2009). Alluvial terraces on the Ionian coast of northern Calabria, southern Italy: Implications for tectonic and sea level controls. *Geomorphology*, *106*(3–4), 165–179. https://doi.org/10.1016/j.geomorph.2008.12.010

Roche, O., Druitt, T. H., & Merle, O. (2000). Experimental study of caldera formation. *Journal of Geophysical Research: Solid Earth*, *105*(B1), 395–416. https://doi.org/10.1029/1999JB900298

Rosi, M., & Sbrana, A. (1987). *Phlegrean fields* (Vol. 9). Consiglio nazionale delle ricerche.

Ryan, H. F., Draut, A. E., Keranen, K., & Scholl, D. W. (2012). Influence of the Amlia fracture zone on the evolution of the Aleutian Terrace forearc basin, central Aleutian subduction zone. *Geosphere*, *8*(6), 1254–1273. https://doi.org/10.1130/GES00815.1

Sacchi, M., Alessio, G., Aquino, I., Esposito, E., Molisso, F., Nappi, R., … Violante, C. (2009). Risultati preliminari della campagna oceanografica CAFE_07–Leg 3 nei Golfi di Napoli e Pozzuoli, Mar Tirreno orientale. *Quaderni Di Geofisica*.

Sacchi, M., Pepe, F., Corradino, M., Insinga, D. D., Molisso, F., & Lubritto, C. (2014). The Neapolitan Yellow Tuff caldera offshore the Campi Flegrei: Stratal architecture and kinematic reconstruction during the last 15 ky. *Marine Geology*, *354*, 15–33.

Salles, L., Ford, M., Joseph, P., De Veslud, C. L. C., & Le Solleuz, A. (2011). Migration of a synclinal depocentre from turbidite growth strata: the Annot syncline, SE France. *Bulletin de La Societe Geologique de France*, *182*(3), 199–220. https://doi.org/10.2113/gssgfbull.182.3.199

Samsonov, S. V., Tiampo, K. F., Camacho, A. G., Fernández, J., & González, P. J. (2014). Spatiotemporal analysis and interpretation of 1993-2013 ground deformation at Campi Flegrei, Italy, observed by advanced DInSAR. *Geophysical Research Letters*, *41*(17), 6101–6108. https://doi.org/10.1002/2014GL060595

Santo, A. P., & Clark, A. H. (1994). Volcanological evolution of Aeolian Arc, Italy: Inferences from 40Ar/39Ar ages of Filicudi rocks. IAVCEI Congress, Abstract Volume, Ankara, 1994. Savelli, C. 2000. Two-stage progression of volcanism 8–0 Ma in the central Mediterranean southern Italy. *Journal of Geodynamics*, *31*, 87–104.

Saunders, S. J. (2004). The possible contribution of circumferential fault intrusion to caldera resurgence. *Bulletin of Volcanology*, *67*(1), 57–71. https://doi.org/10.1007/s00445-004-0360-z

Savelli, C. (1988). Late Oligocene to Recent episodes of magmatism in and around the Tyrrhenian Sea: implications for the processes of opening in a young inter-arc basin of intra-orogenic (Mediterranean) type. *Tectonophysics*, *146*(1–4), 163–181.

Scandone, R., Giacomelli, L., & Speranza, F. F. (2006). The volcanological history of the volcanoes of Naples: a review. *Developments in Volcanology*, *9*, 1–26.

Scarpati, C., Cole, P., & Perrotta, A. (1993a). The Neapolitan Yellow Tuff—a large volume multiphase eruption from Campi Flegrei, southern Italy. *Bulletin of Volcanology*, *55*(5), 343–356.

Scarpati, C., Cole, P., & Perrotta, A. (1993b). The Neapolitan Yellow Tuff - A large volume multiphase eruption from Campi Flegrei, Southern Italy. *Bulletin of Volcanology*, *55*(5), 343–356. https://doi.org/10.1007/BF00301145

Self, S., Goff, F., Gardner, J. N., Wright, J. V, & Kite, W. M. (1986). Explosive rhyolitic volcanism in the Jemez Mountains: Vent locations, caldera development and relation to regional structure. *Journal of Geophysical Research: Solid Earth*, *91*(B2), 1779–1798.

Shulgin, A., Kopp, H., Klaeschen, D., Papenberg, C., Tilmann, F., Flueh, E. R., … Djajadihardja, Y. (2013). Subduction system variability across the segment boundary of the 2004/2005 Sumatra megathrust earthquakes. *Earth and Planetary Science Letters*, *365*, 108–119.

Sibson, R. H. (1995). Selective fault reactivation during basin inversion: potential for fluid redistribution through fault-valve action. *Geological Society, London, Special Publications*, *88*(1), 3–19.

Slingerland, R., & Keen, T. R. (1999). Sediment transport in the Western Interior Seaway of North America: Predictions from a climate-ocean-sediment model.

Smith, R. L., & Bailey, R. A. (1968). Stratigraphy, structure, and volcanic evolution of the Jemez Mountains, New Mexico. *Special Paper—Geological Society of America*, 447–448.

Smith, V. C., Isaia, R., & Pearce, N. J. G. (2011). Tephrostratigraphy and glass compositions of post-15 kyr Campi Flegrei eruptions: implications for eruption history and chronostratigraphic markers. *Quaternary Science Reviews*, *30*(25–26), 3638–3660.

Spence, G. D., Hyndman, R. D., Davis, E. E., & Yorath, C. J. (1991). Seismic structure of the northern Cascadia accretionary prism: evidence from new multichannel seismic reflection data. *Continental Lithosphere: Deep Seismic Reflections*, *22*, 257–263.

Spina, V., Tondi, E., Galli, P., & Mazzoli, S. (2009). Fault propagation in a seismic gap area (northern Calabria, Italy): Implications for seismic hazard. *Tectonophysics*, *476*(1–2), 357–369.

Spina, V., Tondi, E., & Mazzoli, S. (2011). Complex basin development in a wrench-dominated back-arc area: Tectonic evolution of the Crati Basin, Calabria, Italy. *Journal of Geodynamics*, *51*(2–3), 90–109. https://doi.org/10.1016/j.jog.2010.05.003

Stephenson, R. A., & Cloetingh, S. (1991). Some examples and mechanical aspects of continental lithosphere folding.

Tansi, C., Muto, F., Critelli, S., & Iovine, G. (2007). Neogene-Quaternary strike-slip tectonics in the central Calabrian Arc (southern Italy). *Journal of Geodynamics*, *43*(3), 393–414. https://doi.org/10.1016/j.jog.2006.10.006

Thomson, S. N. (1994). Fission track analysis of the crystalline basement rocks of the Calabrian Arc, southern Italy: evidence of Oligo-Miocene late-orogenic extension and erosion. *Tectonophysics*, *238*(1–4), 331–352.

Thomson, S. N., Stöckhert, B., Rauche, H., & Brix, M. R. (1998). Apatite fission-track thermochronology of the uppermost tectonic unit of Crete, Greece: implications for the post-Eocene tectonic evolution of the Hellenic subduction system. In *Advances in Fission-Track Geochronology* (pp. 187–205). Springer.

Tibaldi, A., & Vezzoli, L. (1998). The space problem of caldera resurgence: an example from Ischia Island, Italy. *Geologische Rundschau*, *87*(1), 53–66.

Tortorici, L., Monaco, C., Tansi, C., & Cocina, O. (1995). Recent and active tectonics in the Calabrian arc (Southern Italy). *Tectonophysics*, *243*(1–2), 37–55.

Totaro, C., Orecchio, B., Presti, D., Scolaro, S., & Neri, G. (2016). Seismogenic stress field estimation in the Calabrian Arc region (south Italy) from a Bayesian approach. *Geophysical Research Letters*, *43*(17), 8960–8969. https://doi.org/10.1002/2016GL070107

Trasatti, E., Casu, F., Giunchi, C., Pepe, S., Solaro, G., Tagliaventi, S., … Ricciardi, G. P. (2008). The 2004–2006 uplift episode at Campi Flegrei caldera (Italy): Constraints from SBAS-DInSAR ENVISAT data and Bayesian source inference. *Geophysical Research Letters*, *35*(7).

Trasatti, E., Polcari, M., Bonafede, M., & Stramondo, S. (2015). Geodetic constraints to the source mechanism of the 2011-2013 unrest at Campi Flegrei (Italy) caldera. *Geophysical Research Letters*, *42*(10), 3847–3854. https://doi.org/10.1002/2015GL063621

Troiano, A., Di Giuseppe, M. G., Petrillo, Z., Troise, C., & De Natale, G. (2011). Ground deformation at calderas driven by fluid injection: modelling unrest episodes at Campi Flegrei (Italy). *Geophysical Journal International*, *187*(2), 833–847.

Ulusoy, I., Cubukcu, E., Aydar, E., Labazuy, P., Gourgaud, A., & Vincent, P. M. (2004). Volcanic and deformation history of the Bodrum resurgent caldera system (southwestern Turkey). *Journal of Volcanology and Geothermal Research*, *136*(1–2), 71–96. https://doi.org/10.1016/j.jvolgeores.2004.03.016

Van Dijk, J. P., Bello, M., Brancaleoni, G. P., Cantarella, G., Costa, V., Frixa, A., … Zerilli, A. (2000). A regional structural model for the northern sector of the Calabrian Arc (southern Italy). *Tectonophysics*, *324*(4), 267–320. https://doi.org/10.1016/S0040-1951(00)00139-6

Vilardo, G., Isaia, R., Ventura, G., De Martino, P., & Terranova, C. (2010). InSAR Permanent Scatterer analysis reveals fault re-activation during inflation and deflation episodes at Campi Flegrei caldera. *Remote Sensing of Environment*, *114*(10), 2373–2383. https://doi.org/10.1016/j.rse.2010.05.014

Vitale, S., & Isaia, R. (2014). Fractures and faults in volcanic rocks (Campi Flegrei, southern Italy): insight into volcano-tectonic processes. *International Journal of Earth Sciences*, *103*(3), 801–819.

Walter, T. R., & Troll, V. R. (2001). Formation of caldera periphery faults: An experimental study. *Bulletin of Volcanology*, *63*(2–3), 191–203. https://doi.org/10.1007/s004450100135

Westaway, R. (1993). Quaternary uplift of southern Italy. *Journal of Geophysical Research: Solid Earth*, *98*(B12), 21741–21772.

Wohletz, K., Orsi, G., & De Vita, S. (1995). Eruptive mechanisms of the Neapolitan Yellow Tuff interpreted from stratigraphie, chemical, and granulometric data. *Journal of Volcanology and Geothermal Research*, *67*(4), 263–290.

Wortel, M. J. R., & Spakman, W. (2000). Subduction and slab detachment in the Mediterranean-Carpathian region. *Science*, *290*(5498), 1910–1917.

Zecchin, M., Caffau, M., Civile, D., Critelli, S., Di Stefano, A., Maniscalco, R., … Roda, C. (2012). The Plio-Pleistocene evolution of the Crotone Basin (southern Italy): Interplay between sedimentation, tectonics and eustasy in the frame of Calabrian Arc migration. *Earth-Science Reviews*, *115*(4), 273–303. https://doi.org/10.1016/j.earscirev.2012.10.005

Figures

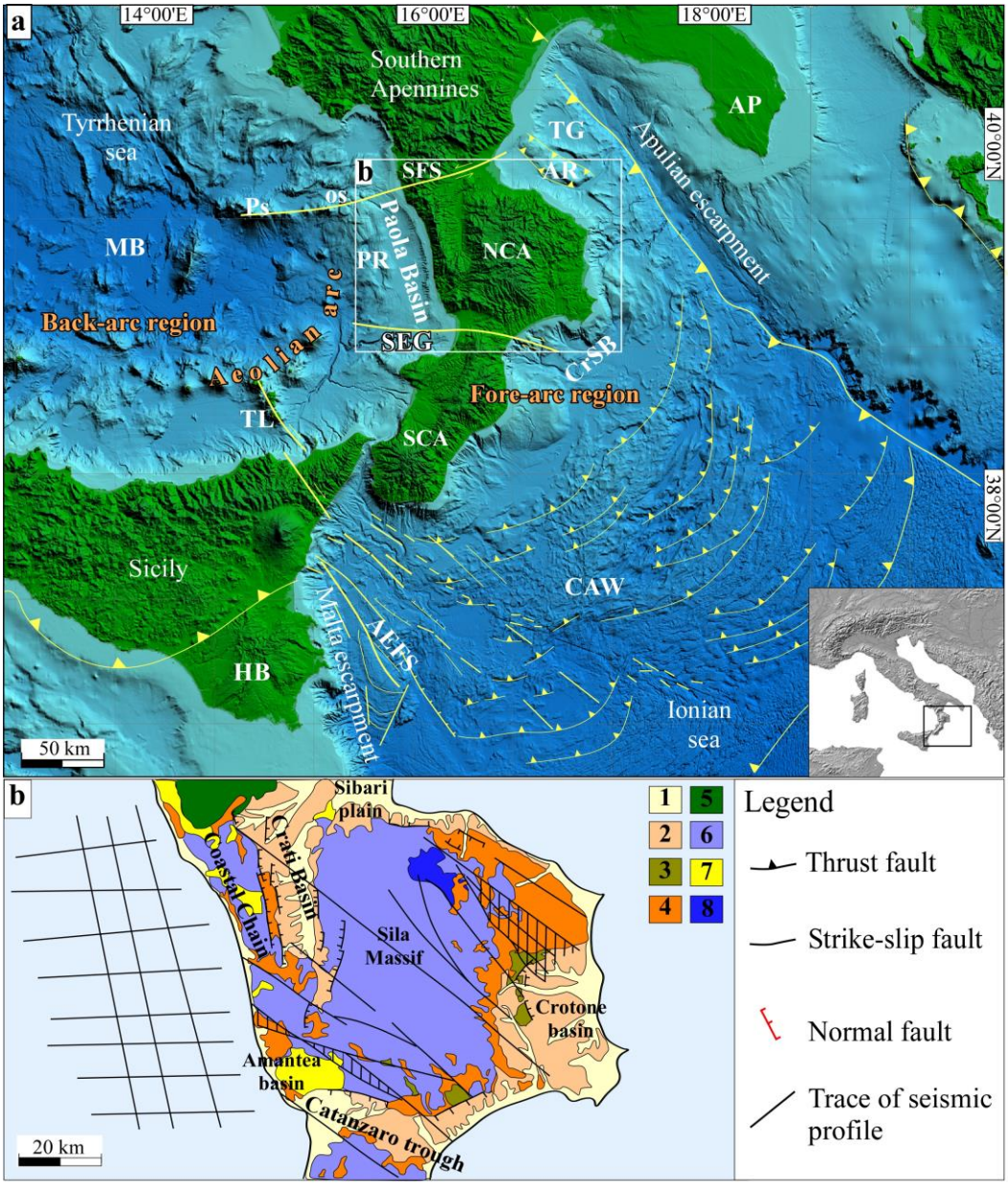

Figure 1. Corradino et al.

Figure 1. (a) Schematic tectonic map of the Tyrrhenian-Ionian subduction system. AEFS: Alfeo-Etna Fault System; AI: Aeolian Islands; AP: Apulian block; CAW: Calabrian accretionary wedge; CrSB, Crotone-Spartivento Basin; HB: Hyblean block; MB: Marsili Basin; N-CPA: Northern Calabria Arc; Os: Ovidio seamounts; PR: Paola Ridge; Ps: Palinuro seamounts; SCA: southern Calabria Arc; SEG: Santa Eufemia Gulf; SFS: Sangineto fault system; TG, Taranto Gulf; TL: Tindari-Letojanni fault. Inset shows the location of the area. (b) Geological sketch map of the Northern Calabrian Arc (after Monaco et al., 1998; Van Dijk et al., 2000, and Tansi et al., 2007) with location of the seismic dataset used in this study. 1: Continental and marine deposits (Holocene-upper Pleistocene); 2: Terrigenous marine deposits (Pleistocene-upper Pliocene); 3: Marine deposits and calcarenites (lower Pliocene); 4: Marine deposits: clays, sandstone and evaporites (Messinian-upper Tortonian); 5: Apennines carbonate units; 6: Igneous and continental-derived metamorphic units; 7: Ophiolitic units; 8: Longobucco cover and Paludi Formation (Paleogene-Mesozoic).

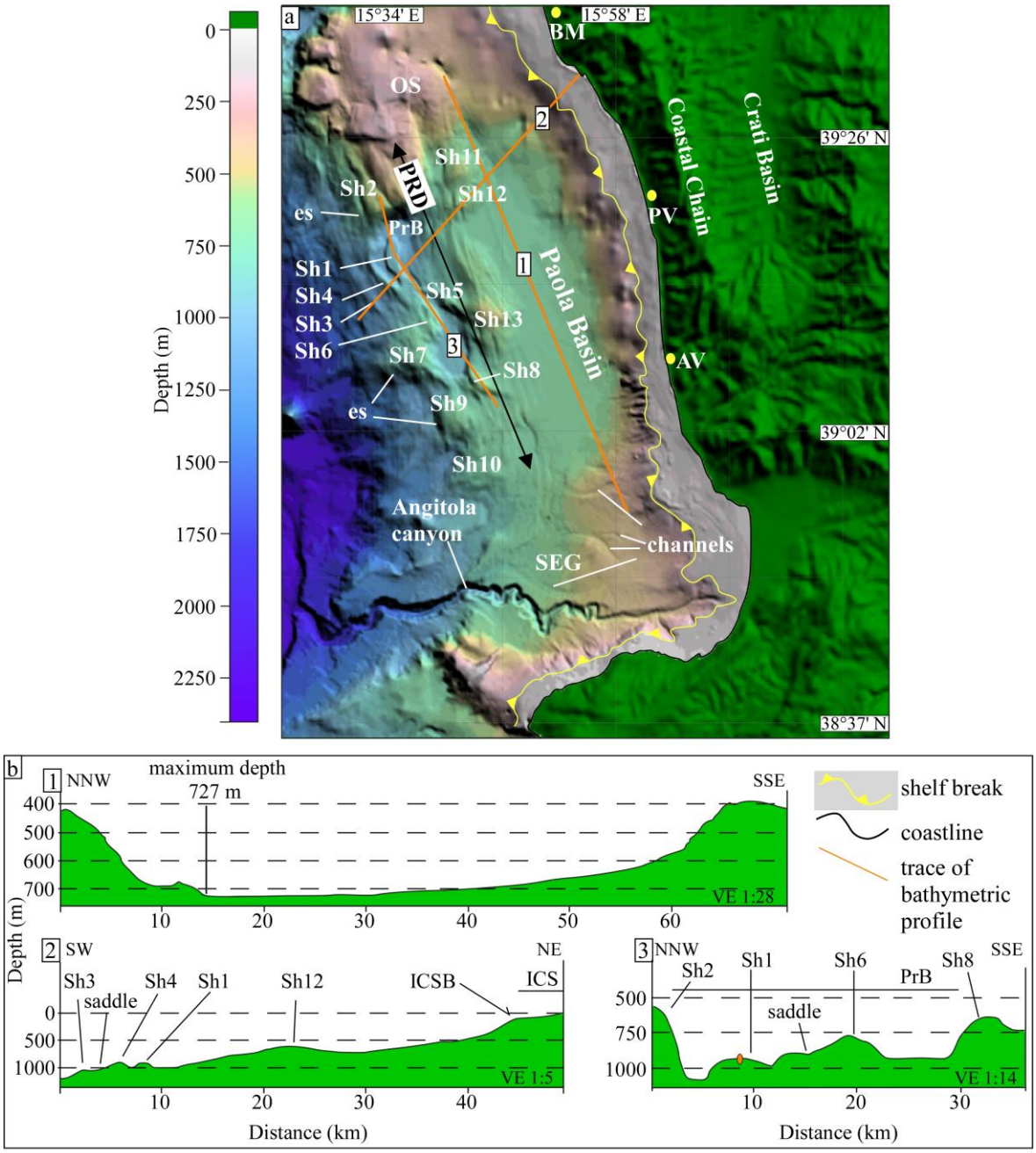

Figure 2. Corradino et al.

Figure 2. (a) Morpho-bathymetric map of the Paola Basin and surroundings. AV: Amantea Village; BM: Belvedere Marittimo Village; es: escarpment; PrB: Propeller basin; PRD: Paola Ridge; PV: Paola Village; SEG: Santa Eufemia Gulf; Sh: Structural high. (b) Bathymetric profiles across the Paola Basin. ICS: inner continental shelf; ICSB: inner continental shelf break; VE: vertical exaggeration.

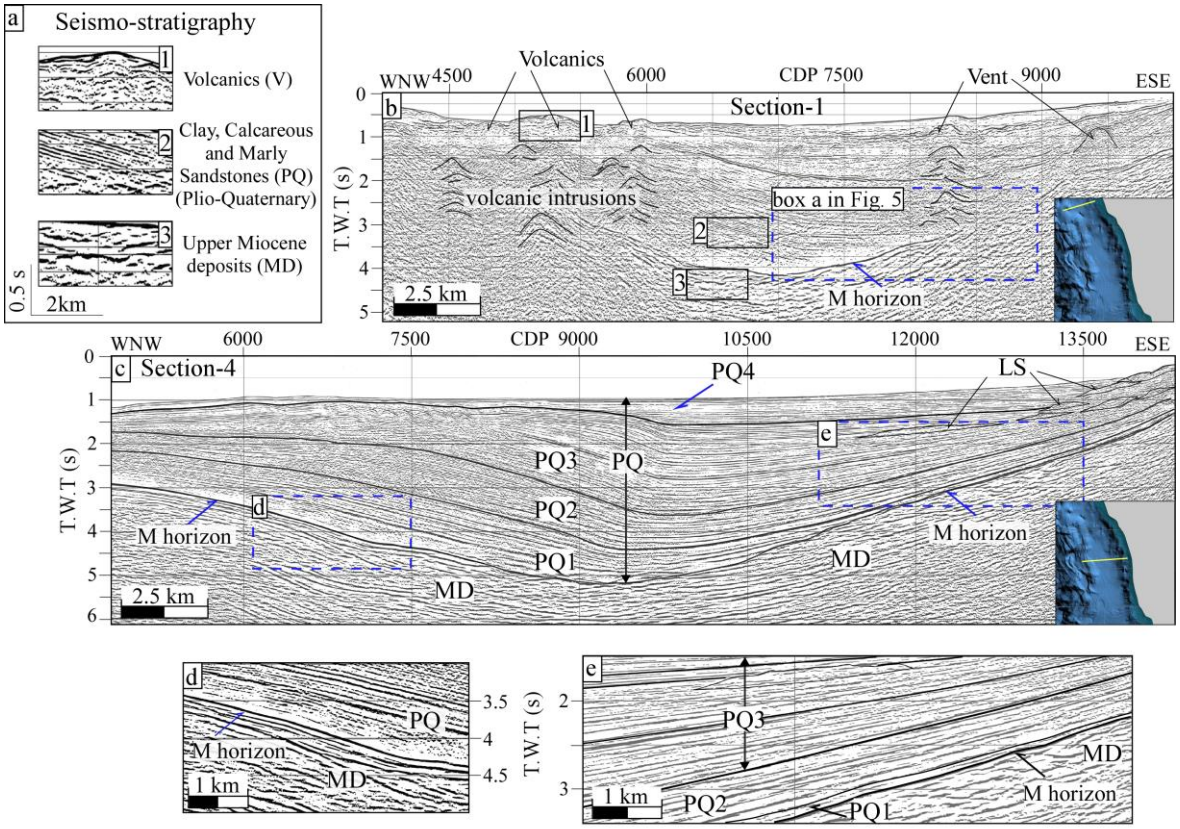

Figure 3. Corradino et al.

Figure 3. (a), (b) and (c) Seismo-stratigraphic units (MD, PQ and V), and subunits (PQ1, PQ2, PQ3 and PQ4) recognized on seismic profiles. Insets show the location of the profiles. LS, Landslide. (d) and (e) display parts of the Section 4 at small scale.

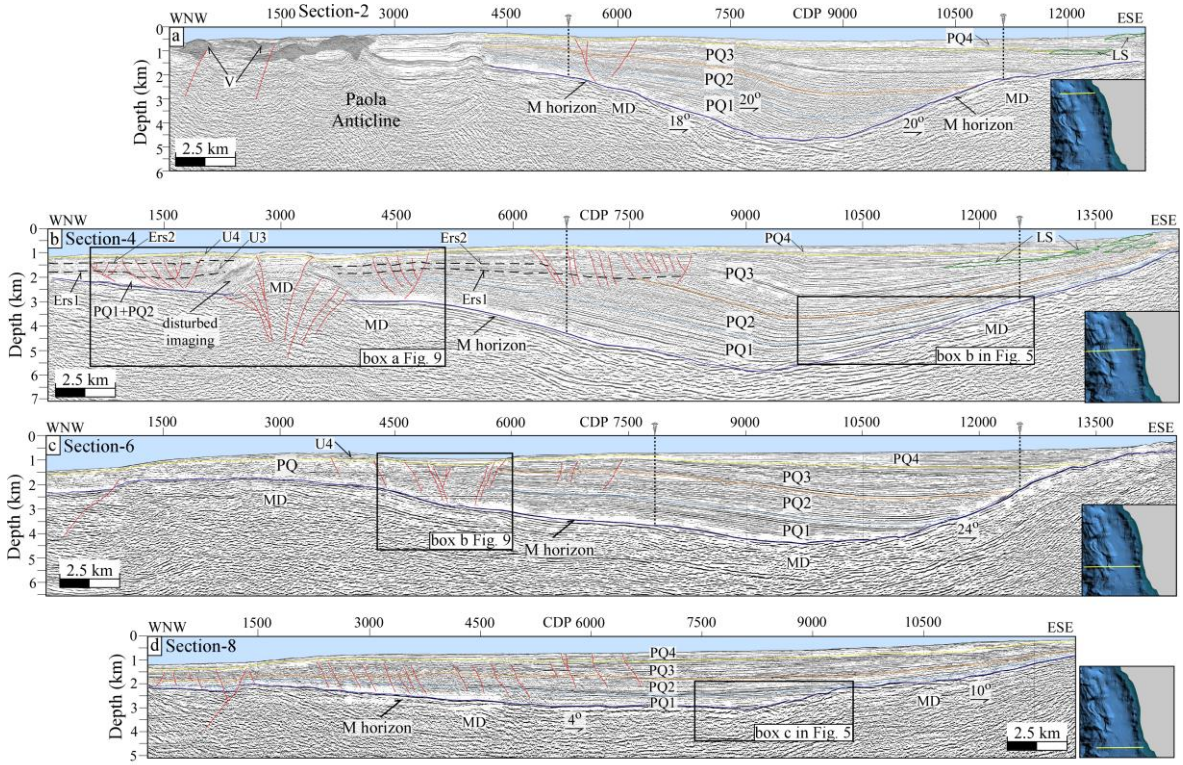

Figure 4. Corradino et al.

Figure 4. Depth-converted EW profiles and their interpretation. MD, Upper Miocene deposits; PQ, Plio Quaternary deposits, PQ1, PQ2, PQ3 and PQ4 subunits recognized on seismic profiles; V, Volcanics; Ers1 and Ers2: erosional surfaces. Insets show the location of the profiles. Grey pins indicate the restoration pin lines.

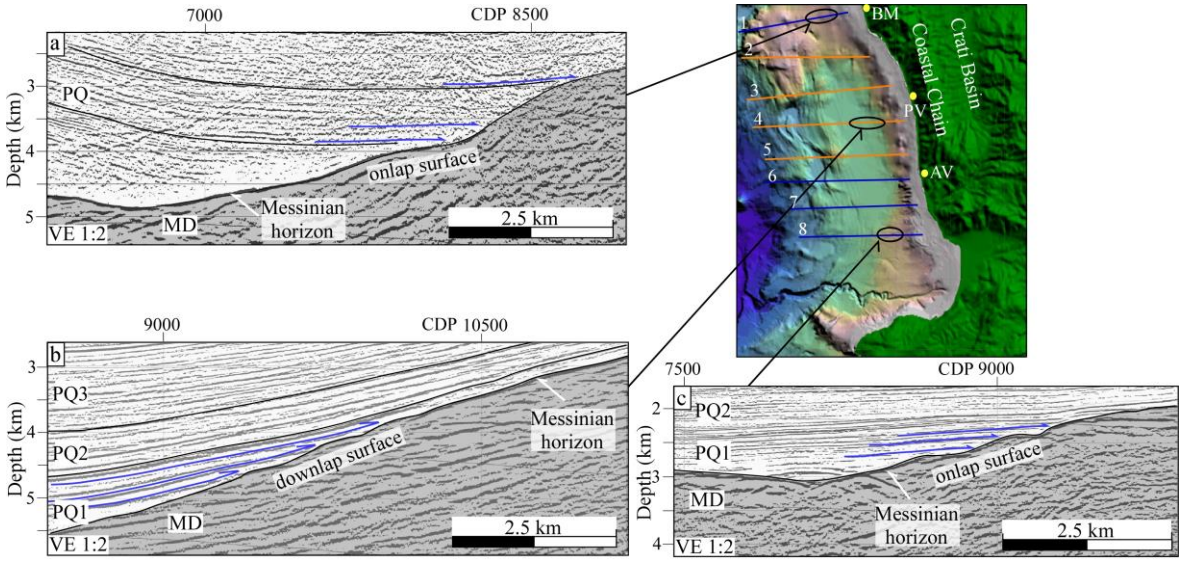

Figure 5. Corradino et al.

Figure 5. Lateral terminations of the Plio-Quaternary deposits onto the eastern flank of the Paola Basin. BM: Belvedere Marittimo village; PV: Paola Village; AV: Amantea Village. See Figs. 3b, 4b and 4d for location of box a, b and c, respectively. Vertical exaggeration 1:2.

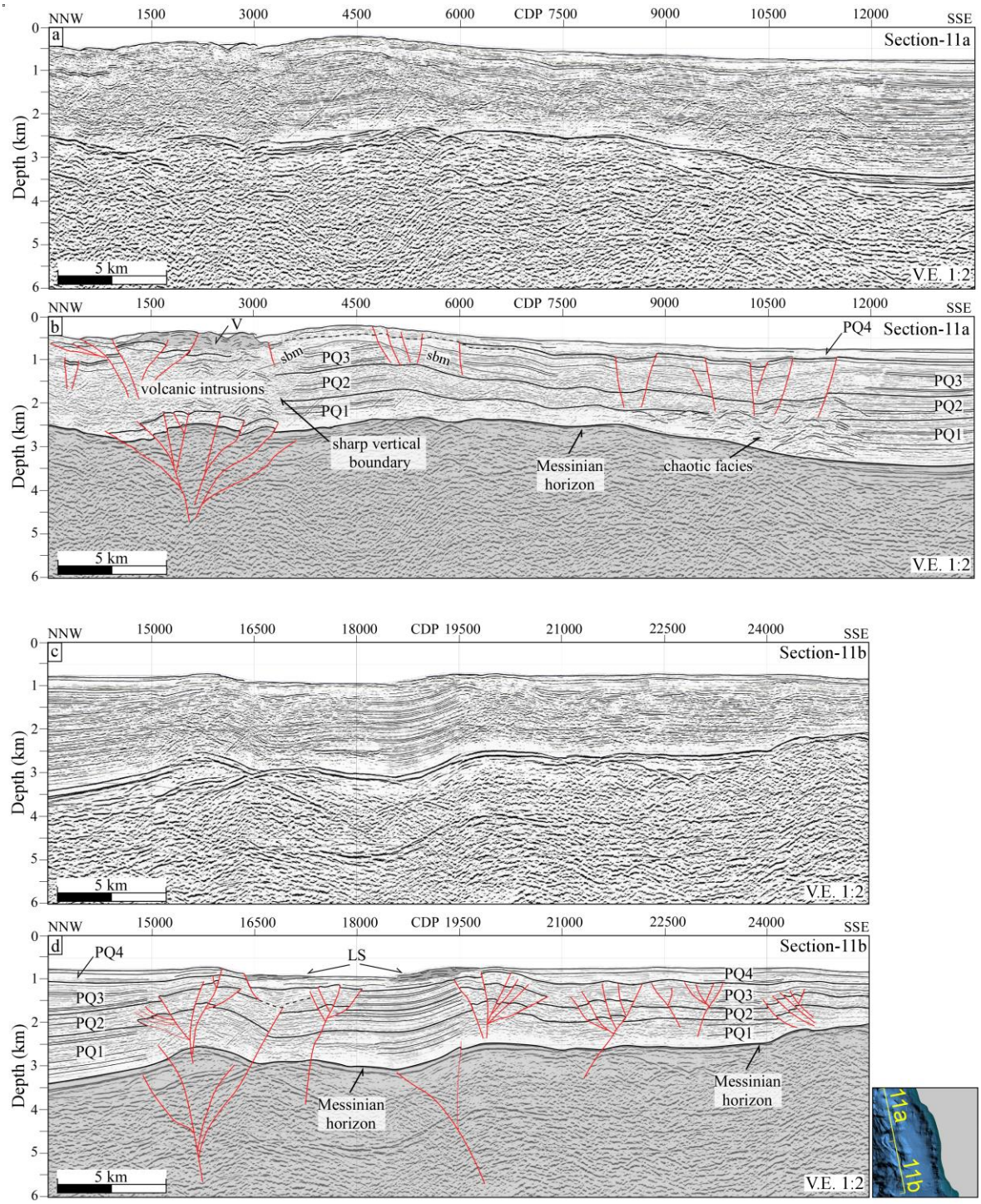

Figure 6. Corradino et al.

Figure 6. Depth-converted "Section-11" profile and its interpretation. PQ1, PQ2, PQ3 and PQ4: subunits recognized on seismic profiles. Inset shows the location of the profile. Vertical exaggeration 1:2.

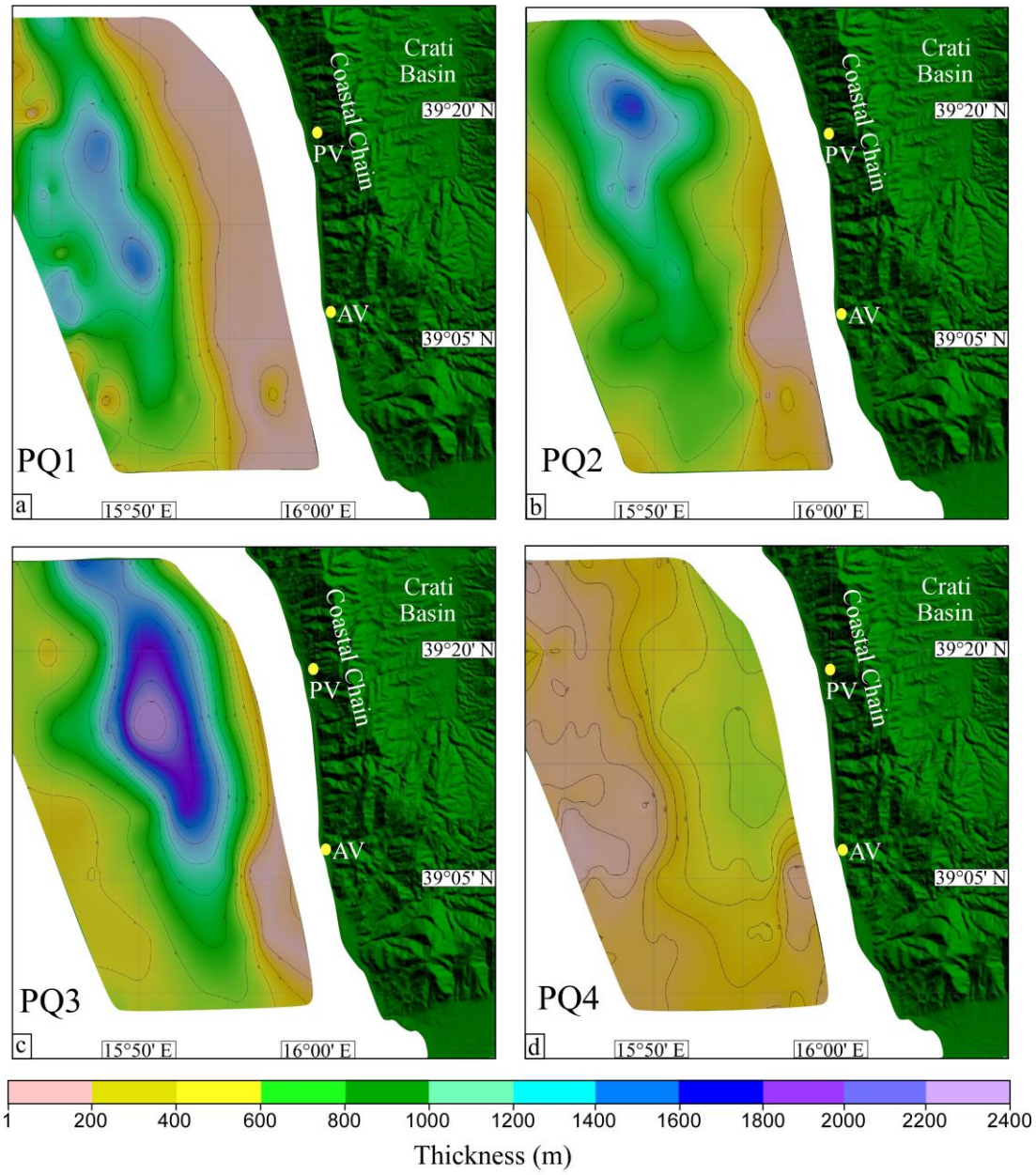

Figure 7. Corradino et al.

Figure 7. (a), (b), (c), and (d) Isopach maps of subunits PQ1, PQ2, PQ3 and PQ4. PV: Paola Village; AV: Amantea Village.

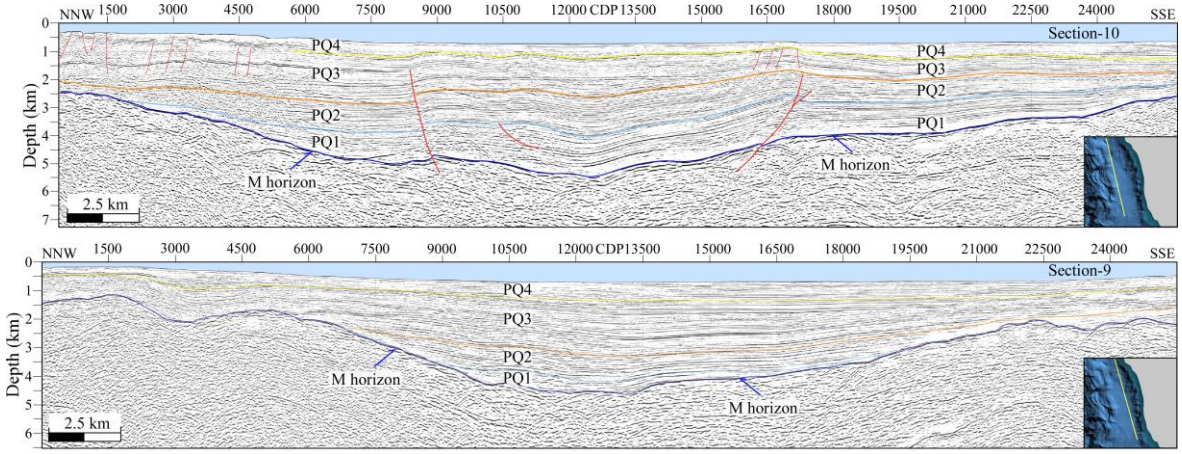

Figure 8. Corradino et al.

Figure 8. Depth-converted profiles “Section-9” and “Section-10” and their interpretation. PQ1, PQ2, PQ3 and PQ4 subunits recognized on seismic profiles. Insets show the location of the profiles. No vertical exaggeration.

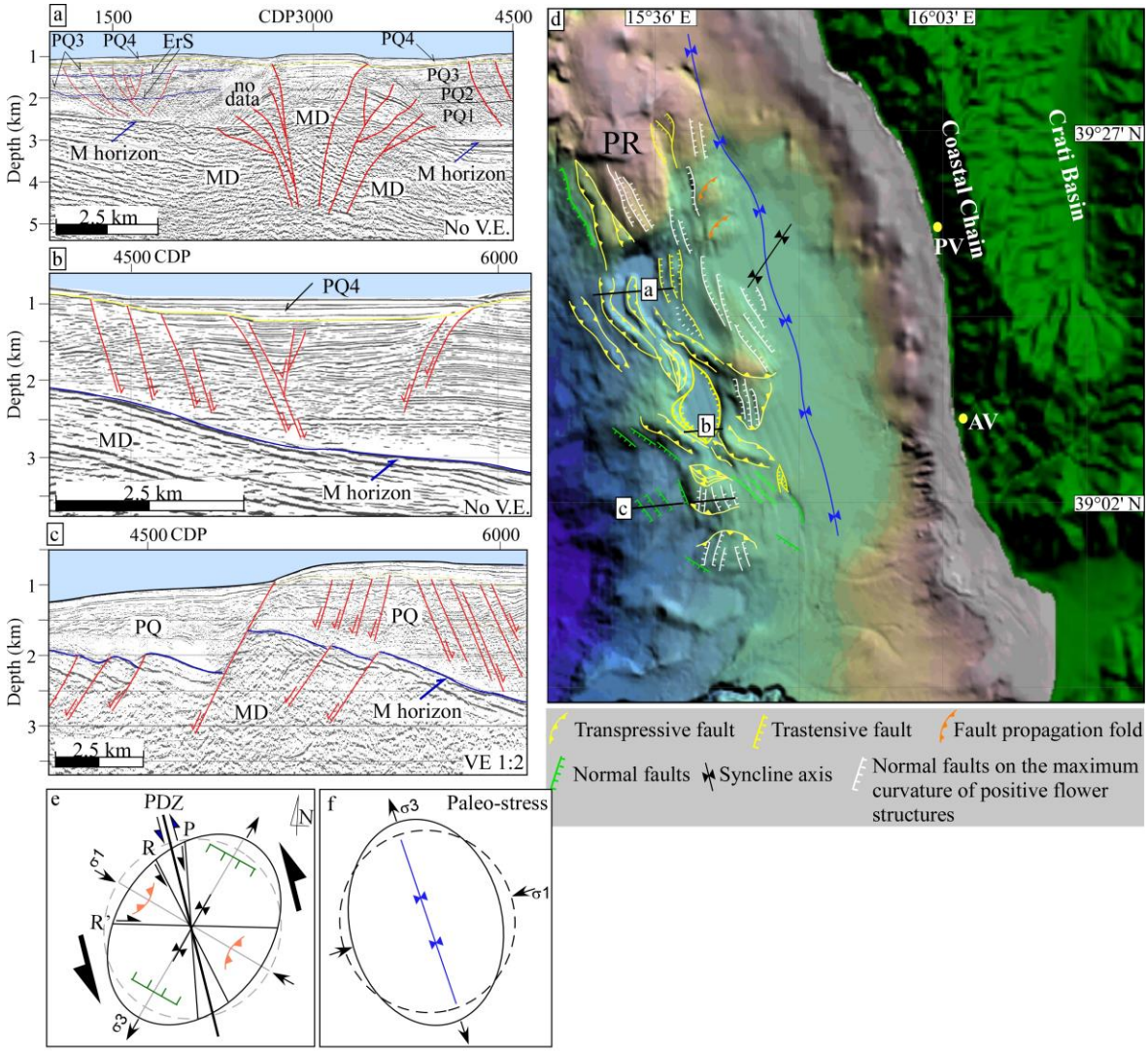

Figure 9. Corradino et al.

Figure 9. Morpho-structural map of the Paola Basin and surroundings. PRD: Paola Ridge; PV: Paola village; AV: Amantea village. Transpressive, transtensive and normal faults that, overall, form the Paola Ridge are shown in the boxes (a), (b) and (c), respectively. (e) and (f) Orientation diagrams of principal stress axes as derived from structural and kinematic data. PDZ, Principal displacement zone; VE: vertical exaggeration.

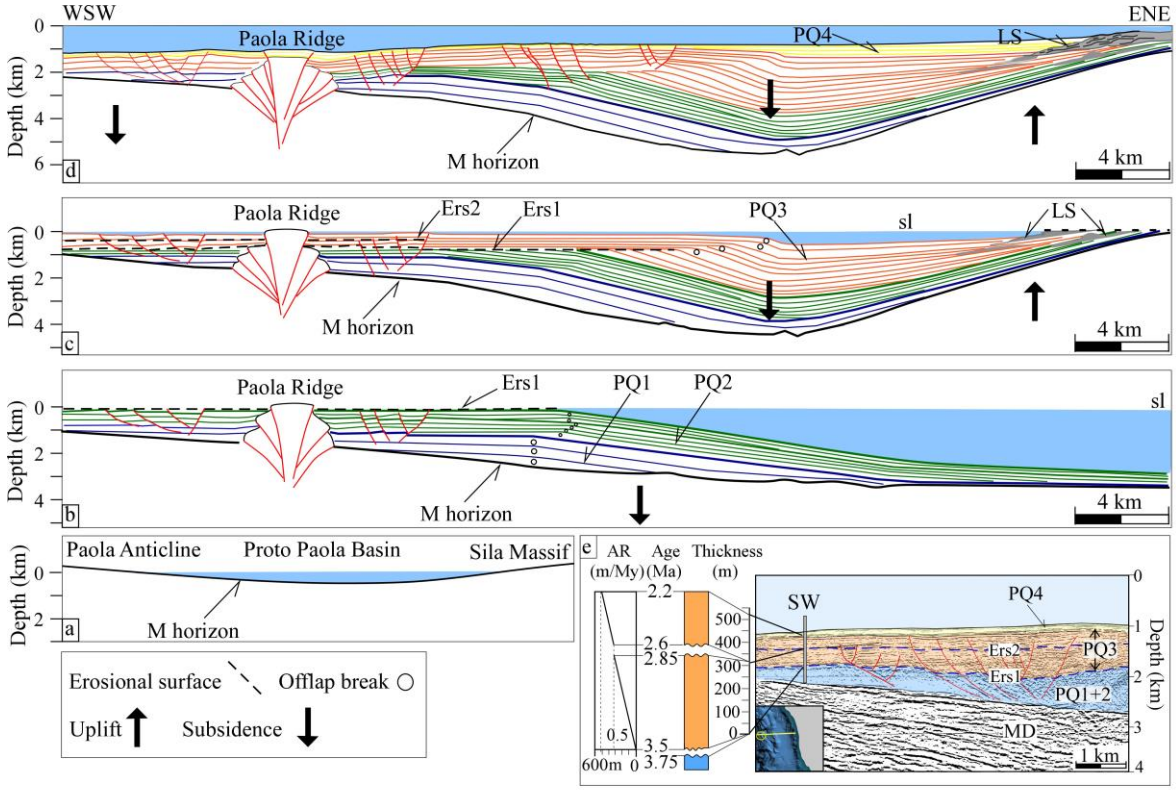

Figure 10. Corradino et al.

Figure 10. (a) Sketch of the proto Paola Basin at the end of the Messinian (Late Miocene). (b), (c) and (d) Stages of the Plio-Quaternary evolution of the Paola Basin corresponding to the deposition of subunits PQ2; PQ3, and PQ4. LS, Landslide; Ers1 and Ers2: erosional surfaces; sl, sea level. See Fig. 11a, b and c for location of sections b, c and d, respectively. No vertical exaggeration. (e) Schematic accumulation rate (AR) plot for the subunits PQ1- PQ4 derived from their thickness and ages assumed for the erosional surfaces (Ers). Inferred age of the top of subunit PQ3 is also reported. The circle in the inset indicates the location.

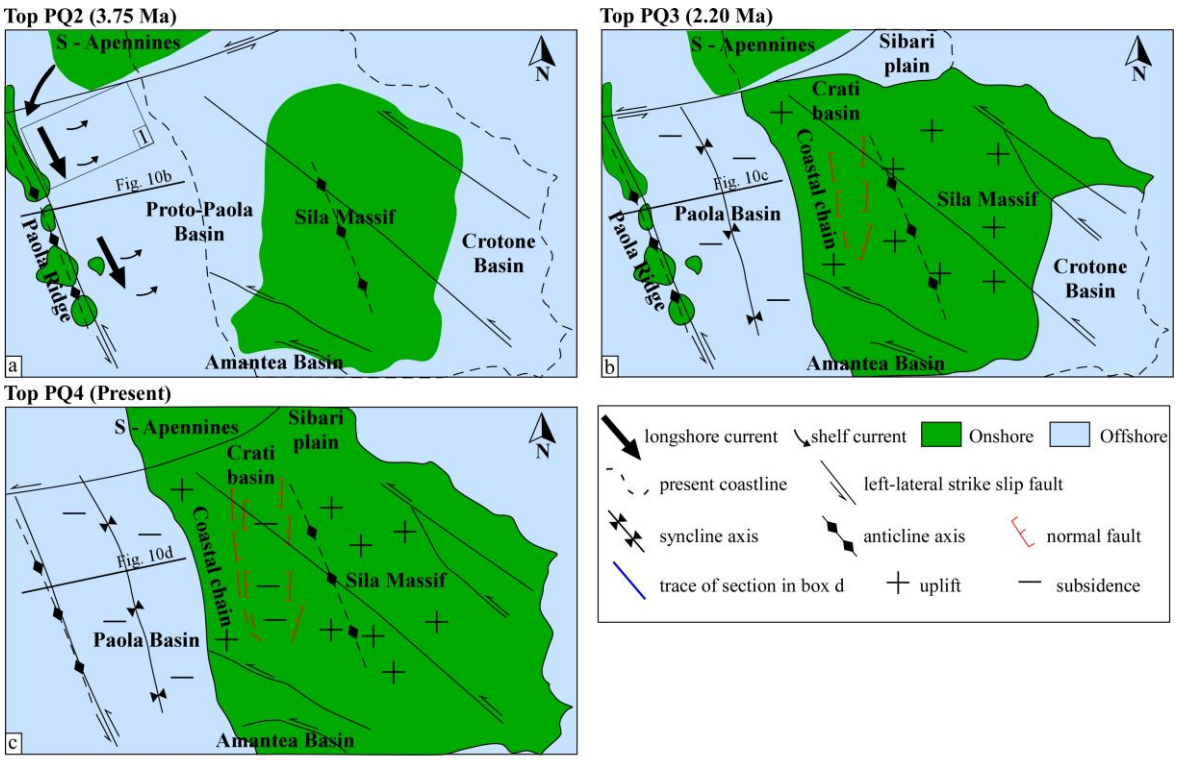

Figure 11. Corradino et al.

Figure 11. Plan view evolutionary model of the interest fore-arc region at the ages of the top of PQ2 (box a), PQ3 (box b), and PQ4 (box c).

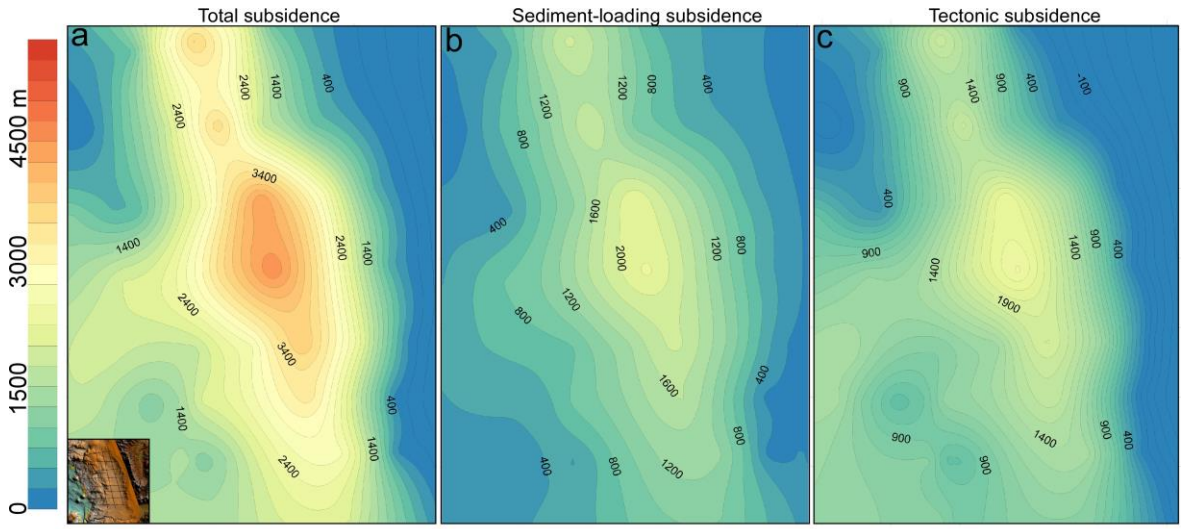

Figure 12. Corradino et al.

Figure 12. Plio-Quaternary (a) total, (b) sediment loading and (c) tectonic subsidence map of the M horizon in the Paola Basin.

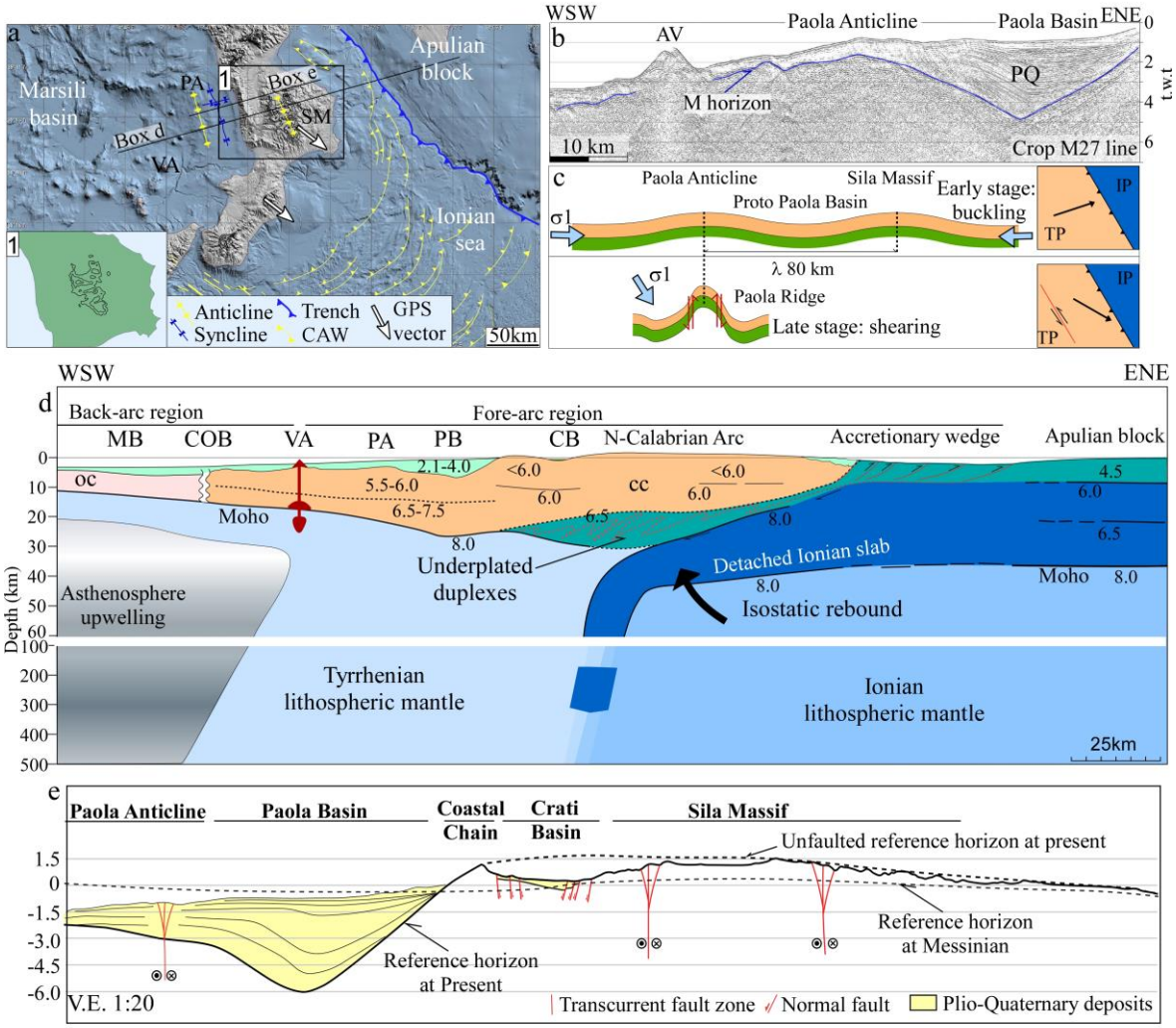

Figure 13. Corradino et al.

Figure 13. (a) Schematic tectonic map showing the northern trench, the accretionary wedge (CAW) of the Tyrrhenian-Ionian subduction system and the axis directions of the Paola anticline (PA), Sila Massif (SM) and Paola synclines. The contour level curves from 1300 a.s.l up to 1700 a.s.l of the Sila Massif are shown in inset 1. (b) Crop M27 profile showing the regional-scale Paola Anticline (modified from Pepe et al., 2010). (c) Sketches of the effects of lithospheric buckling and shearing in the early and late stages of deformation of the proto Paola Basin and surroundings. Insets show the direction of the Tyrrhenian plate (TP) motion vector. (d) Schematic cross-section showing the lithospheric structure across the back- and fore-arc regions of the Tyrrhenian-Ionian subduction system. Structure of the crust based on the results of the DSS seismic refraction data (Morelli, 1975), and the time to depth converted and gravity modelled Crop M27 profile (modified from Pepe et al., 2010). Abbreviations: MB, Marsili Basin; COB, Continent oceanic boundary; VA, Volcanic Arc; PA, Paola anticline; PB, Paola Basin; CB, Crati Basin; oc, Oceanic crust; cc, continental crust. (e) The position of the reference M horizon along the Paola Basin and Northern Calabrian Arc at the Messinian time and at the present-day. Data were derived from the Line Section 4 and by Spina et al., 2011. The positions of the main transcurrent fault zone are also shown. V.E., Vertical exaggeration. Location of sections (d) and (e) are shown in box (a).

Section	Lprd (km)	Lpd (km)	S (%)
2	17.1	16.28	5.03
3	18.9	18	4.76
4	19.37	18.7	3.46
5	16.52	16	3.15
6	15.34	14.9	2.86
7	14.46	14	3.18
10	56.04	55.11	1.66

Table 1. Corradino et al.

Table 1. Crustal shortening across the Paola Basin based on the M horizon recognized of seismic profiles. Lprd, pre-defromation length of the M horizon; Lpd, post-deformation length of the M horizon; S, Shortening percentage.

Conclusions

The results of this thesis, integrated with data available in literature, are relevant for the understanding of deformation mechanisms at different time and spatial scales.

Volcano-tectonic deformations at 1yr-1kyr timescale and 1km spatial scale were investigated in the NYT caldera and its intra-caldera resurgence (Campi Flegrei-Pozzuoli Bay). The analysis of bathymetric and seismic reflection data acquired in the Pozzuoli Bay, coupled with the interpretation of ground deformation maps of the Campi Flegrei, provided new insights into the structural pattern of the NYT resurgent caldera. The NYT collapse caldera displays an almost circle shape with radius of ~8 km. The structural pattern consists of the ~ 3-4 km wide ring fault zone and an uplifted intra caldera region. In the Pozzuoli bay, the ring fault zone corresponds to a series of ~ 60° inward dipping normal faults that allowed the sinking of the NYT caldera floor from ~140 m up to ~ 230 m, moving from the southern sector of the bay to its central part. The development of the normal faults occurred from the inner region of the caldera outward, causing its widening through time. The ring fault zone surrounds the intra caldera resurgence, a ~50 km^2 wide uplifted area with an almost circle shape centred on the Pozzuoli harbor. The resurgence develops along a series of inward-dipping reverse faults characterized by an upwards decreasing inclination of their fault plains from ~70° to ~15°. These structures formed by the reactivation of pre-exiting normal faults developed during the NYT caldera collapse. The structural style of the resurgence is expressed by disjoint uplifted blocks of the caldera floor rocks. Two main blocks are detected inside the resurgent area both off- and onshore, separated by a NNE-SSW trending high-angle normal fault. The most uplifted block includes the area from Mt Nuovo to La Pietra, and the adjacent uplifted sector extends eastwards until Mt Spina. The morpho-bathymetric expression of the two uplifted blocks is represented by a ~5 km wide antiformal structure, surrounded by Bagnoli and Epitaffio valleys. A series of high-angle normal faults forms a graben-like structure as a consequence of the extension regime in the area of maximum curvature of the antiformal structure.

Long-term deformations (Myr timescale) occurring at tens of kilometers spatial scale were studied along the Paola Basin, a forearc segment of the Tyrrhenian-Ionian subduction system. The interpretation of a grid of high-penetration reflection seismic profiles allowed to reconstruct the 3D architecture and the Plio-Quaternary evolution of the Paola Basin. The letter is a NNW-SSE trending asymmetric syncline, bounded by the offshore sector of the Coastal Chain to the East and a limb of the regional-scale Paola Anticline to the West. The Paola Basin hosts up to 5.5 km thick Plio-Quaternary deposits, most of them with an eastward-dipping clinoforms geometry. This pattern is explained with a local circulation of longshore currents that flowed southwards in the restricted gulf between the Sila Massif, Paola Anticline and the Apennines, and dispersed sediments from unknown Apenninic/Sila entry points. The uppermost part of the Plio-Quaternary deposits is characterized by an aggradational internal pattern and a westwards decreasing in thickness, suggesting a sediment supply from the Coastal Chain. In the Early Pliocene the proto Paola Basin extended from the Paola

Anticline until the western flank of the Sila Massif. Since 3.5 Ma, the uplift of the Coastal Chain led to the separation of the proto Paola Basin in the Paola and Crati basins. The tectonic subsidence of the Paola Basin, the uplift of the Paola Anticline and part of the uplift of the Sila Massif are explained through the mechanism of the short wavelength (~ 80 km) lithospheric buckling, resulting from ENE-WSW oriented compressive stress field. The lithospheric buckling, coupled with underplating/underthrusting, and isostatic rebound controlled the folding of the lithosphere along the Northern Calabria Arc. The folding induced tensile stress, resulting in the formation of N-S trending normal faults along the extrados of the Sila Massif anticline. These structures bound the Crati Basin and allow its widening through time. Kilometre scale tectonic features associated with strike-slip restraining and releasing bends formed along the hinge zone of the Paola Anticline, defining the Paola Ridge. Their formation is compatible with a NNW-SSE oriented maximum stress axis. The change in direction of the maximum stress axis from ENE-WSW to NNW-SSE is a consequence of the transition from orthogonal to oblique subduction resulting in the partitioning of strain. Based on a) the oblique subduction of the overriding plate, b) the development of major strike-slip faults in the areas surrounding the Paola basin, and c) the weak deformation of its sedimentary infill, the Paola Basin was classified as a "Neutral Accretionary-type" forearc basin.